D5.1: HIL 15MW development

POLIMI/FIHAC

October 2020

Disclaimer:

This project has received funding from the European Union's Horizon 2020 Research and Innovation programme under grant agreement No 815083.

Project details:

Duration:
1 Sep 2019 - 28 Feb 2023
Grant agreement:
No: 815083

Document information

Deliverable number	D5.1
Deliverable name	D5.1: HIL 15MW development
Reviewed by	Henrik Bredmose (DTU) Mohammad Youssef Mahfouz (USTUTT)
Date	30-10-2020
Work Package and Task	Task 5.1: Innovative experimental testing procedures
Lead Beneficiary for this Deliverable	POLIMI

Authors

Name	Organisation	E-mail
Alan Facchinetti	POLIMI	alan.facchinetti@polimi.it
Simone Di Carlo	POLIMI	simone.dicarlo@polimi.it
Alessandro Fontanella	POLIMI	alessandro.fontanella@polimi.it
Raul Guanche	FIHAC	guancher@unican.es
Tommaso Battistella	FIHAC	battistellat@unican.es
Miguel Somoano	FIHAC	somoanom@unican.es
Javier Sarmiento	FIHAC	sarmientoj@unican.es
Alvaro Rodriguez	FIHAC	alvaro.rodriguezluis@unican.es

Version control

Version	Date	Author	Description of Changes
[Official versions only]	[yyyy-mm-dd]		

Table of contents

1 EXECUTIVE SUMMARY

This work is focused on the development of innovative large-scale experimental testing procedures based on a scaled concept for a 15MW floating offshore wind turbine (FOWT) of the two concrete-based floating substructures designs: a spar (*WindCrete*) and a semi-submersible (*ActiveFloat*). In order to evaluate the impact of the wind-turbine aerodynamic loads over the dynamics of both platforms, and hence over the power cable and mooring system, we propose a methodology that couples two complimentary hybrid testing techniques:

- A multi-fan system able to reproduce the full wind turbine aerodynamic loads in a wave tank.
- A 6_DOF platform able to reproduce the full hydrodynamic performance of a floating wind turbine in a wind tunnel.

Firstly, we define a state of the art of FOWT experimental testing methods for mooring line and cable analysis. This review also considers best practices from other industrial applications where mooring lines and cables are present. Secondly, we investigate the importance of the wind turbine dynamics integration control over the mooring system, power cable and platform performance, with a couple approach in order to face the limitations typically given by scaled problems:

- Froude scale at the wave tank which limits the aerodynamic problem.
- Reynolds scale at the wind tunnel which limits the hydrodynamic problem.

Based on numerical models, the uncertainty of the two different hybrid testing procedures is assessed. Finally, we analyse truncation methods for mooring and cable system integration applied to maximize the size of the tests and reduce potential scale effects. Best practices on the FOWT testing are included, facing two different testing barriers: very deep waters and large footprints.

2 REVIEW OF BEST TESTING PROCEDURES FOR MOORING LINE AND CABLE ANALYSIS

The main function of a mooring system is to restrict the low frequency motions of the floating structure and to resist environmental actions. A correct modelling of mooring system is fundamental in the evaluation of the global response of the platform in floating offshore structures as the mooring lines provide to the stiffness and damping that allowed to maintain the platform in position. Because the mooring system design is usually driven by extreme conditions, a comprehensive analysis of the system should also address other aspects contained in a reliable representation of the loads time histories of the mooring lines, such as the fatigue damage or the effects of the environmental aggressions on the mooring lines and power cables. The importance of the evaluation of such actions for guarantee an appropriate design of the mooring system is presented in (Barrera, Losada, Guanche, & Johanning, 2019b) and (Barrera, Battistella, Guanche, & Losada, 2020a).

2.1 Mooring lines testing

In the experimental testing of a mooring system the main aspects which are investigated are the following:

- The influence of the mooring system on the dynamics of the floater, in terms of displacement under static loads, natural frequencies and damping;
- The load levels of the mooring lines, both as peak loads for ultimate resistance and fatigue loads accumulation.

It is usually difficult to achieve both objectives in the same test campaign because the approaches that must be followed in the two cases are different. While the influence of the mooring system on the dynamics of the floater is reproduced with a quasi-static scaled model of the mooring system, at least in mild to moderate sea states, the inspection of loads or the accurate evaluation of tension-varying stiffness and damping is achieved with a dynamical model of the mooring line. The latter requires a proper scaling and experimental setup, usually unfeasible in wave tank experiments of the whole floating system (moorings and floater).

2.1.1 Simple catenary moorings

The simplest case scenario in mooring lines testing is represented by catenary lines whose dimensions, in terms of depth and radius of anchors, can be fitted inside the wave tank with by applying an appropriate scale factor. An important feature of a mooring line is the restoring force described by the force-displacement curve. The restoring force of a catenary line is mainly due to the weight because the mooring line weight brings the line to the equilibrium when it is perturbed from the resting position. Although the most important parameter for catenary modelling is the weight per unit length, there are other significant parameters such as axial stiffness and diameter which must be taken into account. The axial stiffness observed in tensile test is higher than the correspondent axial stiffness in prototype scale. Because of that, the correct replication of the real axial stiffness is achieved by including calibrated springs within the lines. Accordingly, the total stiffness results from the combination of two stiffnesses, one from the mooring line and the other from the spring (Barrera, Guanche, & Losada, 2019a).

Froude's scaling laws are applied to the mooring dimensions in order to accurately reproduce the hydrodynamic behaviour. This approach maintain the relationship between the inertial and gravitational forces in the model and the prototype scale. Mooring line modelling requires to scale the dominant hydrodynamic loads additionally to the weight of the mooring line, which provides the restoring force and the inertia loads. The weight of the mooring line and the inertia forces are correctly modelled using Froude's laws. However, the hydrodynamic loads due to the drag loads are hardly reproduced correctly because dependent to the Reynolds number, which is normally underestimated compared to the full scale value (Bergdahl, Palm, Eskilsson, & Lindhal, 2016). Nevertheless, in mild and moderate sea states this is normally a minor issue.

2.1.2 Sea bottom friction

Catenary configurations used in spar and semi-submersible platforms are usually designed to have enough line length resting on the seabed, avoiding vertical forces on the drag-embedded anchoring system. Seabed granulometry, compaction and shape of the sand grains have influence in the sea bottom friction, hence an impact on the mooring loads and the dynamic behaviour of the mooring lines. The sand bottom friction can be obtained from a drag test, which consists in dragging a chain at a constant velocity using a carriage located at the top of the flume. The drag force measured during the test determines the seabed friction coefficient (Barrera, Guanche, & Losada, 2019a).

In order to represent the size of the gravel at laboratory scale, the inception of movement is evaluated by determining the Critical Shields number:

$$\mathbf{S} = \frac{\boldsymbol{\tau_{0max}}}{(\boldsymbol{\rho_s} - \boldsymbol{\rho})\mathbf{g}\mathbf{D_{50}}} \quad (\boldsymbol{1})$$

where D_{50} is the characteristic sediment size, ρ_s the sediment density, ρ the water density and τ_{0max} the shear stress parameter depending on the incident waves (Hughes, 1993). Given the flow is scaled by means of the Froude's law, the grain size is scaled as follow:

$$\mathbf{N_D} = \boldsymbol{\lambda} \cdot \mathbf{N_\Delta^{-2.083}} \quad (\boldsymbol{2})$$

where λ is the length scale and $N_\Delta = (\boldsymbol{\rho_s} - \boldsymbol{\rho})/\boldsymbol{\rho}$ the submerged density scale (Barrera, Guanche, & Losada, 2019a).

2.1.3 Deep water moorings

When dealing with model testing of deep water offshore structures the length of mooring lines can be of the order of 1000 m, while the length scale of the structure is 100 m. This poses and issue of mooring scalability when setting up a model test in a wave tank, whose dimensions are in the order of 10 m. If reproduced correctly, mooring lines would force to use small scale factors, which would imply heavy scaling effects, preventing to correctly capture the hydrodynamic behaviour of the floater. It is then a common practice to reproduce the mooring system of a structure with a truncated version of the scaled one. Such approach permits to limit the mooring system within reasonable depths and footprints of anchors, reproducing, at the same time, the correct influence of mooring loads on the structure and possibly investigate the lines tension. In the case of truncation, the mooring line system is normally tested according to a quasi-static approach.

The truncation procedure is a well-established model scale testing method in the Oil and Gas industry (Fan, Qiao, & Ou, 2012). The truncated mooring system has to satisfy some characteristics with respect to the real scale one, as stated in (Stansberg, Oritsland, & Ormberg, 2001): it must reproduce correctly the total horizontal restoring force, model the quasi-static coupling between vessel responses, model a representative level of damping, and tension of the single line (Molins, Trubat, Gironella, & Campos, 2015). This approach, however, has the disadvantage of underestimating the peak forces in the cables, especially during survival load cases (Stansberg, Karlsen, Ward, Wichers, & Irani, 2004). A partial solution to this issue is to use the real scaled mooring lines in the upper section, close to the fairleads, where dynamic loads are more important, and to use actuators to replicate the truncated segments (Argyros, Langley, & Ahilan, 2011).

It is customary to model the cable stiffness by means of springs, reproducing the correct restoring force only in a quasi-static sense (Bergdahl, Palm, Eskilsson, & Lindhal, 2016). This means to achieve the correct force-displacement curve in the different DOFs of the structure. The stiffness behaviour of a mooring line is inherently non-linear, and effort should be put in reproducing this characteristic.

Tests to assess the overall quality of the quasi-static mooring system are free-decay methods and static pull-outs. In a free-decay the frequency of oscillation and the overall damping of the system can be assessed; in static pull-outs it is possible to verify the force-displacement curve, especially in surge and sway motions.

2.1.4 Dynamic testing of mooring lines

While quasi-static analysis is appropriate for determining the tension for low frequency displacements, dynamic analysis is suitable for a wide frequency range. Dynamic scaling of mooring line consists in the reproduction of a scaled mooring system having dynamic similitude with the prototype, scaling, at the same time, the correct tension force characteristics of the full-scale system. In a dynamically scaled model the transversal and longitudinal vibration of the cables are correctly scaled, that is the wave propagation celerity maintains the similitude between model and prototype. Dynamic scaling can be accomplished in several ways (Bergdahl, Palm, Eskilsson, & Lindhal, 2016) by using specific sets of dimensionless groups, depending on the formulation of dynamic equations. Other than the accurate inspection of cable loads, an approach of this kind is necessary when the focus of the experiment is to reproduce phenomena occurring in survival sea state, which can lead to breakage of the mooring system. Among them the tensional shock waves given by snatch loads or the loads generated during the transition from slack cable to taut cable.

The design of chain stiffness using a calibrated spring is a standard procedure and indeed a good way to model first-order effects. However, the method is prone to some discrepancies between laboratory and prototype results, especially in the case of snap loads, where the propagation speed of the tension shock and the tensile stiffness of the cable governs both the peak load magnitude and the cable slack period. Therefore, in spring only models the stiffness of the whole cable in a quasi-static manner and, as a consequence, the resulting snap load events have uncertain magnitude and most likely over-predicted compared to prototype scale (Barrera, Guanche, & Losada, 2019a). In general, the spring stiffness is relevant when the catenary is completely stretched. However, the design of the catenaries using embedded anchors requires anchors without vertical forces. For this reason, although the mooring lines are equipped with springs, they should not provide vertical stiffness. This issue should be addressed in case the mooring lines do not work in a purely catenary shape.

The dynamic behaviour of a cable is tested with forced motion tests. A rotary motion is applied to the fairlead with different circular frequency and amplitude, and the force is measured in one or more locations along the line. The line motion can also be recorded (Barrera, Guanche, & Losada, 2019a). The friction with the seabed can be modelled by deploying sand of correct granulometry inside the basin, and by verifying the seabed-line drag coefficient by dragging the line at constant velocity in the sand and measuring the required force.

The mooring system is not only contributing with a certain amount of added stiffness on the floater, but also with a considerable amount of damping. The mean excursion of the floater due to slowly varying forces is changing the pretension of each line and thus resulting in a different stiffness and damping behaviour. This behaviour has a non-linear character and should be taken into account when testing a mooring system. Another issue to be considered is the relationship between the floater oscillation frequencies and the natural frequencies of the line: damping properties are affected by the change of these frequencies.

The damping of a mooring line can be assessed with model scale tests with two main methodologies:

- Decaying method: the floating structure is tested in a free-decay, and overall damping is measured. Of course, the damping of the sole structure must be known and subtracted from the overall one. From a free decay signal the damping ratio is evaluated through logarithmic decrement and then the damping coefficient is extracted by knowing the mass and added mass of the floater, together with its natural frequency.
- Forced oscillation method: the fairlead of the line is displaced with different amplitudes and frequencies, and the line is subjected to varying pretension. The plot of fairlead tension over displacement gives a closed loop, whose area is proportional to the line damping (Barrera, Guanche, & Losada, 2019a).

2.2 Power cable dynamic analysis

The Oil and Gas industry provides examples of cable dynamic response assessment, like the one developed in the monitoring system of the umbilical cord with lazy-wave configuration installed in the Foinaven Petrojal IV floating production storage and offloading (FPSO) vessel. The cable bending stresses were monitored by a specially developed curvature sensor, while load cells located at the top of the subsea umbilical measured tension (Lyons, Brown, Cook, Walls, & Barnay, 1998). The total stresses in the individual components of the umbilical were derived from this combination, and Rainflow counting techniques were used to assess the fatigue damages. Vessel motions as well as wave/current data were also acquired and stored. To investigate provoked by vortex-induced vibration (VIV), (Lie, Braaten, Kristiansen, & Nielsen, 2007) towed a full-scale prototype-section of the Ormen Lange free-span umbilical from a carriage above the ocean basin. Measured data of bending and axial strain and lateral acceleration in both cross-flow and in-line directions at 10 equally spaced stations, were studied using statistical, modal and fatigue analysis.

Also the wave energy sector provides relevant examples relevant to the cable experimental analysis. In relatively shallow water, the export cable must ensure efficient electrical transmission while alternating taut-slack condition due to dynamic loads from waves, current and the motion of wave energy converter (WEC). In a wave flume, (Martinelli, y otros, 2010) performed dynamic scale tests on a power umbilical connected to a floating WEC model. The umbilical dynamics was observed by a video-camera placed in 4 positions, and a quantitative evaluation of the wire displacements on the mid plane was done with the help of a grid of lines spaced of about 1 cm between them and placed on both the front and the rear windows. An electric extra-flex wire was tested under different regular wave conditions, considering both catenary shape and lazy-wave layout, creating its long-radius hog bend by wrapping the umbilical with polystyrene ribbon stringed into an interweaved sock. The latter configuration appeared to be more suitable as the buoyancy modules decouple the WEC motions from the touchdown point and reduce the hang-off loads at the WEC interface. (Marta, y otros, 2015) assessed the performance of submarine dynamic power cable for floating offshore renewable energy through both static and dynamic mechanical testing. Static performance was obtained from bending stiffness test and tensile test, measuring axial and torsional stiffness. On the other hand, dynamic testing plans included both full cable bending against template test and power cores bending against template test. In addition, the test campaign included the combined dynamic marine movements (pitch, roll and heave) with low-cycles loading fatigue test.

Regarding floating offshore wind power generation, (Taninoki, Abe, Sukegawa, Azuma, & Nishikawa, 2017) conducted a forced oscillation test in a towing tank with a 6.6-kV class three-core XLPE cable on the seabed in order to determine the mechanical forces that act on the cable. A forced oscillation test unit was used to oscillate the top end of the cable with a predetermined force and the strain applied to the wire armour was measured. The changes in the angle between the cable and the seabed were measured using an accelerometer, in order to determine the cable profile change. Besides, the authors used a 6.6-kV cable with specially designed waterproof layers provided around its XLPE insulation to simulate the 66-kV one, on a full-scale 2-MW wind turbine demonstration for approximately two years. The lazy-wave concept was designed to absorb a floater moving distance of ± 40 m, restricting the moving range of the buoy position by a wire and a sinker to minimize changes

in the cable profile near the seabed. However, there are no experimental work regarding the coupled dynamics of power cable in a floating wind environment to our knowledge. Lack of experience with dynamic submarine power cables leads to conservative design.

2.3 Model tests of FOWT

Today, few prototypes of floating wind turbines are currently deployed, so measurements coming from operating systems are rare. Model-scale tests in wave tank or wind tunnel result as cost-effective tools for gathering data used to validate FOWT dynamics behaviours. Codes used to simulate the dynamics of FOWT are still under development, some of them derive from the Oil and Gas industry and are able to simulate correctly the hydrodynamic forcing of waves and the floating dynamics of a structure, however, they often fail to reproduce accurately the turbine aerodynamics and its control system. Moreover, second-order hydrodynamic effects and mooring lines dynamics are still not modelled with sufficient accuracy.

Floating wind turbines are complex systems from the modelling point of view, as they represent a strong coupling between forces related to different physical phenomena. The joint effects of hydrodynamics, structure flexibility, aerodynamics and control system dynamics join together defining the dynamic behaviour of the system. The complexity of the full-scale system reflects obviously on the set-up and conduction of model tests, which intends to reproduce the coupled dynamics or at least evaluate the error generated by a voluntarily or mismodelled system.

Experimental testing of offshore floating wind turbines derives for some extents from experiences gained during experimental testing of offshore facilities, mainly for Oil and Gas purposes, or from the naval field. These engineering fields have added on in a broad know-how which permitted to reach high levels of reliability in the reproduction of hydrodynamic phenomena at model scale or larger scale. However, as stated before, wind turbine simulation involves several factors which are peculiar of the system itself and whose correct reproduction represents a novel challenge with respect to purely naval engineering fields.

2.3.1 Scale issues on FOWT testing

Gravity-influenced phenomena, like wave propagation and wave excitation forces are correctly reproduced at model scale adopting Froude scaling laws. This approach has been extensively used in wave tank experiments involving offshore platforms, ships, harbours and many other civil or naval application.

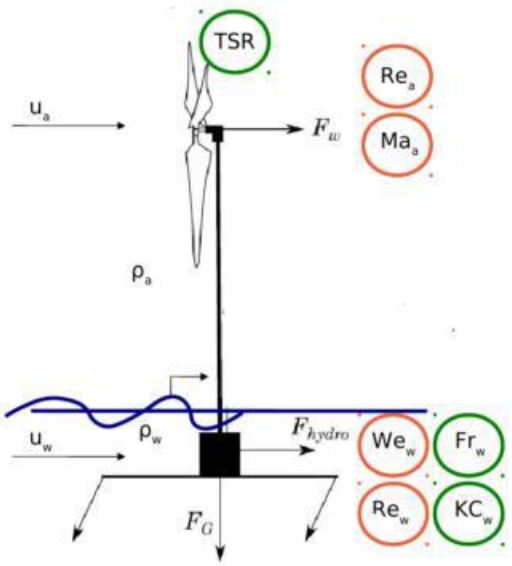

Figure 2-1. Non-dimensional numbers involved in FOWT scaling process ***(Bredmose, Larsen, Matha, Rettenmeier, & Marino, 2012)***.

This is the scaling method adopted also for the wind turbine subsystems subjected to hydrodynamics and inertia loading, such as the floater and the emerged structure mass and stiffness. Froude scaling is however not suited to represent viscous phenomena, which instead obeys to Reynolds scaling. It is well-known after all that Froude scaling results in too low Reynolds numbers, and so in a deviated reproduction of viscous phenomena, both in water and in air. While this issue is often neglected in water, the associated change of Reynolds number for aerodynamics leads to a consistent change in the forces acting on the rotor of the machine, and so to the need of finding strategies to correctly reproduce the aerodynamic thrust. Actually, different testing procedures in floating wind turbine testing are differentiated among them on the basis of what is the strategy adopted to correctly model contemporarily the Froude based subsystem and the Reynolds based subsystem. The following sections are dedicated to a short description of Froude-scaling methodology and the reproduction of aerodynamic loads, with a collection of scientific references.

2.3.2 Froude scaling

The foundation of Froude scaling is the preservation of the ratio between inertia and gravitational forces. Let us define the length scale λ between model and prototype as:

$$\lambda = \frac{L_p}{L_m} \qquad (3)$$

where the subscript p denotes the prototype, and m the model. Now, by requiring that the inertia force on a fluid particle of mass m is equal to the inertia force imparted on it by an acceleration a it is found that:

$$\frac{M_p a_p}{M_p g} = \frac{M_m a_m}{M_m g} \quad \Rightarrow \quad a_m = a_p \qquad (4)$$

Then as the dimension of acceleration is L/T^2 it follows that:

$$\frac{L_p}{T_p^2} = \frac{L_m}{T_m^2} \quad \Rightarrow \quad \frac{T_p}{T_m} = \sqrt{\lambda} \tag{5}$$

this is the scale between prototype time and model scale time (Azcona, y otros, 2014b).

By taking into account a volume of fluid and its density it is possible to obtain the scaling law for masses:

$$\frac{M_p}{\rho_p Vol_p} = \frac{M_m}{\rho_m Vol_m} \Rightarrow \frac{M_p}{M_m} = \frac{\rho_p}{\rho_m}\lambda^3 \tag{6}$$

The Froude number Fr is defined as $\boldsymbol{Fr = \frac{u^2}{gD}}$ where u is the fluid velocity, g is the gravitational acceleration and D is a characteristic dimension of the structure. Assuming a model scale factor of λ and geometric similarity, the Froude model must satisfy the relationship:

$$\frac{u_p^2}{gD_p} = \frac{u_m^2}{gD_m} \quad \Rightarrow \quad \frac{u_p}{u_m} = \sqrt{\lambda} \tag{7}$$

While the Froude number is a primary scaling parameter in these types of model tests and is used in determining the structure responses, the Reynolds number Re effect is not scaled properly in a small scale model (Chakrabarti, 1998). In fact, the Reynolds number for a Froude model is smaller by a factor of $\lambda^{1.5}$:

$$Re = \frac{uD}{\nu} \quad \Rightarrow \quad \frac{Re_p}{Re_m} = \frac{\nu_m}{\nu_p}\lambda^{3/2} \tag{8}$$

The consequence of this difference is that while the prototype flow regime is turbulent, that of the model may necessarily become laminar. The drag coefficients in a laminar flow are normally higher than those found in a turbulent flow. The scaling then is generally expected to be conservative if no corrective measure is taken in scaling. On the other hand, the non-linear damping will produce smaller model response. In order to rectify this deficiency, it is a common practice to artificially stimulate turbulence in a model test by introducing roughness in the flow approaching the surface of the model.

As far as aerodynamics is concerned, the most important non-dimensional group involved in these phenomena is the Reynolds number. While the Froude-scale method captures the wave loading correctly, it does not properly represent the wind loading problem. Using the Froude-scale method, the Reynolds number varies, and it will be much lower than for a full scaled model. Consequently, the aerodynamic forces do not resemble the corresponding scaled loading. This, in general, leads to a reduced lift to drag ratio on a blade profile, which in turn necessitates an increased chord length. The rotor needs to be redesigned to deliver the correct thrust force on the model, because this is the main dynamical effect on the floating turbine. However, the detailed aerodynamics around the rotor is lost (Azcona, y otros, 2014b). Strict Froude scaling will also preserve the thrust coefficient:

$$F_T = \rho_a C_T A u_a^2 \approx \frac{\rho_w}{\lambda^3} \quad \Rightarrow \quad \frac{C_{Tp}}{C_{Tm}} = \frac{\rho_{wp}}{\rho_{wm}} \tag{9}$$

Once the scaling laws for length and masses are defined, the scaling laws for structural properties derive directly. For mooring systems in conjunction with a floating structure, the model deformation due to the wave loading is not negligible. The coupling of loads imposed by the water surrounding the platform with the structure response is known as hydroelasticity. Hydroelasticity deals with the problems of fluid flow past a submerged structure in which the fluid dynamic forces depend on both the inertial and elastic forces on the structure. Therefore, in addition to the Froude similitude, the Cauchy similitude is desired (Chakrabarti, 1998). Noting that the bending

moment in a Froude model scales with λ^4, the Cauchy similitude requires that the bending stiffness must satisfy the following relation:

$$\left(\frac{My}{EI}\right)_p = \left(\frac{My}{EI}\right)_m \quad \Rightarrow \quad \frac{(EI)_p}{(EI)_m} = \frac{\rho_p}{\rho_m}\lambda^5 \tag{10}$$

in which EI is the flexural rigidity, M the vertical bending moment and y the distance to the outer fiber from the neutral axis. Thus, the elastic scaling is achieved by correctly scaling the Young's modulus and the cross-section inertia:

$$\frac{E_p}{E_m} = \frac{\rho_p}{\rho_m}\lambda \quad ; \quad \frac{I_p}{I_m} = \lambda^4 \tag{11}$$

To sum up, Table ***2-1*** shows the main Froude laws of similitude applied during a physical testing.

Table 2-1. Froude scaling laws of similitude **(Sarmiento, Iturrioz, Ayllón, Guanche, & Losada, 2019)**.

Variable	Dimension	Scale Factor
Length	L	λ
Time	T	$\lambda^{1/2}$
Mass	M	$1.025\cdot\lambda^3$
Velocity	LT^{-1}	$\lambda^{1/2}$
Acceleration	LT^{-2}	1
Force	MLT^{-2}	$1.025\cdot\lambda^3$
Pressure	$ML^{-1}T^{-2}$	$1.025\cdot\lambda$

Scaling of waves and wave spectra

From the equations reported in the previous paragraph it is straightforward to derive that the wave height and water depth in the wave tank will scale with λ, while the wave period and current velocity with $\sqrt{\lambda}$. The frequency band for ocean waves of importance to the offshore structure lies in the range of 5 to 24 s, falling the maximum energy of the ocean waves in the area of 10-16 s. Therefore, the model basin should have the capability of generating these waves at a suitable scale with maximum heights in the above range (Chakrabarti, 1998). Generation of high frequency wave components at a small scale is difficult in a wave tank. At a scale of λ, a T_m wave represents a $T_p/\sqrt{\lambda}$ wave. Wave generators seldom have wave generation capability to reproduce waves at frequncies below 1 Hz. Waves at 4-7 s may have significant effect on the dynamic response of floating structures. Therefore, scales smaller than 1:70 do not allow reproduction of these waves. When simulating irregular waves, the significant wave height and the spectral peak period follow the same rules. The peak enhancement factor γ in JONSWAP spectra is not scaled since it is a dimensionless parameter. For long period wave spectra ($\gamma \leq 1.0$) the spectra may be simplified to the Pierson-Moskowitz spectral formulation.

Regarding the wind climate, as it is stated in equation Table ***2-1***, the wind velocity is scaled with $\sqrt{\lambda}$, while the turbulence intensity is kept as it is, being a dimensionless number.

Effects of Froude scaling on dimensionless groups

The Froude scaling approach conserves the following dimensionless groups:

- $KC = \frac{u_w T_w}{D}$: Keulegan-Carpenter number. It is a dimensionless number that qualifies oscillating flows effects on a body. It expresses the ratio between the displacement of a water particle in a sinusoidally oscillating flow and a characteristic dimension of the body. If $KC > 20$ then the flow is quasi-steady, and substantially drag-dominated. Instead, for $KC < 20$ the flow is inertia-dominated.

Among not conserved groups, instead:

- $St = \frac{fD}{u}$: Strouhal number (in water or air). This dimensionless number is rather invariant ($St \approx 0.2$) till Reynolds number is equal to $2 \cdot 10^5$ (subcritical regime). If both Froude and Strouhal numbers are preserved, then the frequency of vortex shedding will be scaled as $f_p = \frac{f_m}{\sqrt{\lambda}}$.

2.3.3 Approaches in FOWT experimental testing: completely physical model

In this section some of the FOWT experimental testing approaches are listed among the ones involving a completely physical modelling of the system.

The first approach listed here involves the coupled simulation of physical wind and waves in a wave tank. The wave tank allows an accurate reproduction of wave propagation and aerodynamic forcing but it is not in general a facility designed to have a contemporary good quality wind generation. Wind is generally provided in open circuit by means of arrays of fans with independent speed control. Layers of vanes and honeycomb provide a low turbulence flux; however, the wind speed is limited (in the order of 2 m/s) and the quality of the flow tends to decade rapidly moving far from the fan array.

A wave tank instead designed from the beginning to allow for coupled wind-wave tests is described in (Fowler, Goupee, Allen, Viselli, & Dagher, 2017).

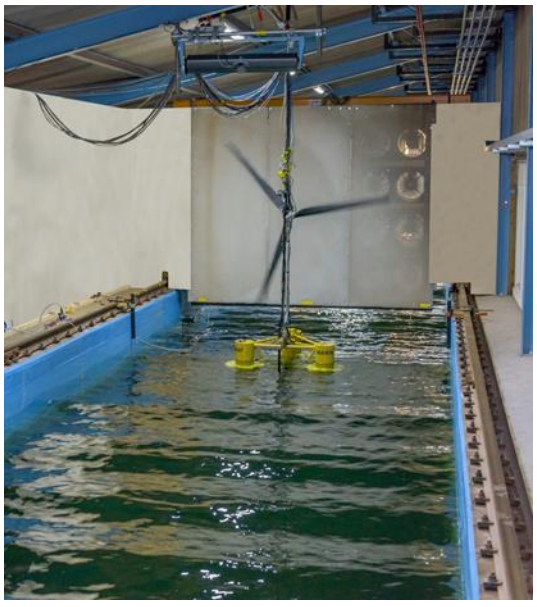

Figure 2-2. Wind-wave tank tests. The turbine in the figure is Froude scaled **(Marinet2, 2020)**.

As it is stated before pure Froude scaling does not reproduce correctly the aerodynamic performances of the turbine. Actually, the lowered Reynolds number resulting from Froude scaled air velocity is resulting in an insufficient level of thrust. This can be corrected by changing the geometry of the blades, because the lower lift to drag ratio found in model scale Reynolds can be compensated by increased chord length (Muller, et al., 2014). The design of the new rotor is of course based on low Reynolds number profiles. In addition to this, also the wind flow velocity can be scaled in a way different from the Froude one, to compensate for the changed rotor

characteristics or for the limited capabilities of the wind generator system (Muller, et al., 2014). This approach is known as Froude-β scaling. The velocity scale is expressed following Froude scaling, but corrected with a factor β:

$$\frac{u_{ap}}{u_{am}} = \sqrt{\lambda}\frac{1}{\beta} \quad (12)$$

With u_{ap} and u_{am} respectively prototype and model air velocity, λ Froude scale factor. For $\beta = 1$ strict Froude scaling is obtained, while for $\beta > 1$ the flow velocity at model scale is higher than the Froude scaled one. If β is different from 1 than the TSR of the machine is altered:

$$\frac{TSR_p}{TSR_m} = \frac{\omega_p R_p}{u_{ap}}\frac{u_{am}}{\omega_a R\_a} = \beta \quad (13)$$

In general conservation of TSR is preferred, but the lack of aerodynamic similarity between prototype and model can justify this approach (Sandner, Bredmose, Jose, & Muller, 2014). The TSR affects the wake effects and this can be important in experiments involving more than one wind turbine. The choice of $\beta > 1$ is a way to reduce the Reynolds number mismatch, taking into account that the geometry of the rotor must be changed anyway and then the detailed aerodynamics around the rotor will not be reproduced correctly.

The advantages of this approach are first and foremost the correct thrust delivery. If the rotational speed is scaled properly, also the 1P and 3P frequencies are preserved. The structural frequencies and deflection are instead subjected to a correct mass and stiffness scaling. Other quantities are instead not conserved: they are the aerodynamic torque, the aerodynamic power, the generator torque and the magnitude of 3P tower shadow forcing (Muller, et al., 2014).

If also the rotor dimensions are scaled according to Froude the air velocity must be increased so to reproduce a sufficiently high thrust, at the expenses of error in the aerodynamic similitude. This is the approach followed in the DeepCWind project (Robertson, M, D, & P, 2013).

A simpler approach is to substitute the rotor of the wind turbine with a drag disc (Guanche, Vidal, Piedra, & Losada, 2011). The drag disk allows the simulation of the wind thrust force under constant wind speeds. Nevertheless, in this case the control dynamics effect is lost. When using the drag disk technique in order to reproduce static wind loading, negative damping dynamics, wind turbine control changes, or turbulent wind speeds cannot be represented (Sarmiento, Iturrioz, Ayllón, Guanche, & Losada, 2019). In the particular case of negative damping dynamics, it has to be noticed that, above the rated speed, turbine thrust force curve usually shows a negative derivative. Because of that, the negative damping cannot be represented based on a drag disk (drag forces derivative is always positive). Besides, this approach can be augmented with a rotating disc of proper mass to reproduce the gyroscopic effects.

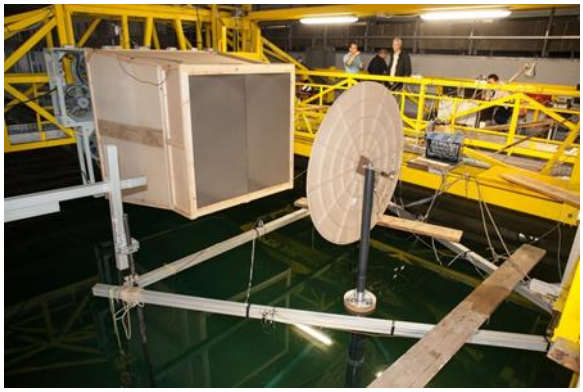

Figure 2-3. Drag disc **(Marinet2, 2020)**.

2.3.4 Approaches in FOWT experimental testing: hybrid testing

The denomination of hybrid testing refers to experiments in which a subpart of the model is not modelled physically in the experimental set-up, but is substituted by a numerical counterpart. This approach is referred to as Hardware in the Loop (HiL) or Software in the Loop (SiL). The numerical subsystem affects the physical one by means of actuators, and is fed by the latter thanks to sensors, that provide some information of the physical model behaviour. The loop is run in real time (Chabaud, Steen, & Skjetne, 2013). During hybrid tests in wave tank facilities the wind turbine loads are obtained by means of real-time synchronized numerical models and the loading is applied by means of an actuator: fans or winches. On the other hand, hybrid tests in wind tunnels reproduce numerically the hydrodynamic behaviour of the floating platform, and force the physical turbine model to follow the simulated platform movements by means a 6 DOFs actuator.

The main advantage of hybrid models in FOWT testing is the decoupling of the physical domains of aerodynamics and hydrodynamics, which, as mentioned before, obeys two different laws and are difficult to reproduce simultaneously. As already stated, it is difficult to reproduce contemporarily Froude and Reynolds scaled phenomena, and proper strategies have to be adopted; moreover, the generation of good quality wind and waves in the same facility is not easy. Is therefore convenient to isolate the two load sources.

Wave tank hybrid testing

In a wave tank setup, the whole hydrodynamic part is reproduced physically, so the floater and the wind turbine are scaled according to Froude laws, allowing correct representations of the wave influence. The aerodynamic part is instead modelled numerically and interacts with the physical subsystem by means of actuators placed in correspondence of the turbine rotor.

Ducted fan: a first solution is the adoption of a ducted fan (Azcona, et al., 2014a). The fan can introduce a variable force that represents the aerodynamic thrust on the rotor. The exerted thrust is determined through a numerical model of the rotor, that, depending on the simulated environmental condition, as well as the wind turbine characteristics, changes the rpm of the fan, controlling the force applied at the tower top to simulate the rotor thrust. The control system of the fan is composed by a brushless motor regulated by an Electronic Speed Controller, feed by an AC/DC power supply. The rotational speed of the motor is regulated with a Pulse Width Modulation signal.

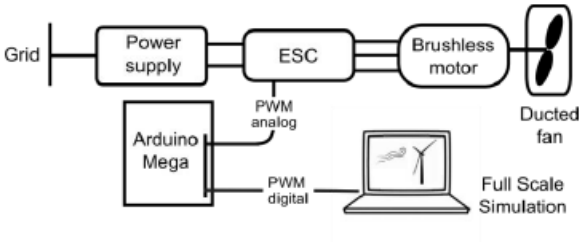

Figure 2-4. Fan control system layout ***(Azcona, et al., 2014b)***.

Figure ***2-5*** describes the integration of SiL inside the physical model. The left part of the scheme represents the numerical substructure, running in full-scale, while the right part represents the physical substructure, realized in model-scale. The input to the numerical model are platform motions (displacements and velocities) and the numerically generated wind field and rotor control operations. The output is the full-scale thrust force, that, once properly scaled, is in turn the input to the fan controller. The fan is then actuated with the proper rpm and provides the computed thrust.

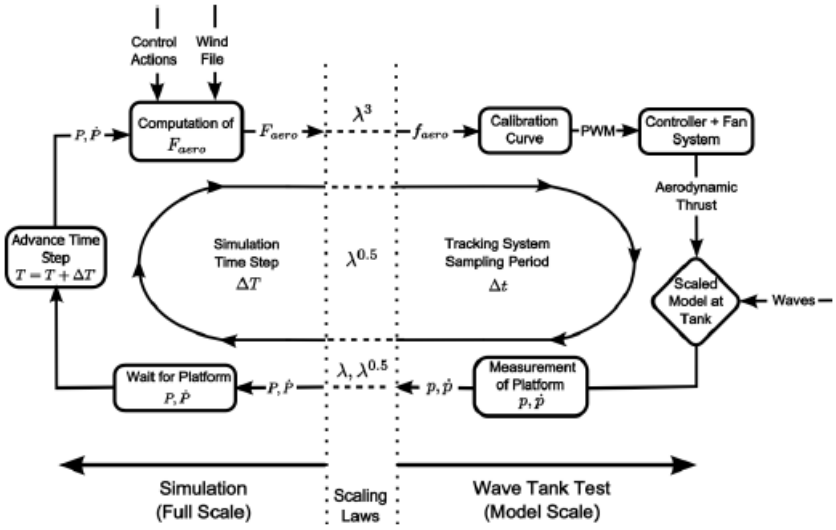

Figure 2-5. Ducted fan SiL integration ***(Azcona, et al., 2014b)***.

The drawback of this technique is that the gyroscopic effects of the rotor and the rotor torque are not reproduced, even if these effects are less important in the overall turbine dynamics.

Winches actuation: a winch system can be used to simulate the aerodynamic loading (Sauder, Chabaud, Thys, Bachynski, & Saether, 2016; Guyedon, Lindeboom, van Kampen, & de Ridder, 2018). The turbine rotor is substituted by a frame where a series of winches are connected and can exert a force trough a system of motors and pulleys. In the setup of (Sauder, Chabaud, Thys, Bachynski, & Saether, 2016) the input to the numerical model were the kinematical data of the physical substructure. Then, based on the wind condition and rotor speed, the force vector exerted by the rotor on the substructure is computed, and mapped into a vector of line tensions that is physically actuated on the model.

In Figure ***2-6*** the red loop represents the inner loop dedicated to the control of the exerted force, and it is running at a higher frequency than the one in blue, that instead collects measurement and compute the load vector to be applied to the frame.

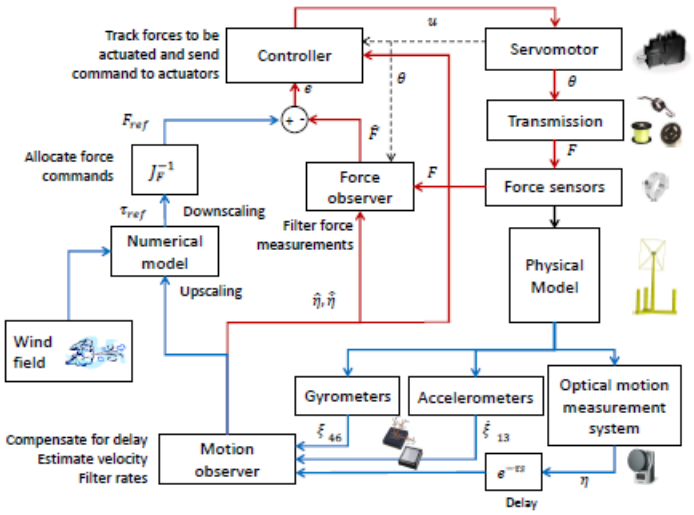

Figure 2-6. The control system scheme of the real time hybrid system in ***(Sauder, Chabaud, Thys, Bachynski, & Saether, 2016)***.

Another example of the winches actuation technique is showed in (Guyedon, Lindeboom, van Kampen, & de Ridder, 2018), where the aim of the work is the comparison of the hybrid system with a completely physical turbine with a rotor scaled for wave tank tests. The experiments show good agreement; deviations in PSD of motions are observed in vertical and sideway direction at 1P frequency, because the winch system is not able to act in these directions. Another limit of winch system is that above a certain frequency the actuation becomes imprecise, leading to deviated results with respect to the scaled model. This demonstrates the importance of correctly evaluate the capabilities of the actuation system.

Multi-fan: another strategy implies the adoption of a multi-fan system (Figure ***2-7***). Figure 2-8 illustrates the basic scheme of the SIL method adopted in (Battistella, Paradinas, M, & G, 2018) to model numerically, in prototype scale, the wind turbine and incoming wind. The movement of the turbine permits the calculation of the relative wind speed seen by the rotor and constitutes the input of the numerical model. Such movements, reduced in three translations and three rotations, are captured by a high definition tracking system (Qualysis), which is able to detect the entity of the six degrees of freedom. The platform positions in subsequent instants are used to calculate the translational and rotational speed of the platform, then, by using the Froude scaling law, the velocity of the rotor is upscaled in prototype scale. The velocity of the rotor completes the set of information necessary to evaluate numerically the forces developed on the rotor. The calculation is carried out by an unsteady Blade Element Momentum (BEM) model, which defines the rotor thrust force and the generator torque. When the data is processed to feed the unsteady BEM the time steps are then upscaled based on the scaling ratio λ. The aerodynamic forces are then scaled back in model scale and sent to the multi-fan to be reproduced at the hub height of the model.

Figure 2-7. An overview of the multi-fan actuator system **(Battistella, Meseguer, & Guanche, 2019)**.

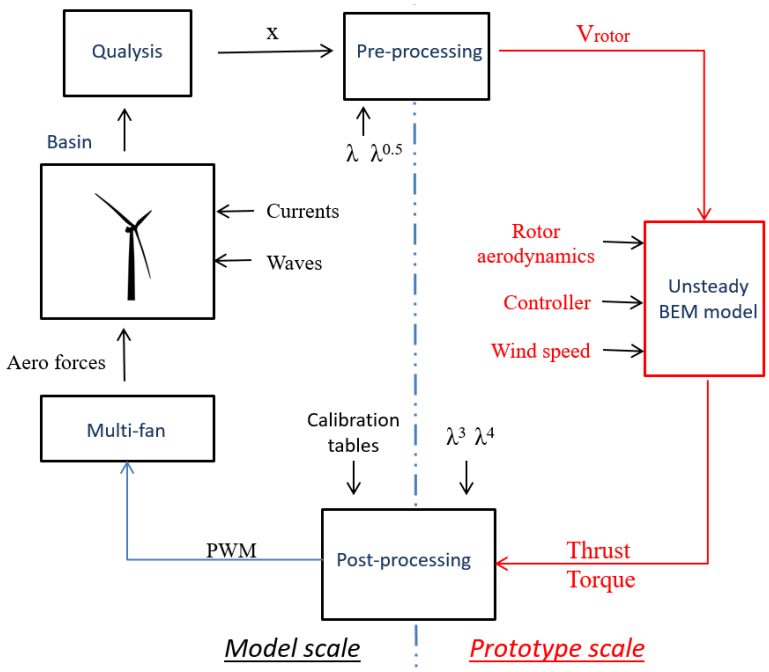

Figure 2-8. Control system of the multi-fan hybrid system in ***(Battistella, Paradinas, M, & G, 2018)***.

The multi-fan consists of up to six fans in which every rotor can be controlled singularly by electro-servomotors (Figure ***2-7***). Each of the propellers produces its own thrust, which generates a force and a momentum capable of reproducing the varied loading of a wind turbine. The number and size of rotors can change so to allow thrust reproduction at different magnitudes; the orientation can be changed to allow the reproduction of aerodynamic torque together with thrust. The agreement of required thrust and effectively simulated thrust is good, with some difficulties of the multi-fan system to track higher frequency oscillations. Moreover, the SIL implemented in (Battistella, Paradinas, M, & G, 2018) does not consider the blades elasticity. Thus, the forces obtained from the BEM do not contain aero-elastic effects. (Meseguer & Guanche, 2019), on the contrary, are capable of solving the Froude-Reynolds scaling conflict using the 6 degree of freedom dynamics of the platform captured in real time as an input in the aero-servo-elastic software. The values are transformed into full-scale positions

and angles to compute the full scale loads in the software. The loads are then scaled to the test model and replicated in the system by means of the multi-fan (Figure ***2-9***).

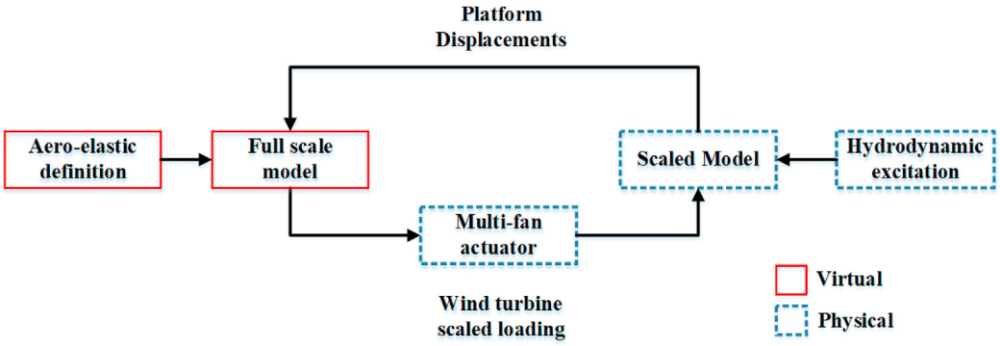

Figure 2-9. HiL scheme implementation **(Meseguer & Guanche, 2019)**.

The SIL of (Meseguer & Guanche, 2019) includes a series of calculations which need to be computed according to the time-scale Froude laws. The challenge of optimizing the computational time when using complex codes, such as aero-servo-elastic to obtain the turbine loading, is solved with a parallel software architecture governing the multi-fan. The multi-threaded architecture permits the parallelization of the different processes, avoiding sequential action and improving the overall response time of the actuator. An overview of the hardware in the loop control scheme is shown in Figure ***2-10***. One thread is dedicated to acquiring data from the platform motion acquisition system. The full-scale computation and load scaling are handled by a second thread. The aero-elastic computation is done when a new value of the tracking system is acquired. The signal processing is also calculated in this thread. The software architecture permits the integration of different methods to calculate the wind turbine load from steady loading to complex dynamics, derived from the turbine controller platform interaction. A third thread is dedicated to shutting down the multi-fan when the test temporization, governed by Froude scale time laws, has not been accomplished, ensuring the detection of anomalous events.

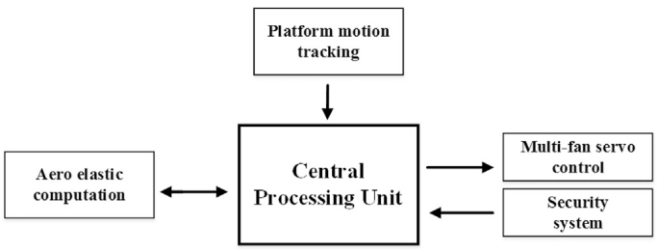

Figure 2-10. Representation of parallel multi-fan architecture implementation **(Meseguer & Guanche, 2019)**.

Wind tunnel hybrid testing

Floating wind turbines hybrid testing has been adopted also in wind tunnel facilities. In this circumstance the turbine aerodynamics are entirely reproduced thanks to the adoption of an appropriate scaling law and the capacity to reproduce high quality winds. On the other hand, the hydrodynamic forcing and the resulting floater motions must be reproduced with a mechanical actuator. In (Bayati, Facchinetti, Fontanella, Taruffi, & Belloli, 2020) a scaled wind turbine model provides rotor and aerodynamic loads, then the forces measured at the tower base are treated as input to a numerical model of the floating platform, together with numerically computed hydrodynamic loads. The resulting motions are imposed to the wind turbine model. The actuation can be made in a reduced number of DOFs, like only surge and pitch, or in all the 6 DOFs. The length scale of the wind turbine

is set so that blockage effects are limited, and, at the same time, avoiding excessive miniaturization of components, while the velocity scale is set to obtain appropriate Reynolds numbers. In the wind tunnel-HIL setup of (Bayati, Facchinetti, Fontanella, Giberti, & Belloli, 2018) the aerodynamic loads coming from the wind turbines are the only ones obtained by the physical simulation. Gravitational loads are computed numerically, because the non- unity of acceleration scale makes impossible to reproduce gravitational restoring, and also inertial loads are modelled by the numerical subsystem, given the difficulty to correctly scale the wind turbine mass. The hydrodynamic loads, hydrostatics, the gravitational restoring of the platform are instead computed numerically as function of the platform state and of the incident wave. The numerical and physical model are joined by a 6 DOF parallel kinematic machine. The main advantage of this approach is that it does not involve a scaled platform model, a possible source of uncertainties, and is applicable to a wide range of platforms. Drawback is the difficulty to run in real time the complete floater model, comprising mooring lines. This is why some simplification must be made to the hydrodynamic model to allow speed of calculations, especially in hydrostatics and in mooring lines dynamics.

2.3.5 Issues in hybrid testing

Hybrid testing requires a setup more complex than the one used for fully physical experiments, and it is subjected to peculiar systematic issues. An extensive explanation is given in (Sauder, Chabaud, Thys, Bachynski, & Saether, 2016) and in reference herein in the article. First of all the numerical substructure is constrained by real time requirements. This means that usually the numerical models must be simplified in order to be able to deliver results inside a time step suitable for the correct reproduction of the experiment. In wave tank hybrid tests this means for example to neglect or limit the calculation of the blade flexibility; in wind tunnel tests is the hydrodynamic interaction of the floater that must be simplified, or the influence of mooring lines. The simplifications to the numerical model or its intrinsic inaccuracy are the first source of errors. This depends then on the degree of fidelity of the adopted numerical model.

Another source of errors are the delays in the input of signals needed by the numerical substructure. The delay in input can be quantified depending on the instrument and measurement chain used, but its effects are difficult to analyse in a comprehensive manner. Moreover, the control system of the actuators is based on the parameters of the physical subsystem being actuated. If these parameters are incorrect, then the control system will not respect the performances needed. After that there are also unstructured uncertainties, that comprise unmodelled dynamics, vibrations, random time delays, varying actuator performances.

2.4 Truncation methods

The hybrid model testing technique can also refer to a combination of experiments and numerical simulations (Stansberg, Ormberg, & Oritsland, 2002). For example it is consider as hybrid model testing the technique that involve (separately) both numerical and experimental activities to design an equivalent truncated mooring system. This technique involves the following tasks: analytical design of a truncated model, model testing using the truncated model, and numerical reconstruction and extrapolation. In order to cope with scalability problem associated with the scaled mooring size, an equivalently passive truncated mooring system can be designed to substitute the full-depth mooring system. The results acquired by the experiments provide the response behaviour including the truncated mooring system. To acquire the responses with the full-depth mooring system, numerical reconstruction and extrapolation should be performed. Numerical coupled analysis on truncated and full-depth models is called numerical reconstruction and extrapolation, respectively. In numerical reconstruction, numerical simulations are performed with the truncated mooring system and the results are compared with the experimental results. Hydrodynamic coefficients such as the damping coefficients are adjusted to make the numerical results fit the experimental results. Finally, numerical extrapolation is performed. In this stage, numerical simulations using the full-depth mooring system are performed with the hydrodynamic coefficients acquired from the numerical reconstruction. The responses of the full-depth system

are then obtained. (Ormberg, Stansberg, Yttervik, & Kleiven, 1999) carried out the model test for a semi-submersible operated both in 335 m full water depth and 116.5 m truncated water depth. The numerical extrapolation of the model test results of truncated water depth to full water depth, were in good agreement with full water depth model test results. (Baarholm, Fylling, Stansberg, & Oritsland, 2006), and (Zhang, Sun, Yang, & Gao, 2009) also carried out hybrid model testing and confirmed the feasibility of the method. The passive hybrid model tests proposed has been regarded as the most reliable method (Stansberg, Karlsen, Ward, Wichers, & Irani, 2004). The difficulty lies in designing the truncated depth system to match the consistency of characteristics of the full depth one (Wang, Luo, Hu, & Li, 2010).

2.4.1 Quasi-static models

Since the equivalent water depth truncated mooring system affects the hybrid model test results directly, researchers have developed several methods to design truncated models automatically and efficiently. (Zhang, Gao, Wang, Jiang, & Zhao, 2012) presented an optimization method to design a moored Floating Production Storage and Offloading (FPSO) system which works at a water depth of 320 m to the truncated water depth of 80 m (the truncation factor was 4). They used an Improved Non-dominated Sorting Genetic Algorithm (INSGA-II), striving to match both the motions responses of the floater and the physical properties of the mooring system considering mainly the static characteristics. (Zhang, Huang, & Guan, 2014) proposed the baton pattern-simulated annealing algorithm for hybrid discrete variables to optimize the static response of a single catenary and the whole catenary system static response in one direction, in order to truncate a turret mooring FPSO from 304 m to 76 m water depth. (Molins, Trubat, Gironella, & Campos, 2015) proposed an optimisation method, using the GlobalSearch Algorithm in Matlab, for designing a truncated catenary mooring system to emulate the real mooring system of the monolithic concrete spar platform WindCrete for a 5 MW wind turbine. The optimization process was focused on adjusting the quasi-static behaviour of the scaled mooring system, and a constant force on the nacelle was used to simulate the wind load.

(Waals & VanDijk, 2004) developed an empirical method to optimize truncated mooring system, assuming that the most important behaviour to model is the wave frequency and low frequency motion of the floater. The truncation strategy consisted in an initial truncation design based on the water depth ratio, optimised in two separate iterative processes: quasi-static response by adjusting length (L), axial stiffness (EA) and submerged weight (W) of the truncated mooring lines; and dynamic response by adjusting mass (M) and diameter (D) of the truncated mooring lines. The truncation factor for the total length of mooring lines considers all the water depth (H) below the fairlead point:

$$\gamma = \frac{H_t}{H_o} = \frac{L_t}{L_o} \tag{14}$$

Nevertheless, the initial truncation design keeps the catenary effects of the bottom section and the top section unchanged. The length reduction for the equivalent mooring lines is obtained by using a truncation factor for the mid-section only:

$$\mu = \frac{L_{m,t}}{L_{m,o}} = \frac{EA_{m,t}}{EA_{m,o}} = \frac{W_{m,o}}{W_{m,t}} = \frac{M_{m,o}}{M_{m,t}} = \frac{{D_{m,o}}^2}{{D_{m,t}}^2} \tag{15}$$

The iterative process of the static load optimisation begins computing the static load curves of the full depth system and the initial truncation design. For a catenary moored system, the system stiffness ($K = EA/L$) of the

region closed to the seabed (region 1) is dominated by the catenary effect, while the submerged weight of the mooring line determines the shape in the equilibrium position:

$$F_W = \frac{K_{1,t}}{K_{1,o}} \quad (16)$$

As the mooring line is lifted to become taut (region 2), the elasticity dominates the system stiffness:

$$F_{EA} = \frac{K_{2,t}}{K_{2,o}} \quad (17)$$

For taut mooring systems, the catenary effect is negligible and F_{EA} is the only factor to adjust. The location of the transition point between these two regions is dominated by the length of the bottom section, whose factor is obtained from the average offset of the parallel mooring lines in region 2 for the full depth and the truncated system according to:

$$F_{L_b} = \frac{\text{offset}_o}{\text{offset}_t} \quad (18)$$

The static load curve of the truncated mooring system for next iteration steps is generated by adjusting the properties as follows:

$$\begin{cases} W_{m,t_{i+1}} = F_W * W_{m,t_i} \\ M_{m,t_{i+1}} = F_W * M_{m,t_i} \\ D_{m,t_{i+1}} = \sqrt{F_W} * D_{m,t_i} \\ EA_{m,t_{i+1}} = F_{EA} * EA_{m,t_i} \\ L_{b,t_{i+1}} = F_{L_b} * L_{b,t_i} \end{cases} \quad (19)$$

2.4.2 Dynamic models

The resulting parameters of the static load optimisation in truncation procedures leads to underestimation of dynamic response because of the shorter mooring lines. The iterative process of the dynamic load optimisation is computed in fully coupled time domain simulations, by applying a set of forced oscillations (or alternatively simulations in waves). Increasing the mass leads to larger dynamic response. However, the diameter may be adjusted to keep the required submerged weight, and thus not to affect the quasi-static behaviour of the system.

The horizontal mooring-induced hydrodynamic damping of the full depth system will be underestimated when the segment diameters are the same (Xu & Ji, 2014). The insufficient horizontal hydrodynamic damping of the truncated mooring systems would induce large discrepancies of the platform motion responses, then the wave frequency dynamics of the mooring line will be underestimated, and the low frequency component will be overestimated at the same time. However, to enlarge the diameters of truncated mooring lines is an efficient way to solve this problem. The similitude of the horizontal damping of the mooring system and mooring line dynamics can be achieved when the diameters come to appropriate values. In order to achieve the static, but also the dynamic similarities, (Ji & Xu, 2014) proposed an optimization design method to conduct model tests of a deep water semi-submersible system with a truncation factor of 7.5. The experimental dynamic responses of

the platform and the mooring lines were compared with the numerical simulation based on the full-time domain coupled dynamic analysis method, showing a good agreement both in full time domain and spectral analysis.

(Jung, Kim, Cho, Hwang, & Sung, 2015) modelled the top and bottom parts of the mooring line with a chain and the predominant middle section with polyester, with an axial stiffness 5 times lower. During the initial truncation process, the lengths of the top and bottom chain were fixed, and only the length of the polyester wire was altered to set the pretension of a single truncated mooring line to match the pretension of the full-depth model. Then, the full truncated mooring system of a FPSO vessel model was constructed using OrcaFlex. The software permitted to analyse both the static and dynamic characteristics based on the time domain. The iterative process of the static load consists in a static pull-out test in which the restoring force was measured while the vessel was pulled over the range of the surge distance. The iterative process used to define the dynamic loading consists in a free-decay test which was conducted by releasing the FPSO vessel from the surge offset and tracking the corresponding vessel's motion in the x direction. The natural period and the damping were then obtained.

Aiming to have a dynamic similarity of the mooring lines and platform between truncated and full-depth mooring systems, (Ferreira, Lages, Afonso, & Lyra, 2016) employed a nonlinear least-squares method for adjusting the design variables. For hydrodynamic analysis through simulations of regular (or irregular) wave tests in time domain, they used a computational program called Dynasim. The design optimization performed to adjust the design variables (mass and diameter of the truncated mooring system) consisted in minimizing the quadratic difference between truncated and full-depth mooring systems, through a weighting objective function. The objective function considers the time series of the restoring force, as well as the motion series in surge, sway, heave and rotation series in roll, pitch and yaw. The resulting equation is the following:

$$f(x) = v\sum_{i=1}^{N}[R_i(x)]^2 + \sum_{j=1}^{6}\left[w\sum_{i=1}^{N}[M_{ij}(x)]^2\right] \qquad (\textbf{\textit{20}})$$

where $R_i(x)$ represents the residual of restoring force normalized by maximum restoring force in the full-depth system. $M_{ij}(x)$ represents the residual of the vessel movements normalized by maximum movement in the full-depth system of the j-th degree of freedom. v and w are the weighting parameters for the restoring force and for motion of the vessel in the j−th degree of freedom, respectively.

Mooring induced damping has significant influence on the horizontal low frequency motions of floating Oil & Gas structures caused by irregular waves. (Fan, Qiao, & Ou, 2012) proposed an optimization model that accounts for the mooring-induced damping generated by the transverse motion of the mooring line due to the low-frequency surge oscillation using a Genetic Algorithm (GA). (Fan, Qiao, & Ou, 2014) used this new method to design the truncated mooring system based on the damping equivalence, in which the mooring damping was calculated by the quasi-static method and the dissipation energy model. The objective function was created with weighted damping forces at different frequencies, and also with the tension force. (Fan, Qiao, Yan, Chen, & Ou, 2017) presented the equivalent design of passive truncated mooring system considering mooring damping equivalence, which in turn reflects into the dynamic characteristics. Thus, the authors effectively reproduced both the static and dynamic characteristics of the full depth mooring system, estimating mooring line damping with an improved quasi-static model considering normal drag forces, tangential drag forces and seabed friction.

(Kang, Zhang, & Sun, 2017) proposed a truncation design for an FPSO, an oil offloading line, and its shuttle tanker. The FPSO was deployed with a spread mooring system, while the shuttle tanker was moored with a single-point mooring system. The passive hybrid truncation method was adopted to make the model test design. The model test results show equivalent static restoring forces. To meet both static and dynamic equivalences for truncation

design, (Ma, Wang, Sun, & Jiang, 2018) made a dynamic truncation for a FPSO with a multi-objective optimization method based on static equivalence for each line. The optimisation algorithm NSGA-II was combined with the slender rod model to optimise the mooring line parameters in the static and dynamic analysis of the truncated system. The mooring forces in the time domain were transferred into the frequency responses for further optimisation, and a coupled dynamic analysis was used to verify the dynamic similarity. (Ma, Zhong, Wang, Kang, & Sun, 2019) validated a single catenary mooring line and a semi-submersible platform mooring system. The new objective function was applied in the dynamic mooring truncation method called DyTrunMoor, by using the multi-objective optimization algorithm NSGA-II and the slender rod model for the static and dynamic similarity. The fitness function for the optimization was constructed with tension amplitudes transformed from time domain. The relationships of wet mass, resultant area and diameter were set up with the following formulas:

$$w = M - \rho A \tag{21}$$

$$A = \frac{\pi D^2}{4} \tag{22}$$

in which, A is the resultant area acting for the inertial force and buoyance force, D is the resultant diameter acting for the drag force.

(Wei, Xiao, Tian, & Kou, Four-level screening method for multi-variable truncation design of deepwater mooring system, 2017) proposed a four-level screening method for designing passive truncated systems. Thus, the high-dimensional objectives were divided into four parts which are optimized successively in four levels by traditional Evolutionary Multi-objective Optimisation (EMO) methods. The four levels of the screening method for multi-variate truncation design were: (1) Initial constraints for each mooring line, (2) Static equivalence of each mooring line using methods such as Non-dominated Sorting Genetic Algorithm (NSGA-II), (3) Static equivalence of the complete mooring system, and (4) Dynamic equivalence of the complete mooring system. The four-level screening method was proved to be effective in designing an asymmetrically truncated system (Wei, Xiao, Tian, & Feng, 2018).

To our knowledge, there are no works entirely devoted to the study of the design of an equivalently passive truncated mooring system for floating offshore wind turbine including the effect of the wind loads on the dynamic response.

3 ADVANCED HIL DEVELOPMENT FOR TURBINE DYNAMICS INTEGRATION: CONTROL SYSTEM

3.1 Methodologies for wind tunnel HIL scale-model experiments

The PoliMi hybrid modelling approach entails replacing the hydrodynamic portion of the scale model test with a numerical simulation that is run in parallel with the actual experiment. The coupling between the physical scale model of the wind turbine and the numerical simulation is provided by real-time measurements and an actuation system.

The hardware-in-the-loop setup is shown in Figure ***3-1***. The floating wind turbine is split into two portions in correspondence of the wind turbine tower-platform interface. One portion consists of the wind turbine and it is governed by the aerodynamic forces, whereas the other is essentially the floating platform and the mooring system and it is governed by gravity and hydrodynamic forces. The wind turbine subsystem is emulated by means of a physical scale model and the wind environment is recreated inside the atmospheric boundary layer test section of the wind tunnel. The rigid-body motion of the floating structure is applied to the wind turbine scale model with an actuation system, controlled by a numerical simulation of the floating platform. The numerical simulation is continuously updated with the real-time measurement of the wind turbine tower-base forces.

Figure 3-1. The hardware-in-the-loop system for wind tunnel hybrid experiments about floating offshore wind turbines.

A scheme of the control strategy on which the hardware-in-the-loop experiment is based is proposed in Figure ***3-2***. The wind turbine scale model is immersed in the scaled wind field recreated inside the wind tunnel and is regulated by a dedicated controller that provides the collective pitch angle β and generator torque Q_G settings.

Tower-base loads $\underline{F}_{RUAG}$ are continuously measured by means of a 6-components load cell. The force input $\underline{F}_{wt}$ to the numerical model is obtained depriving the tower-base loads of the inertia and weight components associated with the wind turbine model:

$$\underline{\mathrm{F}}_{\mathrm{wt}} = \underline{\mathrm{F}}_{\mathrm{RUAG}} - \underline{\mathrm{F}}_{\mathrm{corr}} \quad (\boldsymbol{23})$$

where $\underline{F}_{corr}$ is the wind turbine model inertia and weight. The wind turbine loads $\underline{F}_{wt}$ obtained from Equation 23 correspond to the aerodynamic loads of the rotor and tower and the rotor gyroscopic moments. The simulation of the wind turbine inertia and weight relies entirely on the numerical model.

The $\underline{F}_{corr}$ term of Equation 23 is computed in real-time based on a linear approximation of the system kinematics (i.e. the assumption of small rotations is assumed valid) as:

$$\underline{\mathrm{F}}_{\mathrm{corr}} = [\mathrm{M}]_{\mathrm{t}}\underline{\ddot{\mathrm{q}}}_{\mathrm{a}} + [\mathrm{K}]_{\mathrm{t}}\underline{\mathrm{q}}_{\mathrm{a}} \quad (\boldsymbol{24})$$

where $[M]_t$ and $[K]_t$ are the 6-by-6 wind turbine model mass and gravitational stiffness matrices for the rigid-body platform DOFs and $\underline{q}_a$ is the rigid-body motion of the wind turbine model. The actual value $\underline{q}_a$ is used in place of the command $\underline{q}$ to minimize the effects of actuation delays.

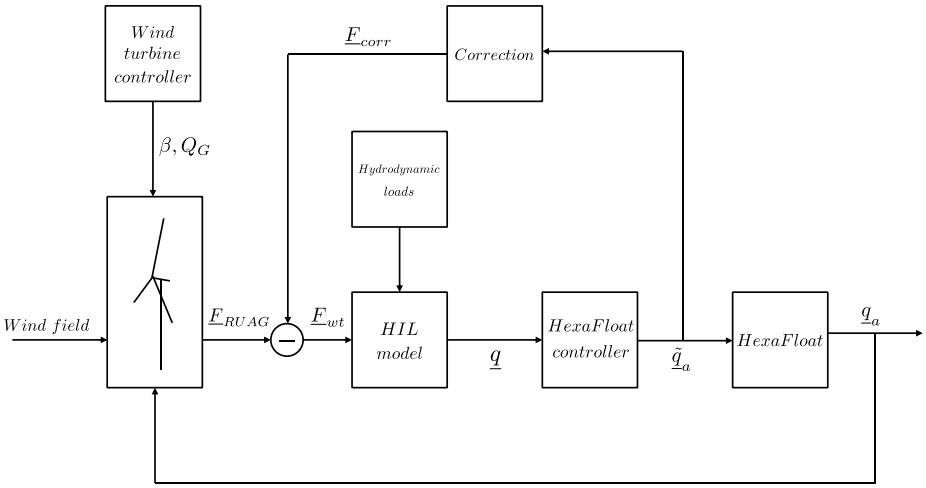

Figure 3-2. Schematic of the control strategy of the wind tunnel hardware-in-the-loop system.

3.1.1 Scaling

The parameters for the hybrid wind tunnel experiment are obtained from scaling the corresponding parameters of the full-scale system. To this purpose, a coherent set of scale factors is required, where the scale factor is defined as the ratio between a given quantity evaluated for the scaled and full-scale systems. The length and velocity scale factors have to be defined first, then the scale factors for all the quantities of interest are obtained by means of dimensional analysis as reported in Table ***3-1***.

Table 3-1. Scale factors for a hybrid wind tunnel experiment about a 10MW floating wind turbine.

Scale factor	Expression	Value
Length	λ_L	1/75
Velocity	λ_v	1/3
Mass	$\lambda_M = \lambda_L^3$	$1/75^3$
Time	$\lambda_T = \lambda_L/\lambda_v$	1/25
Frequency	$\lambda_\omega = \lambda_v/\lambda_L$	25
Acceleration	$\lambda_a = \lambda_v/\lambda_T$	25/3
Force	$\lambda_f = \lambda_a\lambda_M$	1/50625
Reynolds	$\lambda_{Re} = \lambda_v\lambda_L$	1/225
Froude	$\lambda_{Fr} = \lambda_v/\sqrt{\lambda_L}$	$\sqrt{75}/3$

The scaling can be set arbitrarily in a numerical simulation and this key concept is the base for hybrid experiments since it allows to avoid the Froude-Reynolds scaling incompatibility. In the wind tunnel hybrid methodology, the length and velocity scale factors can be set independently, disregarding of Froude similitude whereas this is off course not feasible in conventional wave tank experiments.

When Froude similitude is adopted, the set of scale factors is obtained fixing the same Froude number for the full-scale and scaled systems:

$$\mathrm{Fr} = \mathrm{U}^2/\mathrm{gL} \tag{25}$$

where U is a velocity, g the gravity constant and L a length.

Froude number similitude results into the velocity scale factor λ_v being constrained to the length scale factor λ_L by:

$$\lambda_\mathrm{v} = \sqrt{\lambda_\mathrm{L}} \tag{26}$$

Similarly, Reynolds similitude would require having the same Reynolds number for the full-scale and the scaled system:

$$\mathrm{Re} = \rho\mathrm{UL}/\mu \tag{27}$$

where ρ and μ are the fluid density and dynamic viscosity, U a velocity and L a length. Reynolds similitude also results into a velocity scale factor function of the length scale factor:

$$\lambda_\mathrm{v} = 1/\lambda_\mathrm{L} \tag{28}$$

It is evident that Froude and Reynolds similitude are mutually exclusive.

This is illustrated by means of a numerical example in Figure ***3-3***. The figure shows the Reynolds number reduction attained for different arbitrary combinations of length and velocity reduction factors (the reduction factors in the figure are defined as the inverse of the scale factors used in the equations above). Length reduction factors between 50 and 100 are required to fit a multi-megawatt wind turbine in a common test facility. If Froude similitude is adopted the velocity reduction factor is set according to Equation 26 (red solid line) and it would be between 7 and 10, leading to a Reynolds number between 350 and 1000 times lower than at full-scale. When the wind tunnel hybrid methodology is adopted, the length and velocity scale factors can be set independency one from the other and this is exploited to achieve a higher Reynolds number for the wind turbine scale model and improve the emulation of the wind turbine aerodynamics.

This is further exemplified for a hybrid scale model experiment about a 10MW floating wind turbine that was carried out at PoliMi wind tunnel. In particular, the length reduction factor is fixed equal to 75 to limit the wind tunnel blockage and avoid at the same time an excessive small size of the wind turbine scale model components. The velocity reduction factor was instead set to 3 by comparing the wind speed operating range of the wind turbine with the maximum wind speed that can be achieved inside the wind tunnel. This combination of length and velocity scales is marked by the yellow circle and gives a Reynolds number that is 225 times lower than at full-scale. If a conventional wave tank experiment is carried out based on a scale model of the same size, the velocity reduction factor is around 9 (intersection between the solid red and dashed black lines) and the Reynolds number is 650 times lower than at full-scale.

The Reynolds number achieved in the wind tunnel hybrid experiment is higher compared to a conventional wave tank experiment and this results in a greater fidelity in the modeling of wind turbine aerodynamics.

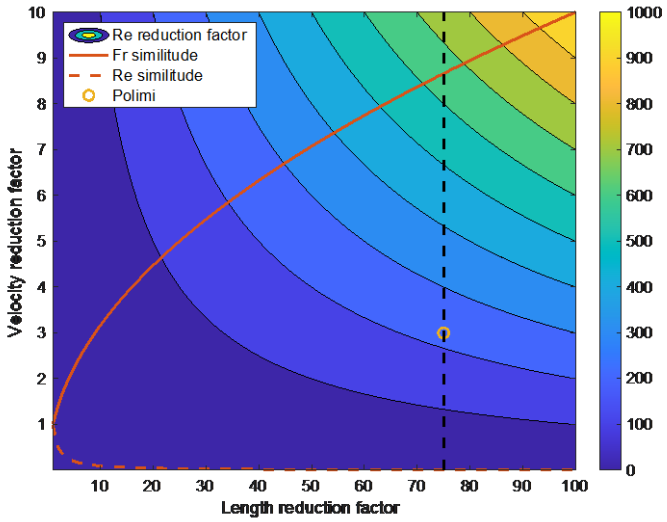

Figure 3-3. The figure shows the Reynolds number reduction attained for different combinations of length and velocity reduction factors. The scaling adopted in the PoliMi HIL simulator is compared with Froude-number similitude for a 10MW floating wind turbine case. As seen, for the same length reduction factor, a Froude-scaled model would experience a Reynolds number approximately three times as lower as in the case of wind tunnel HIL.

3.1.2 Reduced-order model for the HIL simulation

The numerical simulation of the floating platform is based on a reduced-order model that describes the rigid-body (surge, sway, heave, roll, pitch and yaw) $\underline{q}$ motion of the floating wind turbine. The numerical model is based on the equations of motions for the 6-DOFs:

$$([\mathrm{M}]_s + [\mathrm{A}]_\infty)\ddot{\underline{q}} + [\mathrm{R}]_s\dot{\underline{q}} + [\mathrm{K}]_s\underline{q} = \underline{F}_{\mathrm{plat}} + \underline{F}_{\mathrm{wt}} \quad (\textbf{29})$$

where $[M]_s$ is the mass matrix of the floating system (platform and wind turbine) about the rigid-body DOFs, $[A]_\infty$ is the infinite-frequency added mass matrix, $[R]_s$ is a linear damping matrix that is adopted in the model to optionally introduce additional damping in the system (e.g. to match experimental data from wave tank experiments), $[K]_s$ is the floating system gravitational and stiffness matrix. The external loads on the right-hand side of Equation 29 are the sum of platform loads $\underline{F}_{plat}$ and wind turbine loads $\underline{F}_{wt}$. All the quantities in Equation 29 are defined at model scale.

Floating platform loads are the sum of four contributions:

$$\underline{F}_{\mathrm{plat}} = \underline{F}_{\mathrm{rad}}\left(\dot{\underline{q}}\right) + \underline{F}_{\mathrm{we}}(t) + \underline{F}_{\mathrm{visc}}\left(\dot{\underline{q}}, t\right) + \underline{F}_{\mathrm{moor}}\left(\underline{q}, \dot{\underline{q}}\right) \quad (\textbf{30})$$

In order to cope with real-time execution constraints, radiation loads, $\underline{F}_{rad}$, modelling the memory effect, are not implemented by direct calculation of a convolution integral but exploiting a state-space approximation. $\underline{F}_{we}$ are the first- and second-order wave excitation loads, $\underline{F}_{visc}$ the viscous loads and $\underline{F}_{moor}$ the loads exerted by the mooring system onto the floating platform.

Mooring system

The mooring system dynamics are implemented by means of a lumped-mass model. The model is integrated in parallel with the model of the floating structure and it keeps into account the mooring stiffness, inertia, damping, weight, buoyancy, seabed forces and hydrodynamic drag. Bending and torsional stiffness are neglected as well as seabed friction forces. The real-time integration of a mooring system model was preferred to the use of pre-defined look-up tables (i.e. force-displacement data) that would require deploying multidimensional arrays on the HIL real-time controller. Moreover, the integration of a complete mooring line model allows to take into account the velocity-dependent components of mooring line loads, like linear and quadratic damping forces.

Model optimization for real-time implementation

The floating platform model is optimized with respect to the computational effort required to be run in parallel with the physical part of the experiment. The number of computations executed in real-time has been reduced as a compromise between physical consistency of the model output and computational requirements. The main issues that were considered are:

- the number of harmonic components in the irregular wave spectrum. The maximum frequency up to which the spectrum is defined, and its frequency resolution have a significant impact on the effort for simulating wave loads. The frequency resolution is fixed to 0.02 rad/s (full scale) and the upper cut-off frequency after which the spectrum is zeroed to 3.3 rad/s (full scale). Above this frequency the typical JONSWAP spectrum is almost negligible in amplitude;
- the number of elements in the platform members for the calculation of viscous forces. The element size was adapted based on the vertical distance from the mean sea level. Bigger elements are used in the lower part of the platform where the gradient of the wave particle velocity is lower;
- the number of nodes in the mooring lines model. This is lower than what is used in common simulation codes and it is chosen as the best compromise between simulating the mooring line response with good fidelity and low computational effort.

Thanks to these approximations, the model can be integrated in real-time by means of a fourth order Runge–Kutta method and a fixed time step of 0.015 s (model scale) on a 3.0 GHz CPU. This integration time step is upperly bounded on account of the mooring lines dynamics.

3.2 Methodologies for wave tank HIL scale-model experiments

3.2.1 Scaling

The main goal of the wave tank physical modelling is to evaluate the hydrodynamics and fluid-structure interaction processes which govern the behaviour of a marine system. To reproduce with fidelity the main physical phenomena involved on wave-structure interaction, the scaling law has to respect the constant ratio between the gravitational and inertial forces at laboratory and prototype scale. The dominant forces over the platform are dominated by gravity waves, so a correct representation of the hydrodynamic loads can be obtained by fixing the Froude number. Therefore, the quantities defined in the laboratory environment are set such that the Froude number remains constant at both scales.

The best scale factor for a physical model study usually comes from the balance between working at a large scale, which minimizes scale effects and comply with the test facility constraints, such as basin dimensions or wave generation limits. Larger models provide more accurate tests of wave-structure interactions and therefore more reliable results. The consideration of the geometry of the structure, the target water depth, the environmental conditions selected and the size of basin facilities, brings then to the most suitable scale factor λ.

The quantities reproduced and measured in the physical test layout are all scaled down following the Froude's laws. Their translation to prototype scale are obtained multiplying the measured value in model scale with the scaling factor that corresponds to each of them. Table ***3-2*** depicts the Froude scale relations for different entities. The table assumes that the ratio between salt and fresh water is equal to 1.025 t/m^3.

Table 3-2. Froude scaling laws of similitude.

Magnitude	Ratio
Geometry	λ
Time	$\sqrt{\lambda}$
Velocity	$\sqrt{\lambda}$
Acceleration	1
Angular velocity	$1/\sqrt{\lambda}$
Angular acceleration	$1/\lambda$
Angle	1
Mass	$1.025 \cdot \lambda^3$
Force	$1.025 \cdot \lambda^3$
Pressure	$1.025 \cdot \lambda$
Reynolds Number	$\lambda^{1.5}$

The reduced Reynolds number is unavoidable, because coupled testing requires adherence to a consistent scaling scheme, and differing time exponents make Froude and Reynold scaling laws incompatible with each other (Muller, et al., 2014). In floating structure tests, the reduced Reynolds number with an exponent of 1.5 under Froude scaling is usually acceptable because the sensitivity of hydrodynamics to the increased viscous forces is often small. However, as explained in previous paragraphs, testing floating wind turbines presents a challenge to the Froude scaling approach because its aerodynamics are very sensitive to the viscous forces that

begin to dominate at small scales. Thus, the reduced Re number may cause severe reductions in wind turbine performance coefficients (Martin, Kimball, Viselli, & Goupee, 2014).

3.2.2 Wave tank tests HIL method integrating a multi-fan system

The problems related to the scalability of the aerodynamic loads in wave tank test has been tackled with different strategies. Some of them plan to reproduce the turbine scale model by modifying the blades geometry, allowing to compensate for the aerodynamic loads deficit provoked by the low Reynolds number. Others, as already mentioned, are based on hybrid methods which simulate in real time the turbine aerodynamics, reproducing them on the scaled model in parallel with the test execution. Such technique is known as ReaTHM (Real Time Hybrid Model) testing and implies the implementation of HIL (Hardware in the Loop) strategies. The main aspect that differentiate the HIL strategies developed in the last decade relates to the actuator used in to reproduce the aerodynamic forces in the scaled model. This paragraph presents the solution developed at IH Cantabria, which is going to be employed during the test campaign planned in the COREWIND project. This solution makes use of an array of fans located at the model tower top and permits to reproduce the rotor thrust force and other aerodynamic effects relevant for the purposes of wave tank tests. Such actuator is known as multi-fan system.

The multi-fan system (Figure ***3-4***) is formed by an array of fans able to generate with fidelity the aerodynamics simulated numerically in real time.

Figure 3-4. The multi-fan system at the Cantabria Coastal and Ocean Basin **(Battistella, Meseguer, & Guanche, 2019)**.

The device is controlled by a software that regulates the 6 motors independently, reproducing the desired thrust at the hub of the wind turbine model. This setup allows to simulate a wide range of load cases: constant or turbulent wind speed, gust, grid failures, pitch or torque controller failure, among others.

As anticipated, the HIL is run in real time, considering the position and displacement of the platform. In fact, the thrust magnitude is determined at each time step by considering the wind velocity seen by the blades, the aerodynamic characteristics of the rotor and the controller strategy. This is done by means of an Unsteady BEM code.

The aerodynamic loads developed on the turbine rotor were defined numerically by FAST (NREL), whose aerodynamic module (Aerodyn) is based on the Blade Element Momentum method. This tool determines the rotor aerodynamics based on the following information:

- Platform movement: Tracked and passed to the aerodynamic module by Qualisys, a high accuracy tracking motion system based on visual sensors.
- Rotor aerodynamics: Defined based on the geometrical and aerodynamic characteristics of the airfoil mounted on the blades. Such information is provided to the aerodynamic module in each point of the rotor discretization.
- Inflow wind data: The simulated wind is passed to the aerodynamic module by means Full-field input files. Such data is provided in binary format and is based on the coherence models indicated on the IEC standards.
- Controller strategy: The effects of the controller operations on the Thrust forces are considered by the aerodynamic model as it can be interfaced with Servodyn, a dedicated module.

3.3 Definition and analysis of the uncertainties in HIL scale-model experiments

Firstly, we describe the reference floating offshore wind turbines and the reference numerical model used in this project as a preamble to explain our methodology within this context. Then, the second part of this chapter will illustrate the methodology developed in the COREWIND project, to identify, quantify, and propagate the uncertainties expected in hybrid model testing of FOWTs, to the results obtainable during such kind of tests.

3.3.1 Description of the reference Floating Offshore Wind Turbines: Spar and Semi-submersible

This project introduces two new floating platform configurations, both supporting the IEA Wind 15 MW reference wind turbine (Bredmose, y otros, 2019). The two concrete-based floater concepts are a spar (*WindCrete*) and a semi-submersible (*ActiveFloat*), installed in three sites with different water depths and environmental conditions. The IEA Wind 15MW reference wind turbine is an offshore turbine on a monopile structure. Its main features are summarized in Table ***3-3*** and its main performance is shown in Figure ***3-5***. The tower of the turbine will be adapted for each floater design. Therefore, the tower height, tower thickness and tower mass are different for each model.

Table 3-3. Characteristics of the IEA Wind 15MW reference wind turbine (Bredmose, y otros, 2019).

Rated output power	15 MW
Turbine class	IEC Class 1B
Rotor diameter	240 m
Hub diameter	6 m
Rotor-nacelle assembly mass	1017 t
Blade mass	65 t
Distance from Tower Top to Hub Height	5 m
Cut-in wind speed	3.00 m/s
Rated wind speed	10.59 m/s
Cut-out wind speed	25.00 m/s
Minimum rotor speed	5.00 rpm
Maximum rotor speed	7.56 rpm
Rated thrust	2.40 MN

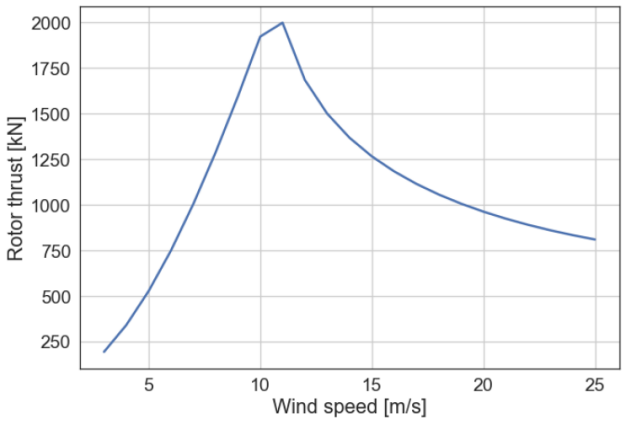

Figure 3-5. Thrust curve of the IEA Wind 15MW reference wind turbine (Bredmose, y otros, 2019).

WindCrete is a monolithic concrete spar platform including both the tower and the floater in a unique concrete member (Vigara, y otros, 2019; Mahfouz, y otros, 2020). The monolithic characteristic means that joints between the tower and the floater are avoided, thus the fatigue resistance is increased since weak points are driven out. The whole structure is in compression state by the use of active reinforcement, and it is designed to avoid traction at any point during the life span of the platform. The tower height is 129.495 m, resulting in a hub height of 135 m (Figure ***3-6***). The WindCrete platform can be divided into the following parts:

- Wind turbine generator (WTG): The substructure is post-tensioned concrete made. Taking advantage of the post-tensioning anchors placed at the top of the tower, a specific steel plate has been designed for the connection between the rotor and nacelle assembly (RNA) and the structure. This round steel plate presents a U-shaped cross section, which acts as a stiff baseplate for the steel tendons, partially or completely closed by an additional upper steel plate, where the connection bolts with the yaw bearing is placed.
- Concrete Tower: The tower is a truncated cone piece. The width of the tower is set to resist the bending moment during the service life of the structure, with a minimum dimension that allows the placing of the post-tensioning tendons and enough concrete cover to ensure the durability of the active and passive reinforcement.
- Substructure: The substructure is divided in three parts listed in the following:
    - Bottom hemi-sphere: The base of the floater presents a hemispheric shape, with the same diameter as the cylinder. This shape is completely favourable in structural terms, distributing the hydrostatic pressures in a compression field around the base, while the post-tensioning steel tendons have continuity along the whole structure. In terms of hydrodynamic properties, the hemispheric shape presents a smaller damping than a flat base.
    - Cylinder buoy: The cylinder is the main part that ensures the buoyancy needed as well as allows the placing of the ballast in its base to achieve the needed pitch and roll stiffness.
    - Tapered transition piece: The transition between the tower and the floater connects the tower and the floater. This transition is designed to minimize the curvature of the geometry changes, where the losses and deviation forces of post-tensioning are more significant.
- Station keeping system: The station keeping system is designed with three mooring lines distributed each 120º with delta arrangement. The fairlead points should be installed close to the center of gravity of the structure to avoid pitch coupling motions that will increase the tension range of the mooring lines, and thus reducing its lifespan.

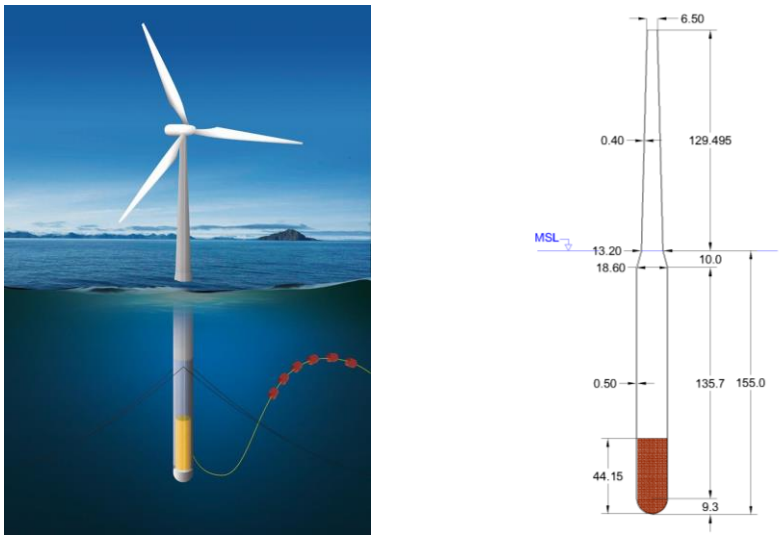

Figure 3-6. Overview (Vigara, y otros, 2019) and sketch of WindCrete platform (Mahfouz, y otros, 2020).

ActiveFloat platform has been developed by COBRA and is currently being designed by COBRA and ESTEYCO (Vigara, y otros, 2019; Mahfouz, y otros, 2020). The platform is a semi-submersible concrete floater, which means that it has enough water-plane area inertia to face tilting angles with large righting moment. The three external vertical columns placed at 120 degrees, are connected to a central shaft that holds the connection with the tower that ends in the turbine. The three vertical columns are connected to the central shaft through three prismatic pontoons below the sea level. The vertical columns provide the buoyancy and stability to the system while the pontoons are structural members, as the central shaft from where the turbine loads are transferred and also add heave damping. The platform external columns have the same height as the central cone where the access platform is located. The platform is made of reinforced concrete, except for the tower that is made of structural steel. Circular heave plates are provided at the bottom of each external column, in order to increase damping. The column diameter is kept equal towards to the pontoons beam. The pontoons have a rectangular cross-section member with a central bulkhead that split the span of the pontoon decks. Table ***3-4*** summarizes the main dimensions of the ActiveFloat platform and Figure ***3-7*** shows a schematic with the following main parts:

- Wind Turbine Generator (WTG): It is worth noting that only the nacelle, hub and blades are here considered parts of the WTG.
- Steel tower: A steel tower is fitted on top of the lower concrete tower piece.
- Foundation: ActiveFloat is a unique body which comprises the following parts:
    - External columns: Three cylindrical towers positioned in the perimeter of the foundation each 120º. These columns emerge above the sea level which provides the stability to the platform. They shall be also water filled to ballast the platform.
    - Pontoons: The prismatic beams joining the central column with the external ones. They are beam-like rectangular-cross-section elements which provide resistance to bending moments and act as water ballast tanks.
    - Central column: Conical tower which acts as the tower foundation. Its height is the same as that of the outer columns and holds the access platform and tower flange on top. It is a dry space to allocate the ballast system, HVAC, etc.
- Mooring system: the mooring system consists of anchors, mooring lines, connectors and links. It is composed of several catenary mooring lines (chain, fibers or mixed systems).

Table 3-4. Main dimensions of ActiveFloat platform (Mahfouz, y otros, 2020).

Hub height above sea level	135.00 m
Columns diameter	17.00 m
Columns separation (center to tower center)	34.00 m
Columns height	35.50 m
Central cone base diameter	19.60 m
Central cone top diameter	11.00 m
Tower base diameter	10.00 m
Tower top diameter	6.50 m
Tower length	120.50 m
Pontoons height	11.50 m
Heave plate cantilever	4.00 m
Overall beam	83.90 m

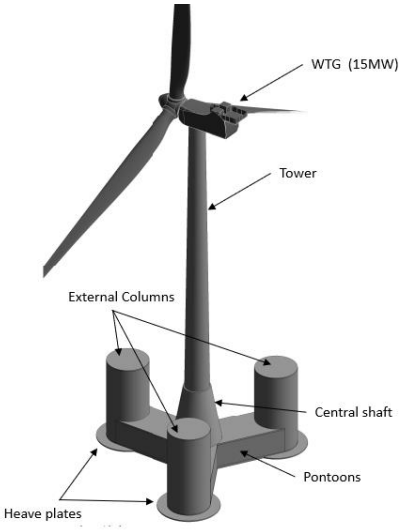

Figure 3-7. Overview of ActiveFloat platform (Mahfouz, y otros, 2020).

3.3.2 Description of the reference numerical model used: OpenFAST

OpenFAST (Jonkman & Buhl Jr, 2005) is a NREL's open source tool for simulating the coupled dynamic response of wind turbines (Figure ***3-8***). OpenFAST joins aerodynamics models, hydrodynamics models for offshore structures, control and electrical system (servo) dynamics models, and structural (elastic) dynamics models to enable coupled time-domain nonlinear aero-hydro-servo-elastic simulation. OpenFAST accounts for the gravitational loads, the behaviour of the control and protection systems (ServoDyn), and the structural dynamics of the wind turbine including the elasticity of the rotor and tower, along with the elastic coupling between their motions and the motions of the support platform (ElastoDyn). The module AeroDyn uses the BEM approach with empirical corrections to calculate the rotor aerodynamics generated by the field inflow (InflowWind). The wind fields are created using the NREL tool TurbSim. The module HydroDyn adds the capability of simulating time-domain hydrodynamic effects from linear hydrostatic restoring, added-mass and damping contributions from linear radiation including free-surface memory effects, incident-wave excitation from linear diffraction,

and nonlinear viscous drag including sea-current loading. The open source code also includes a nonlinear quasi-static mooring line module (MoorDyn).

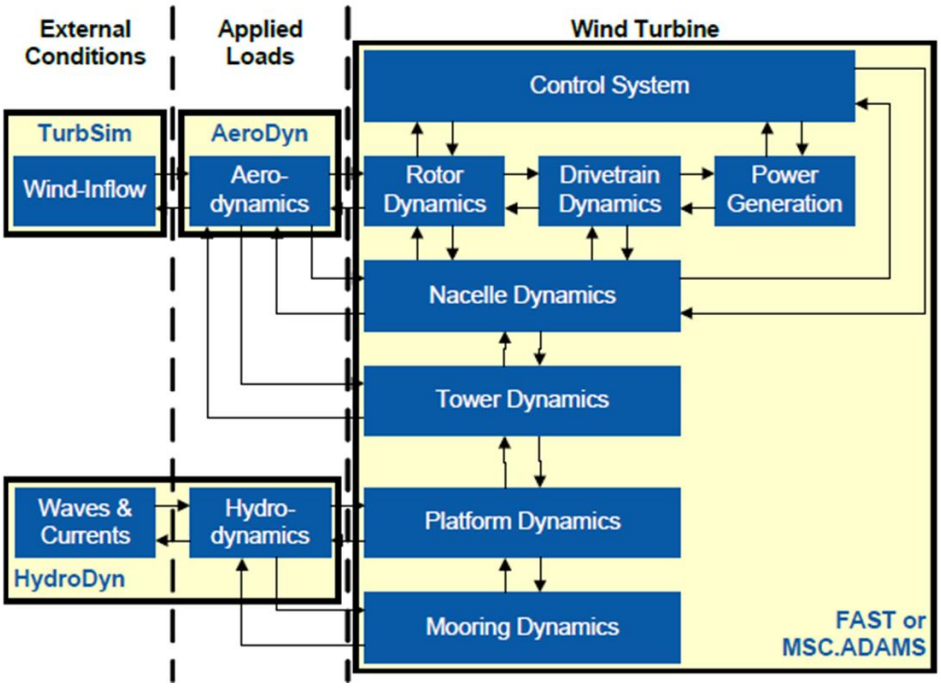

Figure 3-8. Schematic of OpenFAST modules and their interfaces.

Three sites are selected for designing the solutions (Vigara, y otros, 2019). The environmental conditions and depths are different so the project conclusions will include sensitivity aspects to this criteria:

- **Site A:** West of Barra Island, Scotland (UK). A depth of 100 meters is the design depth of this location. Information source is the LIFES50+ project.
- **Site B:** Gran Canaria Island (Spain). A depth of 200 meters is the design depth of this location. The information for this site is mainly obtained from the ELICAN project.
- **Site C:** Morro Bay (USA). A depth of 870 meters is the design depth of the site. The information was provided by the FIHAC.

Representative load cases of Site B were selected to check the time and frequency domain responses of ActiveFloat floating system (Mahfouz, y otros, 2020). Table ***3-5*** shows the simulations done to identify the systems properties of the ActiveFloat floater. Firstly, simulations of regular waves in the absence of wind are done. Afterwards, representative cases of DLCs 1.3, 1.6 and 6.1 (IEC 61400-3, 2009) were carried on to check the performance of the floating wind turbine at different sea states, wind turbulence and sudden grid loss. The values for extreme wind and waves as well as the wind-wave relationships were chosen based on values from (Vigara, y otros, 2019) for the Gran Canaria site. The turbulence class was chosen following the turbine's class shown in (Bredmose, y otros, 2019). Pierson-Moskowitz spectrum is used to model the irregular waves while including the effect of second order waves and forces at irregular sea states.

Table 3-5. Load cases used for models verification **(Mahfouz, y otros, 2020)**.

Name	Duration [s]	Waves	Wind [m/s]	Turbine
Regular Waves	1500	Regular; Hs = 2 m, Tp = 6 s	-	Parked
DLC1.3	5400	Irregular; Hs=2m, Tp=6s	Turbulent ETM; 8, 10.5, 16, 20, 25 m/s	Operational Active control
DLC1.6	5400	Irregular; Hs=5.11m, Tp=9s	Turbulent NTM; 8, 10.5, 16, 20, 25 m/s	Operational Active control
DLC6.1	5400	Irregular; Hs=5.11m, Tp=9s	Turbulent EWM50; 41.2 m/s	Idling Active control

3.3.3 Methodology

Results of model test activities are affected by uncertainties that often are not evaluated properly for controlling the level of the test reliability. Experimental uncertainties rise from several sources: uncertainties affect the excitation of the system, are present in the proprieties of the scaled model, and alter the data measured (Robertson A. , 2017). Recent works have addressed the evaluation of uncertainties in testing of floating wind turbines during wave tank campaigns, following guidelines of several standards of interest. The present work intends to resume the uncertainties included in scaled model tests of floating wind turbines in both wave tank and wind tunnel layouts. Then, a study focused on the identification, quantification and propagation of uncertainties will be done with a particular focus on the uncertainties related with the implementation and application of the HIL strategies.

HIL strategies implemented in wave tank environment plan to reproduce the aerodynamic loads in the physical model by an actuation system that permits to avoid scaling problems, reducing cost barriers for floating wind turbine design validation in realistic coupled wind and wave conditions. The key issue in a hybrid modeling approach is the quality of the dynamic coupling between experiment and simulation. The accuracy of the HiL simulations is the error between the output of the HiL simulator and what the output of the true system would be with a hypothetical real system. In order to assess the relationship between coupling system performance and accuracy of the results in wave tank testing, (Hall, Goupee, & Jonkman, 2018) quantified the sensitivity of the floating wind turbine response respect the coupling quality by simulating errors in the hybrid coupling system. The sensitivity results was then used to determine tolerances for motion tracking errors, force actuation errors, bandwidth limitations and latency in the hybrid coupling system, producing performance specifications to use as targets when designing a hybrid coupling system.

In the case of the IH Cantabria multi-fan system (Figure ***3-4***), the coupling location between physical and numerical sub-models is at the aero-rotor interface. Aero-rotor coupling considers: experimental modeling of mooring system, floating platform and wind turbine tower; and numerical modeling of the aerodynamic loads and rotor inertia to capture details such as gyroscopic forces. Moreover, true-to-scale rotor elasticity can also be modeled numerically (Meseguer & Guanche, 2019), representing an improvement over current capabilities in wind-wave testing because Froude-scaled rotor blades are typically overly rigid.

(Hall, Goupee, & Jonkman, 2018) used simulations in FAST (Jonkman & Buhl Jr, 2005) to determine performance requirements for a hybrid coupling system and study the relationship between coupling system performance and the resulting coupled model accuracy. Running simulations incorporating coupling errors provided information on requirements for the quality of the hybrid coupling system. By observing the discrepancy induced in the results of interest, the sensitivity to these errors introduced in the hybrid coupling were calculated and acceptable error tolerances determined.

Firstly, it is necesary to identify all the possible sources liable to uncertainty, introduced by the fact that the hybrid system is modelled by means of the combination of a numerical simulation, sensors, actuators and control softwares. Then, the uncertainties identified are weigthed in order to prioritizing the most relevant and consequently optimize the propagation procedure. Once the Quantities of Interest (QOI) are defined, a selection of load cases relative to the Gran Canaria site for the ActiveFloat floater (*Table **3-6***) was performed. Such load cases were picked in order to obtain a comprehensive baseline set. Each load case and type of error were initially examined separately. Simulations are run in OpenFAST (Jonkman & Buhl Jr, 2005) for levels of errors defined by assuming a Normal distribution of each QOI variable. Each simulation lasts 3600 s, with a calculation frequency of 0.01 s. In a real case, however, different types of coupling errors are present simultaneously. Thus, after assessing the Gumbel distributions of the resulting mean discrepancy level for each single QOI, a Monte Carlo simulation was run (Park, Kim, & Song, 2013) with error sources acting concurrently in order to assess the effect of combined errors levels.

Table 3-6. Extremal load cases used for the analysis of uncertainties.

Name	Duration [s]	Waves	Wind [m/s]	Turbine
DLC1.3	5400	Irregular; Hs=2m, Tp=6s	Turbulent ETM; 10.5 m/s	Operational Active control
	5400	-	Turbulent ETM; 10.5 m/s	Operational Active control
DLC1.6	5400	Irregular; Hs=5.11m, Tp=9s	Turbulent NTM; 10.5 m/s	Operational Active control
	5400	Irregular; Hs=5.11m, Tp=9s	-	Operational Active control
DLC6.1	5400	Irregular; Hs=5.11m, Tp=9s	Turbulent EWM50; 41.2 m/s	Idling Active control
	5400	-	Turbulent EWM50; 41.2 m/s	Idling Active control

3.3.4 Identification of the uncertainty sources

Uncertainties in hybrid scale model experiments may rise due to several reasons.

Numerical model

OpenFAST (Jonkman & Buhl Jr, 2005) simulations in the time domain for the coupled dynamic response of floating wind turbines have certain limitations. Such limitations cannot be quantified in the approach used in this work, as it is run by following a numerical approach. Such limitations can be shortly resumed as follow:

- The viscous effects of water needed for calculating the platform response cannot defined with accuracy (unless calibrated with experimental data) with potential theory.
- The hydrodynamics of the platform is represented according to the Cummin's equation. Some simplifications are applied:
    - In the case of radiation, all the Degrees of Freedom (DOF) of movement are linearly superimposed.
    - In the case of diffraction, waves are linearly overlapped, and wave force increases linearly with the wave height (some interaction between waves is introduced with the QTFs, but it is a non-linearity of only 2nd order).
    - Diffraction forces are computed prior to the simulation, considering the floating system in the rest configuration.
- The wind turbine aerodynamics is described by means of a Blade Element Momentum model (BEM).
    - Semi-empirical corrections are used to introduce 3D effects and unsteady effects as the wake dynamics and the dynamic stall.
    - The BEM model neglects the effects on the aerodynamics ones due to the movement of the rotor inside the wake.
- Finally, accuracy of wind in the wave tank, wave and current in the wind tunnel, are also limited by the irregular wave and the turbulent wind models used.

Physical model

Fabrication and materials for the manufacturing of the scaled model have tolerances associated to their properties:

- For the wave tank:
    - Dimensions, geometry at the water-plane and geometry of the mooring lines (dry weight density and length).
    - Platform weight and mass distribution (Center of Gravity (COG) and radius of gyration).
    - Platform heading, orientation of the mooring lines, fairlead position, location of anchor points.
    - Mooring stiffness and tower stiffness.
    - Damping and pretension of the mooring lines.
    - Bottom friction of the mooring lines.
- For the wind tunnel:
    - Geometry, mass, mass distribution and bending stiffness of the wind turbine tower and of the rotor blades.
    - Weight and weight distribution of the wind turbine scale model.
    - Performance of the wind turbine actuators (pitch actuators, generator).
    - Aerodynamic performance of the wind turbine rotor. The rotor of the wind turbine scale model is designed according to performance-scaling. Despite this, discrepancies with respect to the full-scale target are usually present.

Environmental uncertainty

Parameters concern the reference met-ocean characterization as inputs:

- For the wave tank:

Incident and reflected wave conditions (significant wave height, spectral wave peak period); current definition (average speed, RMS speed, stability).

- For the wind tunnel:
  Wind turbulence, as the reproduction of large integral length scale contributions is limited by the size of the test chamber cross section.

Measurement uncertainty

Measurements are collected by instruments and sensors that define the parameters related to the test setup configuration, the geometry and proprieties of the model and the reproduced environmental conditions. Sensors are also used to identify the quantities that describe the system response during the different test campaign scenarios.

Hybrid coupling

In this case, inaccuracies are the result of limitations in the hybrid coupling system in terms of measurement and actuation error levels, bandwidths, and latency. (Hall, Goupee, & Jonkman, 2018) divided the sources of uncertainty into specifications for the performance envelope of the coupling system and specifications for the quality of the coupling system.

- The following specifications concern the performance range of the coupling system:
  - Maximum displacements.
  - Maximum velocities.
  - Maximum accelerations.
  - Bandwidth of motions.
  - Maximum forces and moments.
- The last four specifications concern the precision of the coupling system (*Figure **3-9***):
  - Error tolerances for motion tracking of the physical model.
  - Error tolerances for force actuation on the aero-rotor coupling.
  - Required motion tracking or actuation bandwidth.
  - Acceptable latency levels.

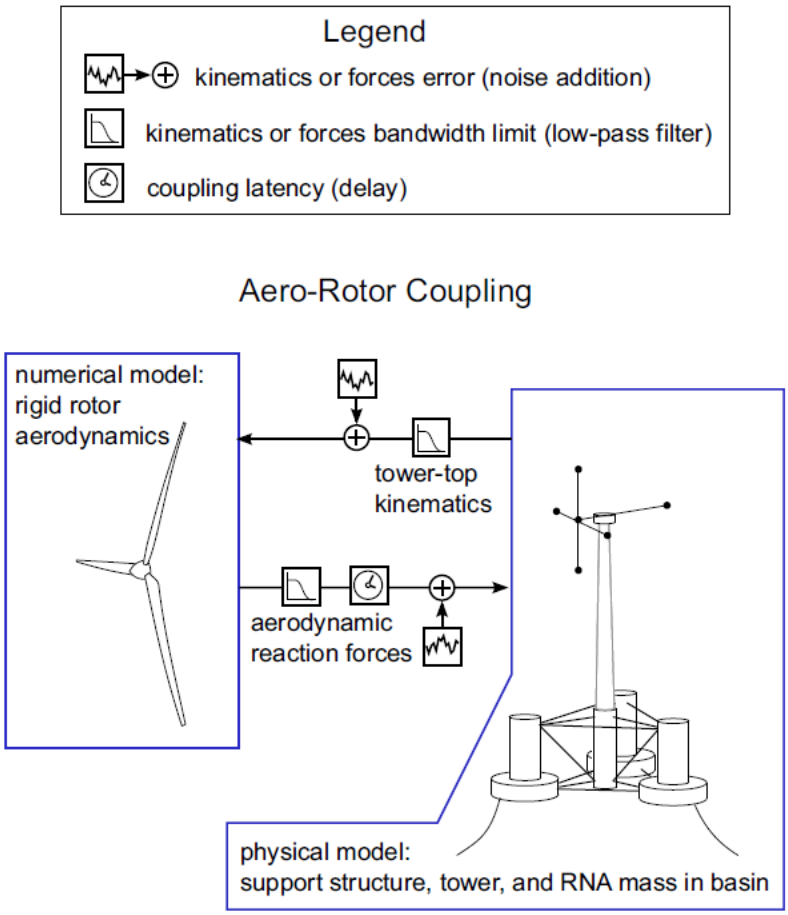

Figure 3-9. Flowchart of communication and error introduction in hybrid coupling simulations **(Hall, Goupee, & Jonkman, 2018)**.

3.3.5 Uncertainty quantification in ocean basin

For the sake of computational manageability, we firstly define the Quantities of Interest (QOI) to be evaluated from all the possible sources liable to uncertainty. (Barrera C. , Guanche, Rodríguez, Armesto, & Losada, 2020b) performed a sensitivity study to determine the most significant *mooring parameters* over the numerical outcomes, changing each of them at a time according to a percentage from a reference value. Their results showed a relevant dependence on the length, and in smaller extent, on the weight-diameter. (Robertson, et al., 2018) used a value of 0.1 m uncertainty in the full-scale geometric dimensions, while (Kim & Hermansky, 2014) suggested a tolerance of ± 0.05% of linear dimensions larger than 2 m. In the case of mooring system, as the unstretched lines' length of 614 m in prototype scale (Mahfouz, y otros, 2020), last case would be more restrictive resulting a value of 0.307 m uncertainty. Regarding the weight, (Robertson, et al., 2018) measured a systematic (ASME-based approach) or type B (ISO-based approach) uncertainty of 0.616%, and a random or type A uncertainty of 0.028%. While the systematic type is defined as the accuracy that measures how close the results achieved at the model would be to the real value of the fully operating floating wind turbine, the random type would be related to the repeatability observed in the results at the model (Desmond, Hinrichs, & Murphy, 2019). The total standard uncertainty of a measurement can be calculated doing the square root of the sum of the squared values of types A and B uncertainties (Kim & Hermansky, 2014). In this case, the total standard uncertainty will be the 0.617% of the 561.252 kg/m as the mass per unit length of the line in prototype scale (Mahfouz, y otros, 2020), i.e. 3.463 kg/m. *Figure **3-10*** shows the Probability Density Functions (PDF) of the

Gaussian or Normal distributions N(μ,σ) for the most significant mooring parameters, being μ the mean and σ the standard deviation.

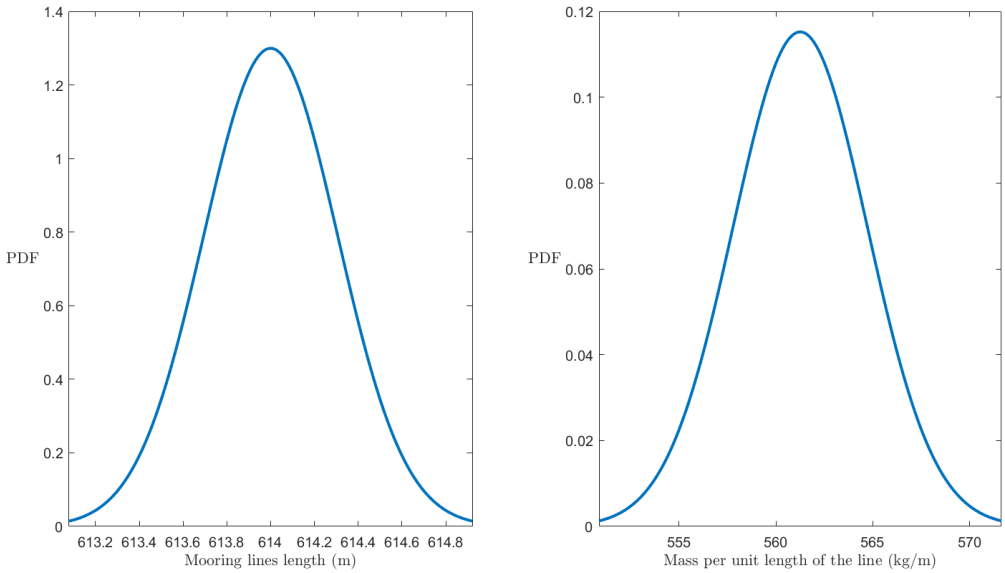

Figure 3-10. Normal distributions of mooring lines length and mass per unit length.

The Quantities of Interest to be evaluated from all the possible *platform parameters* liable to uncertainty are: the metacentric height (GM); the Inertia related to the pitch rotation about the centre of mass (I_{yy}). (Robertson, y otros, 2018) used a value of 0.05 m uncertainty in the full-scale geometric dimensions in the vertical distance from the Mean Sea Level (MSL) to the Centre of Mass (CM), and thus in the metacentric height. The authors also suggested a systematic and a random uncertainty of 1% and 0.008%, respectively, when calculating the I_{yy}. Thus, the total standard uncertainty of the 45.825 x 10^9 kg·m^2 as the I_{yy} value in prototype scale, will be 0.458 x 10^9 kg·m^2. The Gaussian distributions of the platform parameters are plotted in Figure ***3-11***.

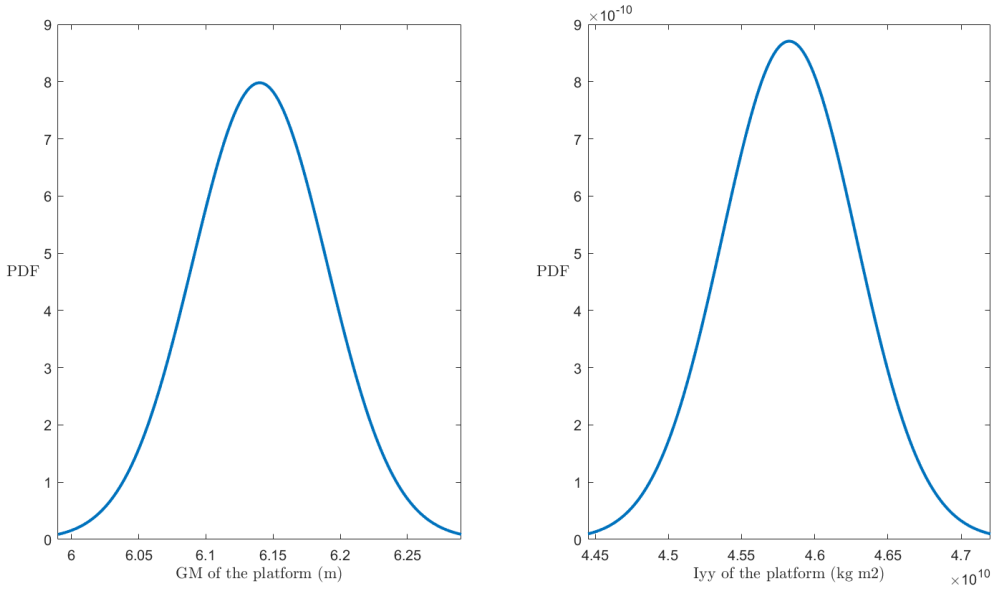

Figure 3-11. Normal distributions of platform metacentric height and Inertia for pitch rotation.

Concerning the precision of the *hybrid coupling*, the OpenFAST code was modified to quantify: the sensitivity to limited force actuation bandwidth, and the sensitivity to latency in the overall coupling system's response. Limited coupling bandwidth is realized by adding a first-order low-pass filter to the forces calculated by aeroelastic model of the FAST simulation (Hall, Goupee, & Jonkman, 2018). For the uncertainty quantification of limited force actuation bandwidth, we assume an effectiveness of a hybrid coupling below 2 Hz. Considering a scale factor of 1/40, the full-scale values of the first-order low-pass filter cut-off frequency used to simulate the bandwidth limitation, would follow a Normal distribution with $\mu = 2\ Hz/\sqrt{40} = 0.316\ Hz$ and $\sigma = 0.01\ Hz$. On the other hand, latency in the overall coupling system's response is modeled by adding a delay of a discrete number of time steps (each of 0.01 s) in the reaction forces from the aero-rotor coupling. To quantify this delay, we use in the full-scale geometric dimensions a Normal distribution of $\mu = 0.05\ s \cdot \sqrt{40} = 0.32\ s$ and $\sigma = 0.01\ s$. Figure ***3-12*** shows the Probability Density Functions (PDF) of the Gaussian distributions for these key parameters for the effectiveness of a hybrid coupling.

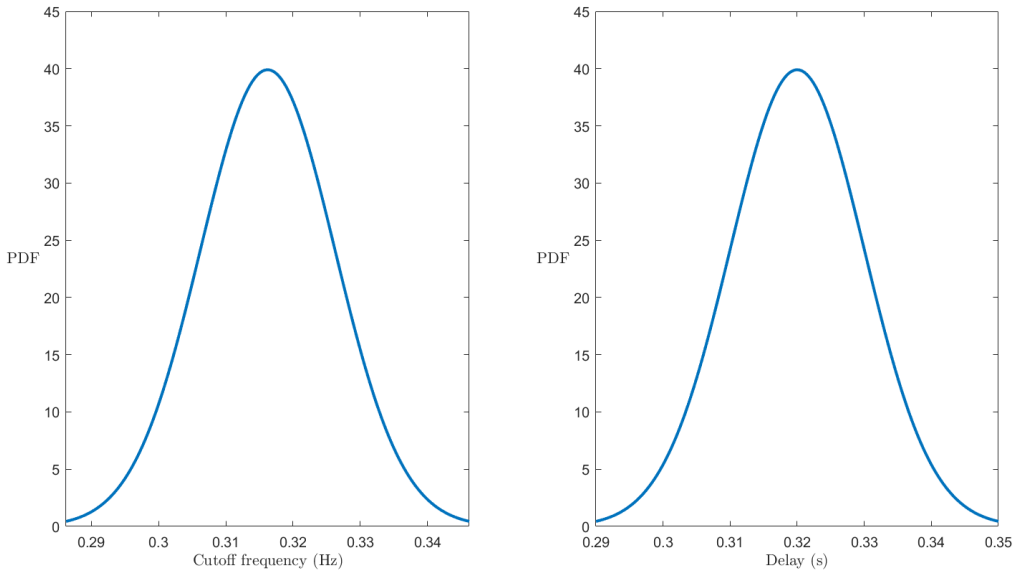

Figure 3-12. Normal distribution of the cut-off frequency of the first-order low-pass filter and delay in the reaction forces from the aero-rotor coupling.

3.3.6 Uncertainty propagation of mooring, platform and multi-fan parameters

To assess the propagation of experimental uncertainty in ocean basin testing of the Activefloat wind turbine, a numerical model of the true system validated in (Mahfouz, y otros, 2020) is used. Thus, we neglect any extra inaccuracy in the numerical propagation. We quantify discrepancies by taking the absolute difference between the mean of the time-series output of the perturbed simulation and that of the baseline simulation:

$$\textbf{Mean dicrepancy} = \left| \frac{\sum_{i=1}^{n} x_i'}{n} - \frac{\sum_{i=1}^{n} x_i}{n} \right| \qquad (31)$$

where x is the time-series of the quantity of interest in the baseline simulation, x' is the same QOI in the perturbed simulation, and n is the number of recorded samples. The time-series analysed are related to some of the parameters which describe the platform behaviour, those are surge displacements and platform pitch rotations, nacelle accelerations along the x-axis, and the tensions on the fairlead of the windward mooring line.

Mooring parameters

The resulting discrepancy level calculated in the outputs of the 31 different level of error set in the mooring lines length were fitted by a Gumbel distribution for each of the six load cases. The results are plotted in Figure ***3-13***. The DLC 1.6 without wind presents a notably lower mean discrepancy in platform surge displacements. This load case also exhibits lower uncertainty values in pitch rotations of the platform, while DLC 1.6 and DLC 6.1 show a higher mean discrepancy. Besides, the uncertainties in windward mooring fairlead tension do not seem to vary too much between the different load cases.

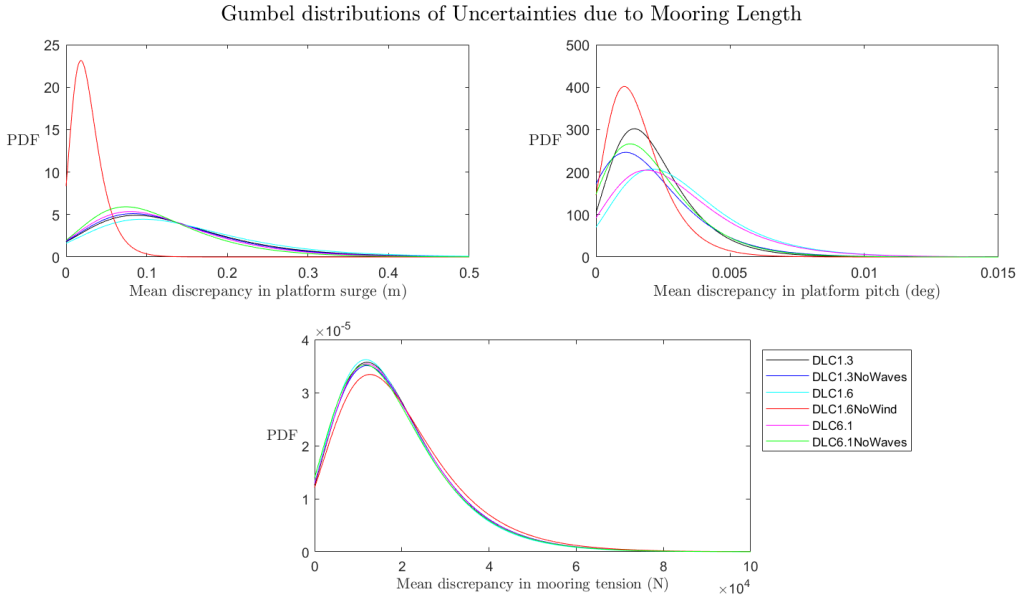

Figure 3-13. Gumbel distributions of mean discrepancies due to mooring length in platform surge and pitch, and windward mooring fairlead tension.

In order to define the minimum number of simulations necessary for each load case for obtaining statistical reliable results (regarding the uncertainty propagation of mooring length), we repeat this procedure for different simulations randomly taken and calculate the Most Probable Mean (MPM) discrepancies of the Gumbel distributions. This value of the Gumbel distribution corresponds to the 37% percentile and is given by:

$$\mathbf{MPMean} = \mu - \mathbf{0.45} \cdot \boldsymbol{\sigma} \qquad (\textbf{\textit{32}})$$

where μ is the mean and σ the standard deviation of the mean discrepancy obtained from each simulation. Figure ***3-14*** shows how the MPM varies with the number of simulations in surge displacements and pitch rotations of the platform response, and in tensions on the windward mooring line. As we can see, this value seems to converge to 8 simulations (black dashed line) for every load case.

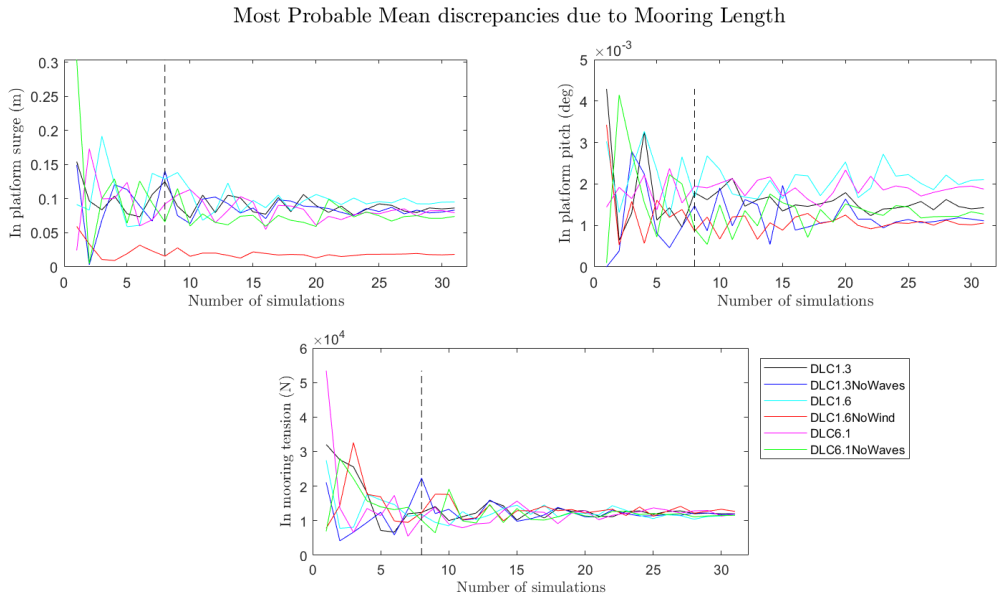

Figure 3-14. Most Probable Mean discrepancies due to mooring length as a function of the number of simulations in platform surge and pitch, and windward mooring fairlead tension.

On the other hand, Gumbel distributions of mean error level averaged in surge displacements and pitch rotations of the platform response, as well as in tensions on the windward mooring line, fitted with 31 different errors levels regarding the mooring lines mass per unit length are plotted in Figure ***3-15***. Although tendencies are similar in platform surge and mooring tension, the propagation of the mooring weight uncertainty is not as relevant as the mooring length one, as (Barrera C. , Guanche, Rodríguez, Armesto, & Losada, 2020b) had already concluded. DLC 1.6 present lower uncertainties in pitch rotations of the platform, while the DLC 6.1 without waves exhibits a higher mean discrepancy.

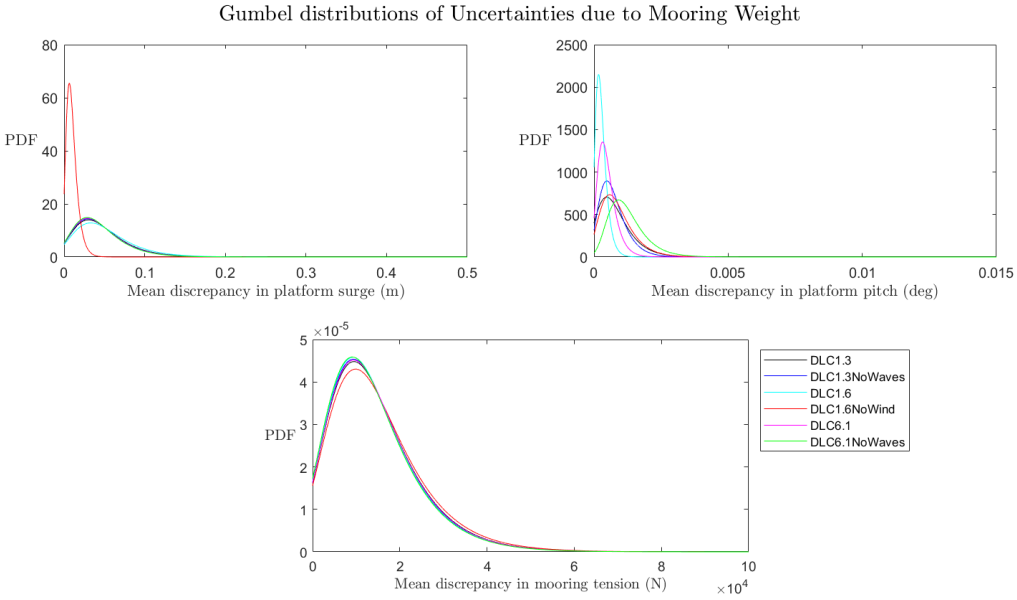

Figure 3-15. Gumbel distributions of mean discrepancies due to mooring weight in platform surge and pitch, and windward mooring fairlead tension.

Next, Figure ***3-16*** shows how the Most Probable Mean discrepancies of the Gumbel distributions due to the mooring weight varies with the number of simulations. As in the previous case of the mooring length, the MPM seems to converge from 8 simulations (black dashed line) for every load case of the outputs analysed.

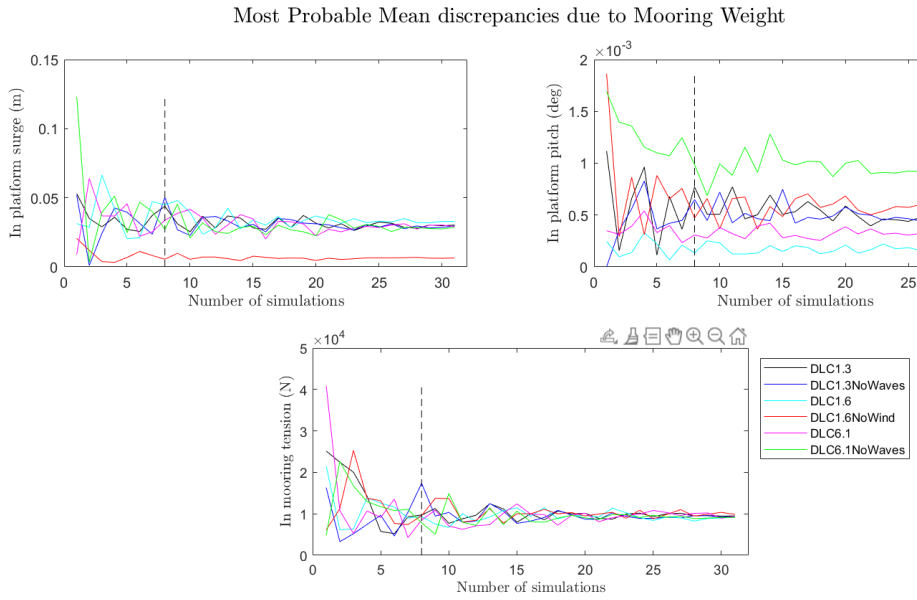

Figure 3-16. Most Probable Mean discrepancies due to mooring weight as a function of the number of simulations in platform surge and pitch, and windward mooring fairlead tension.

Platform parameters

To quantify the propagation of inaccuracies on the geometric measurements related to the platform, it would be necessary to modify and run AQWA to create new platform inputs for OpenFAST. For the sake of computational manageability, and having already seen that the MPM seems to converge from 8, it was considered to simulate 8 amounts of error in the GM for each load case assuming to obtain statistical reliable results. The resulting mean discrepancy level averaged for the outputs analysed were fitted by a Gumbel distribution and plotted in Figure ***3-17***. The DLC 6.1 with and without waves present lower and higher uncertainties, respectively, in surge displacements of the platform. Regards the platform pitch rotations, the DLC 1.6 with and without wind exhibit a lower and a higher mean discrepancy, respectively. The DLC 1.6 also presents lower tension of the windward mooring fairlead, while DLC 1.3 shows a higher mean discrepancy.

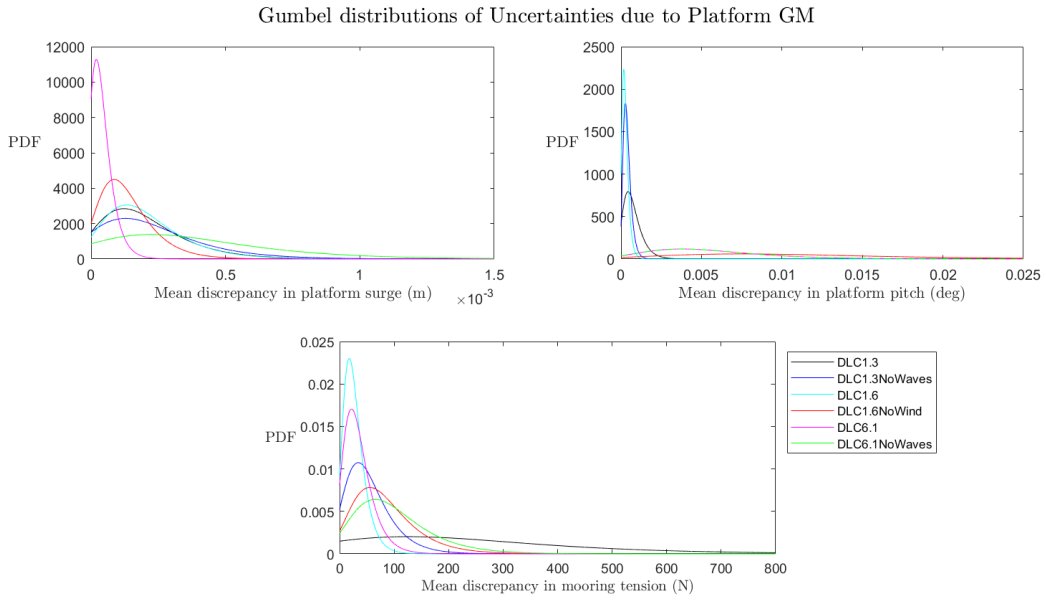

Figure 3-17. Gumbel distributions of mean discrepancies due to metacentric height in platform surge and pitch, and windward mooring fairlead tension.

Besides, Gumbel distributions fitted with 8 values of mean discrepancy level due to introduced errors in the Inertia I_{yy} are plotted in Figure ***3-18*** for each load case of the outputs analysed. The three cases with coupled loads of wind and waves, present higher uncertainties in platform surge displacements. Pitch rotations of the platform are negligible in comparison to those ones because of the metacentric height inaccuracies. Although the DLC 1.3 tendency of Gumbel distributions of both platform parameters are similar in mooring tension subplot, propagation of I_{yy} uncertainties also exhibits significantly lower values for every load case.

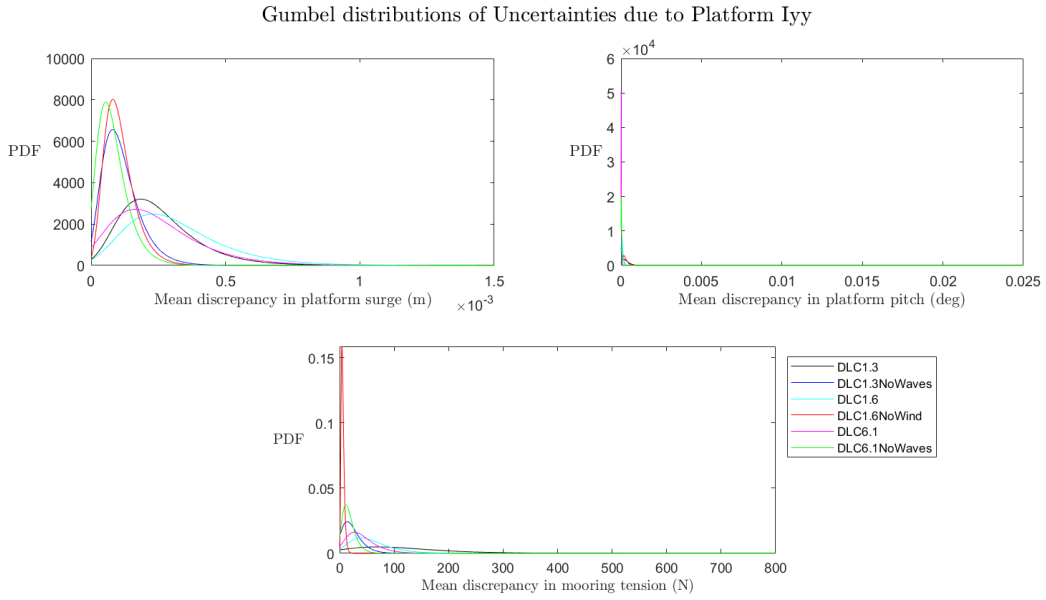

Figure 3-18. Gumbel distributions of mean discrepancies due to Inertia for pitch tilt rotation in platform surge and pitch, and windward mooring fairlead tension.

Multi-fan parameters

For the multi-fan bandwidth uncertainty, as for the mooring ones, we analyze the outputs in 31 different bandwidth amplitudes. However, for this parameter, we only repeat the Gumbel fitting procedure for the four load cases in which the turbine is operative (Figure ***3-19***). DLCs 1.3 with and without waves show higher mean discrepancies in surge displacements and in pitch rotations of the platform response, as well as in tensions of the windward mooring fairlead.

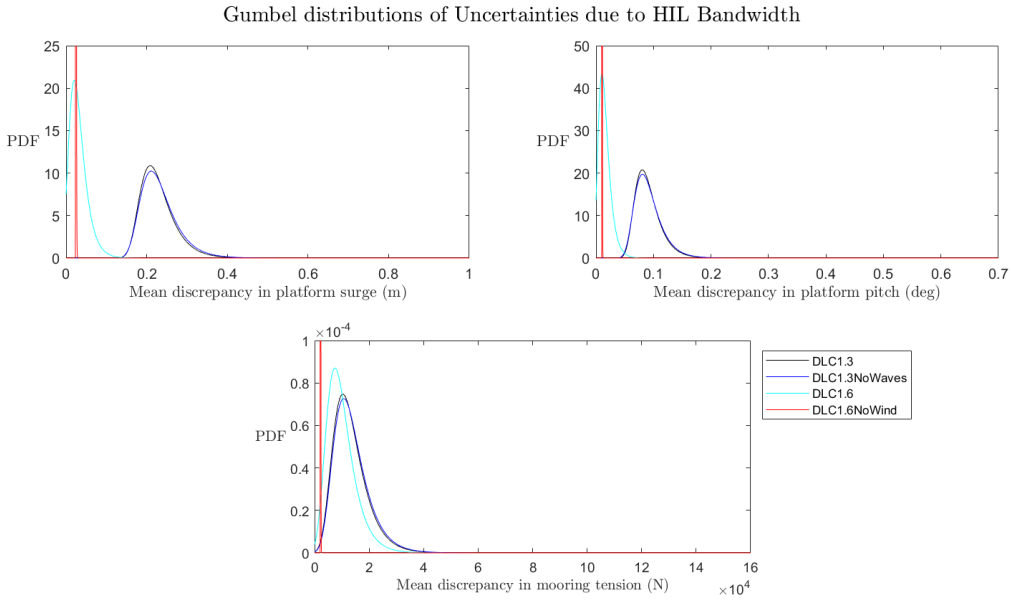

Figure 3-19. Gumbel distributions of mean discrepancies due to limited force actuation bandwidth in platform surge and pitch, and windward mooring fairlead tension.

On the other hand, for uncertainties due to the latency in the multi-fan system response, we simulate 5 levels of delay for the four load cases in which the turbine is operational, due to the limitation of the time step to 0.01 s. Moreover, in this case, the elasticity of the turbine is not considered in OpenFAST otherwise the applied delays would have caused a dynamic structural instability of the platform. Although tendencies are similar, the propagation of the multi-fan latency uncertainties is notably higher than the actuation bandwidth one. The resulting Gumbel distributions for the outputs analyzed are shown in Figure ***3-20***.

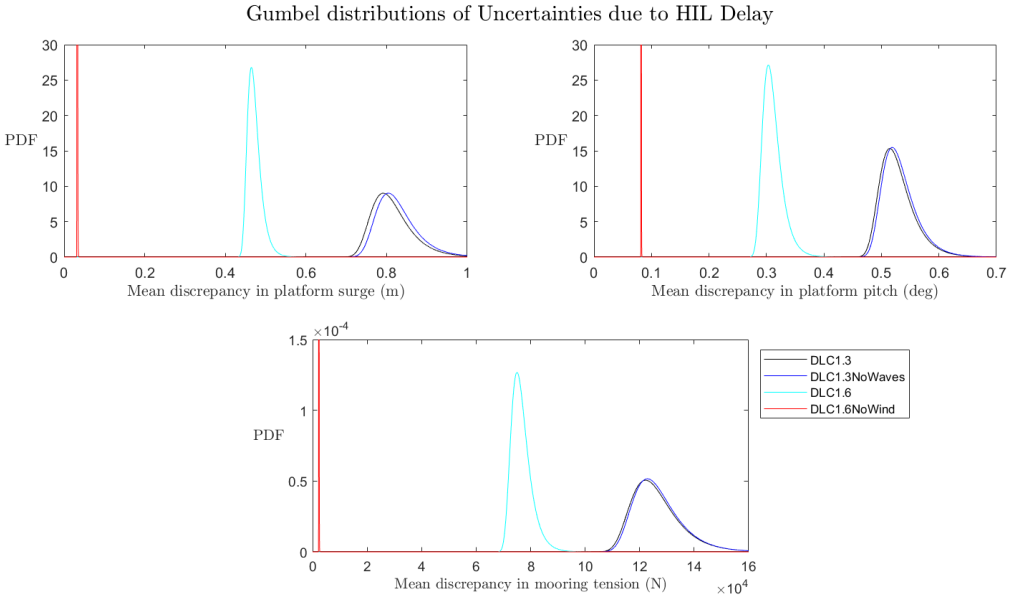

Figure 3-20. Gumbel distributions of mean discrepancies due to latency in the multi-fan system response in platform surge and pitch, and windward mooring fairlead tension.

3.3.7 Uncertainty coupling propagation in ocean basin

For the sake of computational manageability, we run 1000 simulations for each of the load cases considering wind, waves and the turbine in operative stages. Random amounts of errors were introduced in the mooring length, in the metacentric height and in the force actuation bandwidth. Being necessary to modify and run AQWA to introduce GM inaccuracies, the introduced discrepancies of this parameter are randomly taken from 8 equidistant values in the Cumulative Distribution Function (CDF) with a 99% confidence level. In order to confirm the statistical results obtained with the combination of the mentioned parameters, it was assessed the Gumbel distributions of the resulting mean discrepancy level averaged and calculate the Most Probable Mean (MPM) value for different number of simulations. Figure ***3-21*** shows that the MPM of combined discrepancies seems to converge in all the outputs analysed for both load cases (DLCs 1.3 and 1.6).

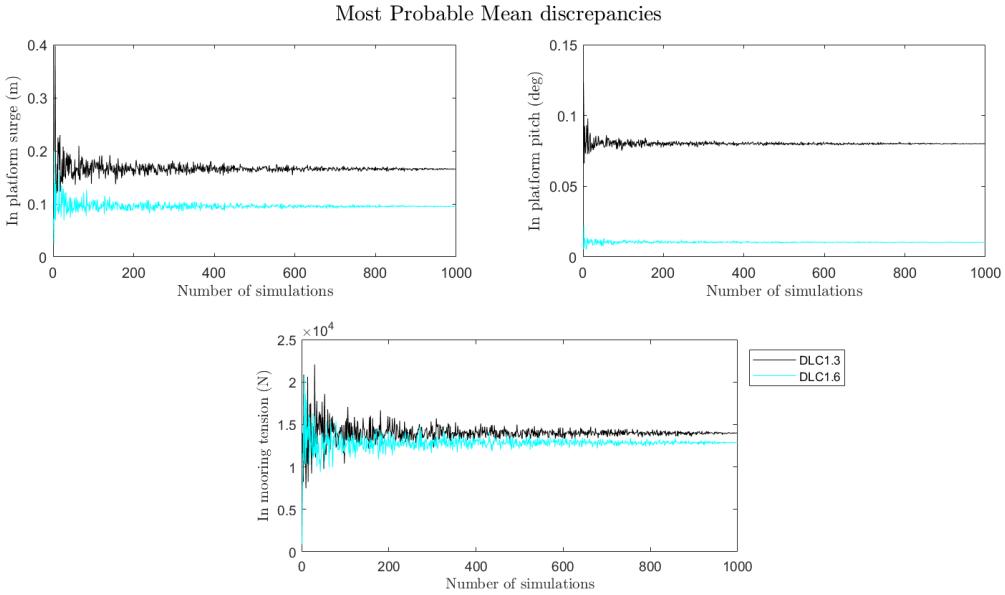

Figure 3-21. Most Probable Mean discrepancies due to coupled inaccuracies as a function of the number of simulations in platform surge and pitch, and windward mooring fairlead tension.

In order to analyse the effect of coupled inaccuracies on the propagation, Figure ***3-22*** and Figure ***3-23*** show the Gumbel distributions of the mean discrepancies due to the three parameters and the ones due to a single parameter separately for DLC 1.3 and DLC 1.6, respectively. For both load cases, the mean discrepancy due to the metacentric height is trivial in surge displacements and platform pitch response, as well as in tensions of the windward mooring fairlead. For DLC 1.3, the Gumbel distributions obtained by combining the different sources of uncertainties maintain the discrepancy levels of the one found for the actuation bandwidth in platform pitch rotations. Nevertheless, the effects of the mooring length are dominant in windward mooring fairlead tensions. Respecting the platform surge displacements, as Gumbel distribution of uncertainties due to the mooring length has higher standard deviation but lower mean than that due to the actuation bandwidth, the Gumbel distributions obtained by combining the different sources of uncertainties is defined by both parameters.

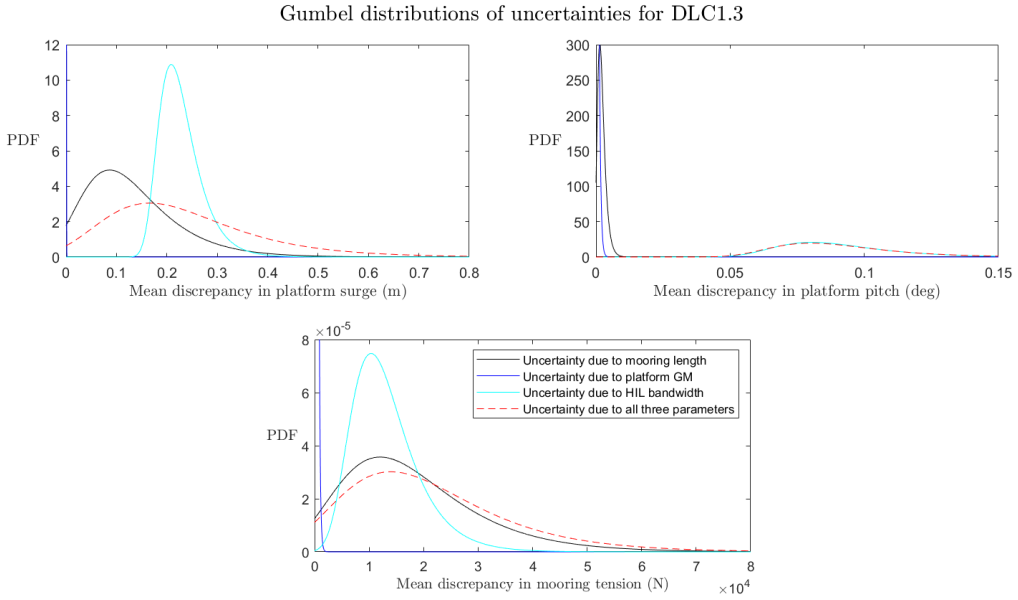

Figure 3-22. Gumbel distributions of mean discrepancies due to coupling inaccuracies in platform surge and pitch, and windward mooring fairlead tension for DLC1.3.

The Gumbel distributions obtained by combining the different sources of uncertainties for DLC 1.6 present lower values than for DLC 1.3 in surge displacements and pitch rotations of the platform response, and quite similar in tensions of the windward mooring fairlead. Besides, tendencies of the parameters effects are similar for both load cases in platform pitch rotations and in mooring tensions. However, as Gumbel distribution of uncertainties due to the mooring length has both higher standard deviation and higher mean than that due to the actuation bandwidth, the effects of the mooring length are dominant in platform surge displacements for DLC 1.6.

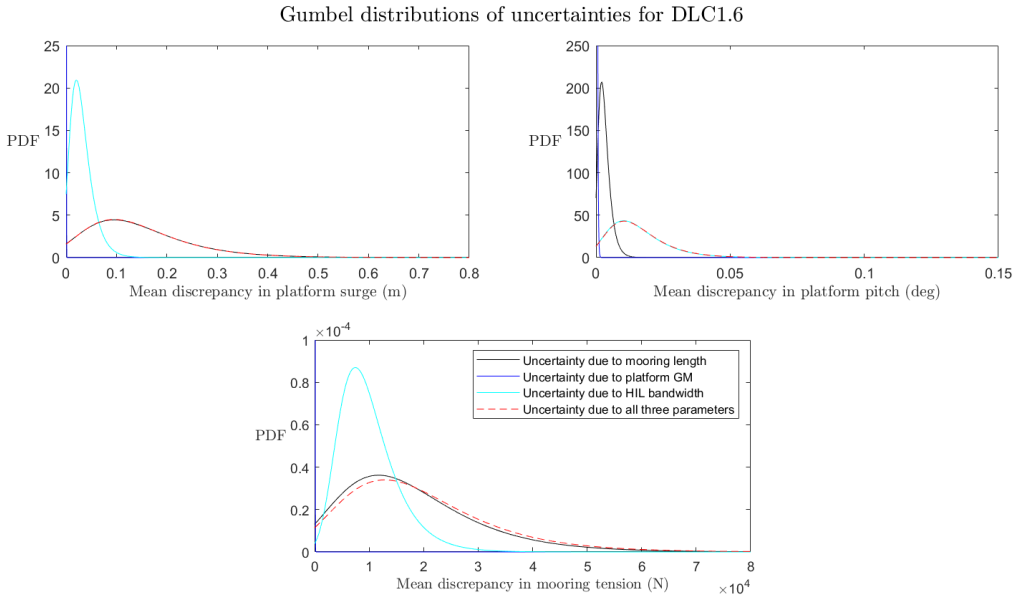

Figure 3-23. Gumbel distributions of mean discrepancies due to coupling inaccuracies in platform surge and pitch, and windward mooring fairlead tension for DLC1.6.

3.3.8 Uncertainty analysis in wind tunnel

Two kind of modeling errors are considered:

- The aerodynamic behavior of the full-scale rotor is not perfectly matched by the scale model rotor. The effects of inconsistencies in the rotor performance are proved by means of numerical simulations;
- The global response of the floating system that is simulated in the scale model experiment is affected by the HIL coupling; the effects of the HIL coupling on the platform motions are shown based on the results of a previous wind tunnel test campaign.

Rotor aerodynamics

The Reynolds number achieved in wind tunnel hybrid experiments is greater than in conventional wave tank experiments. However, it is still lower than what is experienced by the full-scale wind turbine in the corresponding operating conditions. For the rotor aerodynamics to be representative of the full-scale system, the rotor must be redesigned according to a performance scaling procedure. Despite this, some differences persist between the scale-model and full-scale rotor, which affect the simulation of the floating wind turbine response in the experiment.

The rotor of the PoliMi wind turbine scale model was designed to match the aerodynamics of the DTU 10MW RWT. The scale model rotor is compared to the rotor of the IEA-15-240-RWT in Figure ***3-24***. The thrust coefficient for the scale model is much higher than for the RWT. A new rotor must be designed to match the IEA-15-240-RWT.

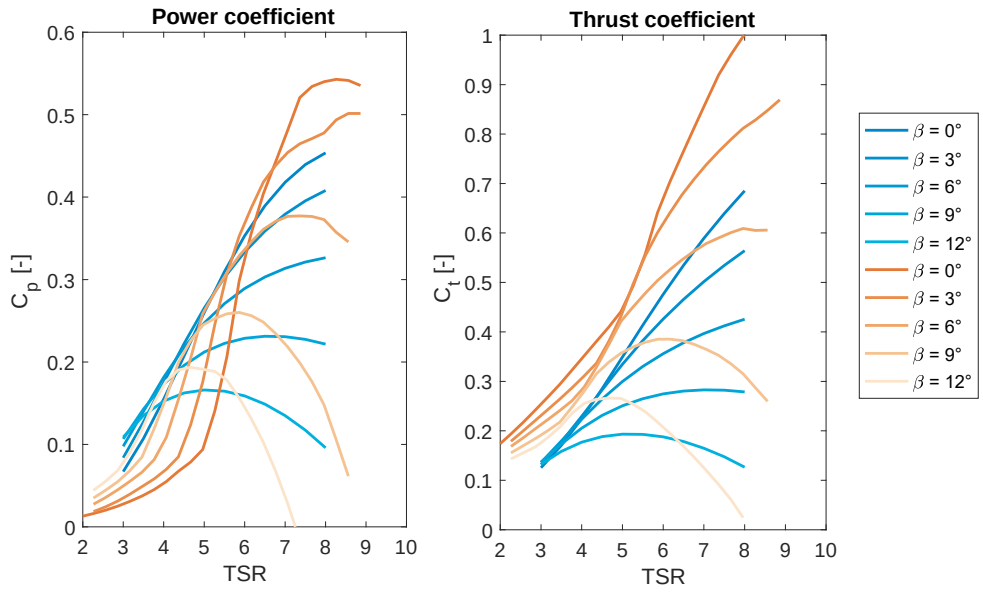

Figure 3-24. The IEA-15-240-RWT (blue) is compared to the PoliMi wind turbine scale model (orange) in terms of power (left) and thrust (right) coefficient. The coefficients are reported for several values of tip-speed ratio (TSR) and rotor collective pitch angle β.

In order to assess the inaccuracies introduced by a performance-scaled rotor in the simulation of a floating wind turbine response, the case of a 10MW floating wind turbine is considered in place of the 15MW designs of this project. In detail, the floating system is formed by the DTU 10MW and the INNWIND.EU TripleSpar platform. Once a new scale model rotor is designed to match the IEA-15-240-RWT, the same procedure may be used to verify the impact it has on the emulation of the floating wind turbine response.

In Figure ***3-25***, the power and thrust coefficients of the DTU 10MW are compared to those of the PoliMi scale model. In this case, the thrust coefficient, which was the target of the performance-scaling design, is much closer to full-scale. Larger differences are found for the power coefficient, which is anyway close to target in operational conditions (TSR = 6-9).

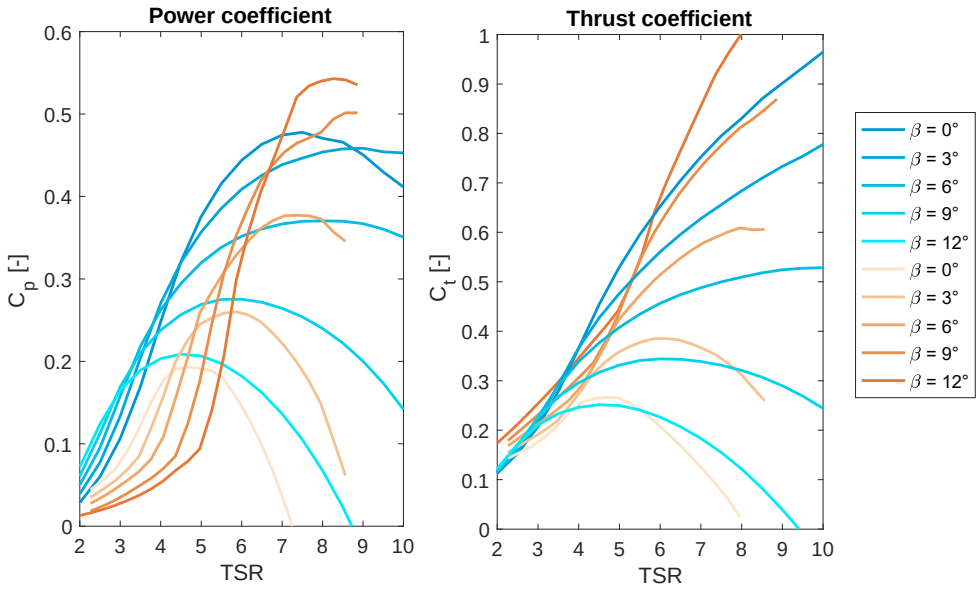

Figure 3-25. The DTU 10MW (blue) is compared to the PoliMi wind turbine scale model (orange) in terms of power (left) and thrust (right) coefficient. The coefficients are reported for several values of tip-speed ratio (TSR) and rotor collective pitch angle β ***(Belloli, y otros, 2020)***.

The effects of the scaled aerodynamics are evaluated by means of numerical simulations in FAST v8.16. To support the results of the comparison between numerical simulations, the power and thrust coefficient of the FAST model of the PoliMi wind turbine scale model are reported in Figure ***3-26***. The power and thrust coefficients obtained from the numerical model are slightly different than those of the real scale model, but the comments to Figure ***3-25*** also apply to Figure ***3-26***.

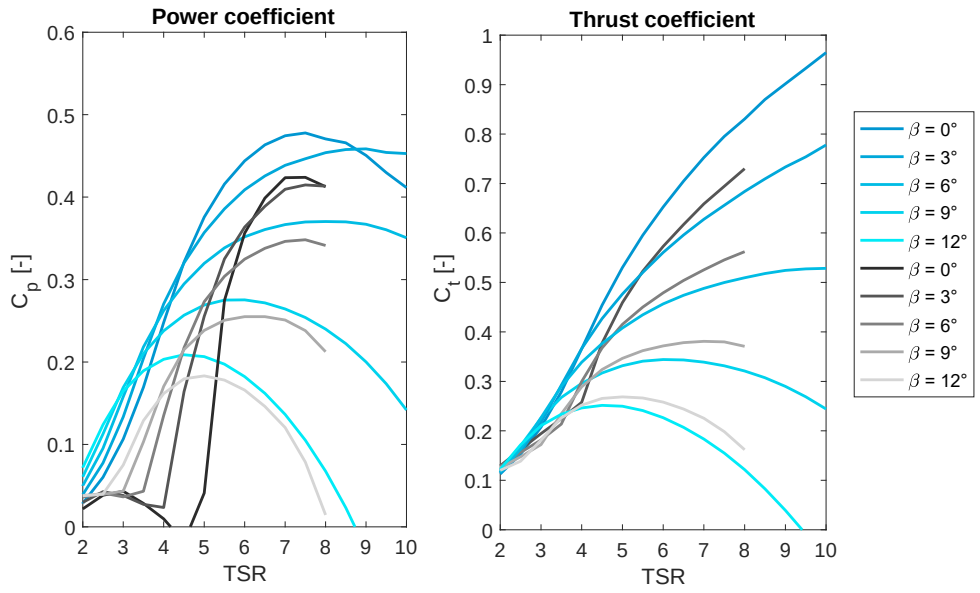

Figure 3-26. The DTU 10MW (blue) is compared to the FAST model of the PoliMi wind turbine scale model (grey) in terms of power (left) and thrust (right) coefficient. The coefficients are reported for several values of tip-speed ratio (TSR) and rotor collective pitch angle β.

In above-rated winds, the global response of the floating wind turbine (formed by the DTU 10MW and the INNWIND.EU TripleSpar platform) is largely determined by the coupled platform-rotor dynamics which is set by the collective pitch controller. Floating wind turbines may experience an unstable motion and large loads in above-rated conditions, and a correct emulation of the above-rated dynamics in scale model experiments is therefore necessary. A wind-step case with still water is considered to evaluate the inaccuracies introduced by the performance-scaled rotor in the floating platform response. The surge and pitch motions of the full-scale system and of the hybrid scale model system are compared in Figure ***3-27***. There is a difference in the steady-state response (Table **3-7**) which is ascribed to the highest thrust coefficient of the scale model; the oscillations for the scale model are slightly less damped than for the full-scale system.

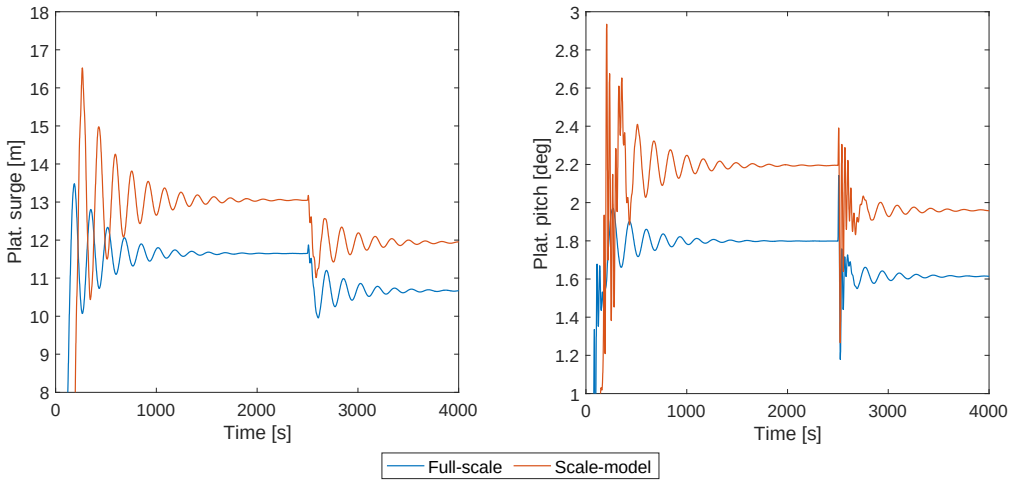

Figure 3-27. Platform surge and pitch response for a 13-14 m/s and 14-15 m/s wind step (the scale-model response is reported at full-scale).

Table 3-7. Percentage difference of the static surge displacement and static pitch rotation in scale-model experiments compared to full-scale.

Wind speed [m/s]	Static surge displacement	Static pitch rotation
13	10,73%	17,97%
14	10,64%	17,65%
15	10,89%	17,80%
16	11,44%	18,24%

HIL coupling

The effect of the HIL coupling system (measurement of the tower base forces and motion control) must be assessed comparing the platform response obtained from a simulation based on the stand-alone HIL numerical model, to the platform response obtained from an equivalent HIL simulation in still-air. Given the absence of experimental data for the floating concepts of this work, the effect of the HIL coupling system is evaluated with reference to a previous test campaign that was carried out within the EU H2020 LIFES50+ project. The aim of the wind tunnel experiment was to investigate the global dynamics of the floating system formed by the DTU 10MW and the OO-Star Wind Floater semisubmersible (Müller, Lemmer, & Yu, 2013). The experiment used the setup described in Section ***3.1***.

The platform surge and pitch response in a surge and pitch free-decay test for the numerical simulation and HIL simulation is reported in Figure ***3-28***. The corresponding dynamic properties for the two platform modes are reported in Table ***3-8***.

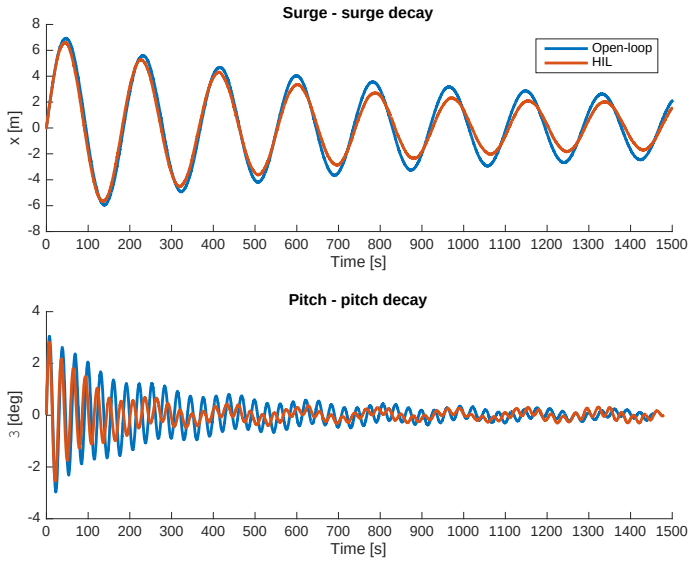

Figure 3-28. Surge and pitch DOFs response for a surge and pitch free-decay test. Comparison between stand-alone numerical simulation (Open-loop) and HIL simulation (HIL).

Table 3-8. Decay analysis for free-decay surge and pitch tests. The stand-alone numerical simulation (OL) is compared to the HIL simulation (HIL) in terms of natural period T_n and relative damping coefficient for the platform surge and pitch modes.

	Surge		Pitch	
	OL	HIL	OL	HIL
T_n [s]	183.5	183.7	31.0	27.9
Rel. Damping [-]	2.15E-02	2.97E-02	1.84E-02	2.77E-02

A pink-noise simulation was carried out with the stand-alone numerical model and the HIL system. Zero-degree heading waves were generated according to a pink noise spectrum of frequency 0.003-0.05 Hz. The FRF between the wave elevation and the platform surge, heave and pitch motions, which is shown in Figure ***3-29***, is examined. The FRF amplitude is coincident with the response amplitude operator (RAO) for the above-mentioned platform motions. The analysis is limited to three platform DOFs being the response of the others negligible for 0° waves.

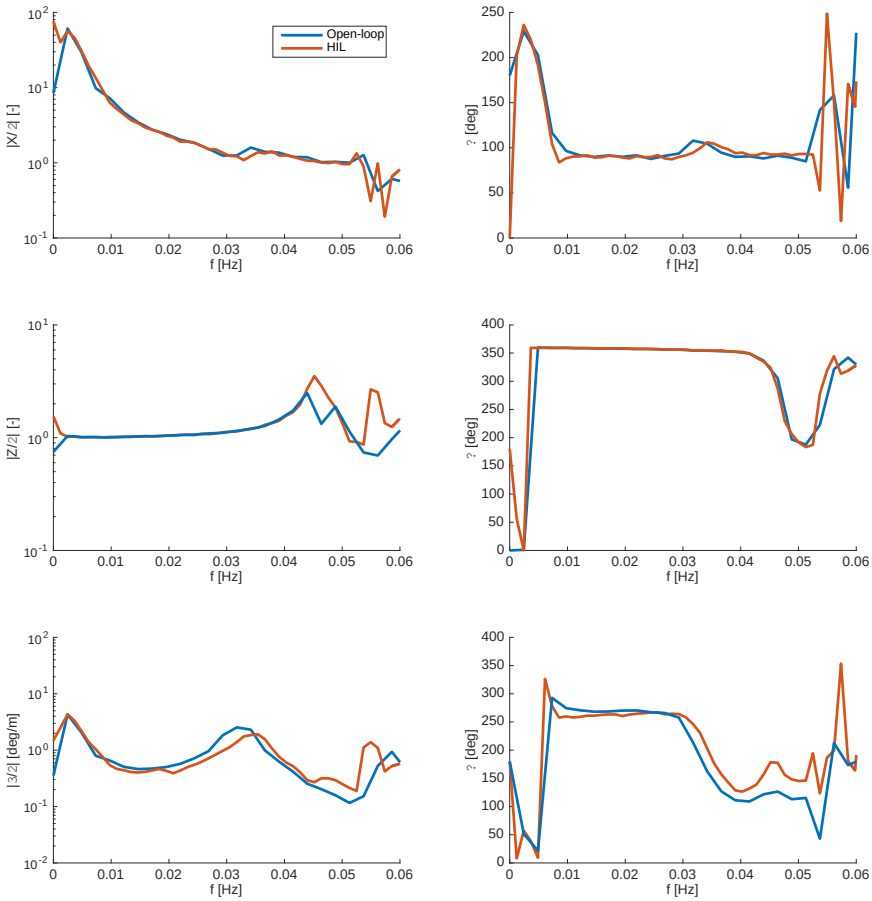

Figure 3-29. Frequency response function (amplitude left column, phase right column) between the wave elevation and the platform surge, heave and pitch response based on pink-noise zero-degree waves. Comparison between numerical simulation (Open-loop) and HIL simulation (HIL).

The HIL coupling has some effects on the dynamics of the floating platform, which are almost negligible except for the pitch motion. The pitch HIL coupling modifies the pitch DOF frequency and damping, which is slightly higher than in the numerical simulation.

3.4 Suggested usage of HIL scale-model experiments

Scale model tests are needed in order to evaluate the hydrodynamic performance of the platform under waves, currents and wind action, as well as to assess the forces over the mooring system and the tendons. Furthermore, these tests are useful in the calibration of hydrodynamic numerical models, allowing their validation for different configurations.

3.4.1 Validation of numerical models

Due to scaling effects and other inevitable differences between the scaled model and the full-scale floating offshore wind turbine, (DNVGL-RP-0286, 2018) recommends to base the model validation on consideration of two separate numerical models: one representing the desired design at full scale ("design model"), the other representing the experimental model at full-scale ("model of the model"). Comparisons between the experiment and numerical model should be done with the "model of the model". When validating numerical models with this approach, conclusions for the "design model" should be drawn with caution based on the conclusions valid for the "model of the model".

Hybrid experiments allow to assess the code prediction capability only with respect to the part of the system that is emulated by means of hardware in the HIL simulator. Moreover, it is advisable that the same numerical model is used in the HIL simulator and in the code to be validated.

3.4.2 Direct assessment of new concepts

If a concept that has been model tested is altered, two possibilities arise:

- If a numerical model that has been calibrated by the first model test results exists and it is proven to be valid also after the concept has been altered, numerical simulations are to be preferred for the assessment of the new concept. Remark: Nonlinear hydrodynamic effects may alter significantly if geometrical changes to the model are significant or the water depth change (DNVGL-RP-0286, 2018).
- Else, a new experimental scale-model test campaign should be carried out.

Usually it is too expensive to test all the conditions required for the assessment of a new concept. Thus, it is preferable to test only the most critical conditions, or those for which the uncertainty of numerical simulations is the highest, and then rely on a calibrated/validated comprehensive model to assess all the other conditions.

3.4.3 Limitations

A challenge with real-time hybrid testing relates to the complexity of the control system used to connect the physical model to the numerical simulation. Actuators may have a physical limitation to emulate high frequency loads and motions. The capacity of the actuators to produce load/motion variations at frequencies and in the range of amplitude that are important for the behaviour of the considered floater should be verified.

Moreover, there are limitations specific for the test facility:

- in wave tank tests, the basin size required to model catenary lines properly can limit the possible scale of the test unless truncation is applied;
- in wind-tunnel tests, the wind-tunnel cross section size can limit the emulation of the wind turbulence component related to large-scale vortices; moreover, if the area of the cross-section occupied by the rotor is large, blockage effects may occur.

3.5 How to combine scale-model data from different methodologies

Real-time hybrid model testing of floating offshore wind turbines can be defined by two substructures: one physical and one numerical, where one aims to reproduce the system hydrodynamics and the other aims to simulate the aerodynamic part of the system. During hybrid model testing of a floating wind turbine in a hydrodynamic facility, the hydrodynamic loads are physical, while the aerodynamic loads are numerical; the opposite will be true for HIL model testing in a wind tunnel. For hybrid ocean basin tests, position sensing is used as input to the numerical model; while for HIL wind tunnel tests, force sensing is the input to the numerical substructure.

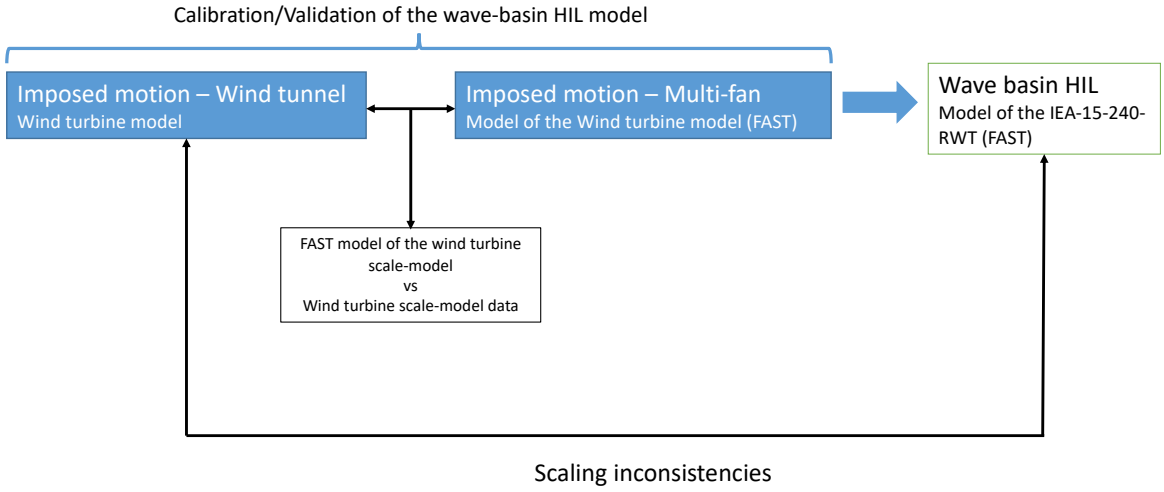

Figure 3-30. Flow-chart of the calibration/validation procedure that must be carried out before wave tank experiments.

(Thys, Fontanella, Taruffi, Manjock, & Belloli, 2019) recommended the procedure illustrated in Figure ***3-30***, which suggests how to perform hybrid scale model experiments with a floating wind turbine combining wind tunnel and ocean basin activities:

1. **Performing HIL model tests in a wind tunnel** for the validation of the aerodynamic model that will be used in the ocean basin tests. For the verification, wind tunnel tests with a physical wind turbine connected to a 6 DOF actuators controlled by real-time simulations of the floating platform subject to hydrodynamic loads, are necessary.

2. **Performing real-time hybrid model tests in an ocean basin**, using the previously validated aerodynamic model. The tests with a physical model of the floating wind turbine without the rotor geometry, coupled to a force actuator controlled by the simulated aerodynamic loads, are used for calibration of the platform and hydrodynamic model as well as for final verification.

Ideally, additional iterations of the process would be preferred, but could be difficult to realise, since costly and time taking. Consequently, we propose a common strategy to combine different methodologies from wind tunnel and wave tank HIL scale-model experiments in order to tackle the problems related to the scalability of the dynamic environmental loads. Previously to commencement of the testing campaign planned for analysing the performance of the structures under relevant conditions, calibration tests of every environmental condition to be used in the tests as well as model characterization tests are to be carried out.

3.5.1 Calibration for the HIL wave tank experiments

Environmental calibration tests will begin simulating the wind, with the absence of the model, in a wind tunnel facility.

Calibration of the reduced-order model for the wave tank HIL

The aerodynamic model that simulates the wind turbine in wave tank experiments must be calibrated against experimental data. To ease the procedure, a simplified motion and load condition is considered. A steady and uniform wind is considered, the wind turbine is forced to move in the surge direction only. The surge motion is selected because it causes a large and uniform variation of the wind speed seen by the rotor. In detail, the surge motion is mono-harmonic

$$\mathrm{x} = \mathrm{A}\sin(2\pi \mathrm{f} \mathrm{t}) \tag{33}$$

where A and f are the amplitude and frequency of motion respectively.

Several mono-harmonic motions must be investigated, which are obtained from the combination of different values of amplitude and frequency. Frequencies should be selected in the low-frequency range for the platform designs, as large motions are expected in this range of frequencies, where the rigid-body motion modes of the floating platform are excited in resonance. The maximum frequency must be limited to avoid exciting the first tower fore-aft flexible mode.

Different amplitudes must be tested for each combination of frequency and mean wind speed. The values of amplitude are selected based on the maximum surge velocity

$$\max(\dot{\mathrm{x}}) = \Delta \mathrm{V} = 2\pi \mathrm{f} \mathrm{A} \tag{34}$$

Having defined

$$\Delta \mathrm{V}^{*} = \frac{\Delta \mathrm{V}}{\mathrm{V}} \tag{35}$$

The amplitude values are selected to achieve, for any pairing of wind speed and motion frequency, a given value of $\Delta \mathrm{V}^{*} \ll 1$.

Calibration of the multi-fan system

Once we have calibrated and validated the aerodynamic model, we proceed to calibrate the multi-fan system **to reproduce the measured aerodynamic loads on the RNA in the wave basin facility**. The multi-fan system used for simulating the wind is to be calibrated in dry conditions. The calibration allows to limit the error of the generated thrust at less than 3% of the target value. This calibration consists on the following steps:

- Fixed multi-fan thrust calibration: the multi-fan is mounted on a fixed tri-axial load cell. Calibration on the thrust applied by the multi-fan is to be carried out.
- Dynamic multi-fan thrust calibration: the multi-fan is mounted on the tri-axial load cell. The load cell is mounted on a hydraulic actuator which moves the assembly back and forth following a sinusoidal signal programmed. Calibration on the thrust applied by the multi-fan is to be carried out.

3.5.2 Calibration for the HIL wind-tunnel experiments

The calibration of the HIL numerical model used in wind-tunnel experiments requires to run several characterizations tests in the wave tank.

Floating platform and mooring system characterization tests

Characterization tests are a set of essential trials to know the platform scale-model properties as well as the platform and mooring system response. Table ***3-9*** outlines the parameters obtained from each characterization test.

- Firstly, tilts tests are to be carried out in still-water to evaluate the initial stability of the structure and to obtain its GM. Tilt tests in roll and pitch movement are to be performed, with ballast located on the floating structure in a specific position and by measuring the angle of heel.
- Secondly, decay tests shall be conducted to obtain decay curves for the free condition (for heave and pitch/roll) unaffected by mooring. Decay curves will output damping (linear and non-linear, separately) and natural periods of the model. Minimum of 5 iterations of each tests are to be carried out to obtain the best approach filtering possible human errors during execution. The rest of DOFs shall be kept as much still as reasonably possible. They shall be monitored to discard any potential coupling during the execution.
- Thirdly, static offset tests shall be carried out to verify the stiffness of the soft-mooring arrangement, whose springs will have been independently calibrated. Tests shall be performed with all the different soft-mooring arrangements to be used during test campaign. Motions and forces will be simultaneously measured for this aim.
- Finally, decay tests shall be conducted again to obtain decay curves for the condition with soft mooring (this time for all 6 degrees of freedom).

Table 3-9. Summary of characterization wave tank tests.

Tests	Configuration	Results
Tilt tests	Roll	Metacentric height and GZ curve
	Pitch	Metacentric height and GZ curve
Decay tests	Without Mooring System (Heave, Roll, Pitch)	Natural periods
		Non-dimensional damping coefficient
	With Mooring System (6 DOF)	Natural periods
		Non-dimensional damping coefficient
Static offset tests	0° (positive Surge)	Platform + Mooring system stiffness
	90° (negative Sway)	Platform + Mooring system stiffness
	180° (negative Surge)	Platform + Mooring system stiffness

Calibration of the reduced-order model for the wind tunnel HIL

Once we have calibrated and validated the hydrodynamic model, we proceed to calibrate the HexaFloat actuation system to reproduce the measured movements on the base of the tower in the wave tank facility. The 6-DOFs parallel kinematic robot used for simulating the waves is to be calibrated in still-air conditions, while the wind turbine scale-model is mounted to this mechanism by means of a 6-components load-cell to measure the forces at the base of the tower.

3.5.3 Calibration of environmental conditions

Previously to the tests, calibration tests of every environmental conditions are to be carried out. Calibration is required to allow the comparison of scale-model test results from the two hybrid experiments, as shown in Figure ***3-31***.

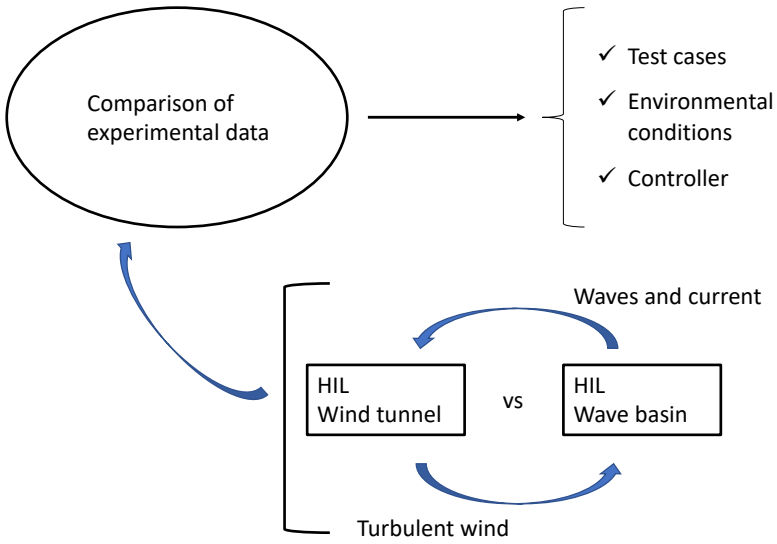

Figure 3-31. Comparison of scale-model test data from the wave tank and wind-tunnel hybrid experiments.

Calibration tests are performed in absence of the model in the basin in order to avoid disturbances.

Wave tank

Calibration is required for:

- Irregular waves associated to Severe Sea State (SSS) and Extreme Sea State (ESS). A free surface sensor array is installed at the control position during calibration as well as during testing. Two arrays composed of seven wave resistive wave gauges are installed during the calibration tests. One of these is located at the reference origin of the physical model and is removed after the calibration tests. The second array, located on the left of the basin, is kept in place during the rest of the tests. The comparison between the measurements performed at the reference location during the wave calibration tests, and measurements at the same reference location during the physical modelling tests, provides an indication of the test repeatability and, thus, a confirmation of the local incident wave conditions at the structure. During model testing, the control array (wave gauges and current sensors) is placed at the same position than during the calibration tests, meanwhile the physical model is located at the centre of the ocean basin.
- Current velocities. The current speed is measured by means of an Acoustic Doppler Current Profiler (ADCP), which is only installed during the calibration phase. The calibrated current is replicated during the tests.

Wind tunnel

- The vertical profile of the average wind speed and three-component turbulence at the scale model location is measured with an automatic traversing system mounting three-components velocity sensors (multi-hole probes or hot-wire anemometers). Calibration is repeated for any wind condition.

4 MOORING AND CABLE SYSTEM INTEGRATION: TRUNCATION METHODS FOR VERY DEEP WATERS OR LARGE FOOTPRINTS

Inside innovative experimental testing procedures, this chapter is focused on the analysis truncation methods to be applied on the Floating Offshore Wind Turbine (FOWT) testing to maximize the size of the tests and reduce potential scale effects. Two different testing barriers will be faced: depth and footprint. Based on numerical methods, the uncertainty of the methodology proposed will be assessed and included on the resulting best practices.

4.1 Motivation

Increasing demand for offshore wind energy is driving to exploit this resource in waters deeper than 60 m and lead to the deployment of floating offshore wind turbines. Testing this emerging technology in ocean basins is an important step in the design process to reduce risks and validate numerical simulations. However, worldwide ocean basins are not deep enough to simulate floating offshore platforms at reasonable model scales, larger than 1:100 (Luo & Baudic, 2003), to obtain reliable physics that govern the system behaviour. These limitations related to footprint size or water depth may be solved by performing an equivalent truncation method to reduce the mooring system size, maintaining the physical characteristics of the original one.

This way, the truncation procedures allow large scale test in the basin, reducing the scale effects which influence the representability of the physics that govern the system behaviour. The truncation method consists in designing a truncated system set-up using a numerical tool and validating it against model tests performed with this truncated mooring system. Then, the resulting calibration is used in full-depth numerical simulations in operational conditions, to assess the behaviour of the full-depth mooring system.

4.2 Objectives

This chapter is intended to provide a methodology to perform mooring truncations in wave tank tests addressing modelling limitations related to water depth and mooring footprint size. Most of the methodologies already implemented and validated are focused on solving limitations related to the footprint size. Moreover, most of the methodologies are focused on a generic offshore structure (Oil & Gas). The methodology to be developed is intended to address at the same time restrictions related to the footprint size and water depth, and specifically designed for floating offshore wind turbines.

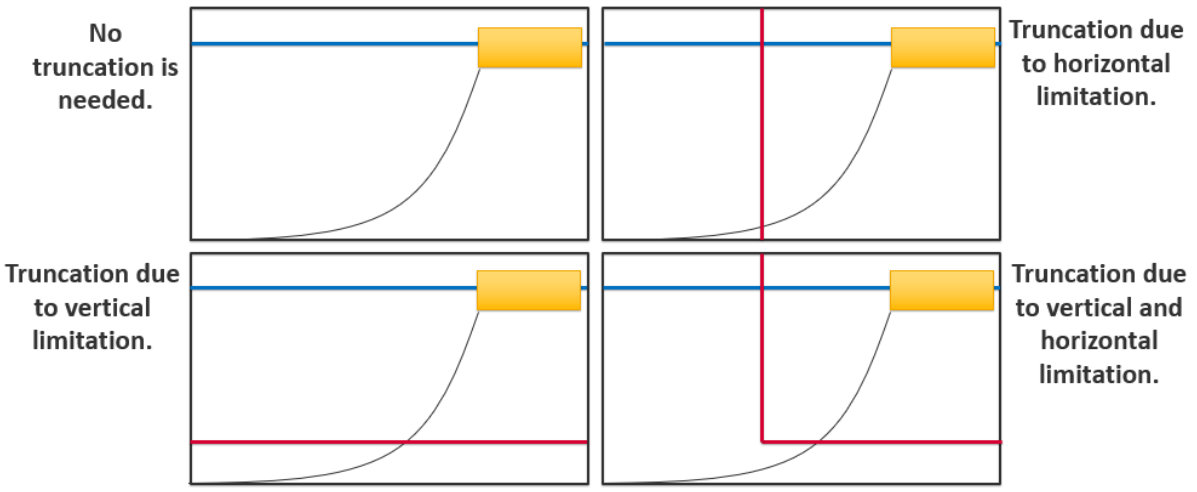

Figure 4-1. Static offset for an objective and a truncated line for very deep waters or large footprints.

In order to achieve this main goal, a series of **specific objectives challenging for floating offshore wind energy**, are proposed:

- Represent first-order behaviour.
- Represent second-order dynamics.
- Maintain natural periods of linear and non-linear damping.
- Study the effect of wind and the influence of wind turbine.

4.3 Methodology of comparative analysis

The truncation methodology is based in the numerical modelling of the mooring lines, and a brief description of the available numerical models is required to fully understand the truncation steps.

4.3.1 Mooring lines modelling

The motion of a submerged line can be described by means of non-linear equations that must be solved numerically. This can be done with a quasi-static model, which are based on the catenary line and ignores dynamic effects on the line, or with a dynamic model, based on the solution of the line differential equation with a Finite Element Method (FEM) and that captures dynamic effects such as the shock loads. Both approaches are described in detail below.

In the field of offshore floating wind turbines, the influence of mooring system has been documented in several studies. In (Matha, Bischoff, Fetcher, & Kuhn, 2011) the quasi static model predicts higher platform motions than the dynamic one, and in (Masciola, Robertson, Jonkman, Coulling, & Goupee, 2013b) it is showed that platform motions are influenced by mooring dynamics only in extreme sea states but that mooring dynamics are fundamental in the prediction of loads in all load cases.

Quasi-static models

Simplified modelling approaches exist that focus on the calculations of the forces exerted by lines on a floating object. Among them, the quasi-static method assumes a static model of the chain, that is resolved at each time step of the simulation using the catenary line equations, given the position of the fairlead, and considering that the line is contained in a vertical plane:

$$\mathbf{x}(\mathbf{H_F},\mathbf{V_F}) = \frac{\mathbf{H_F}}{\boldsymbol{\omega}}\left[\ln\left(\frac{\mathbf{V_F}}{\mathbf{H_F}}+\sqrt{1+\left(\frac{\mathbf{V_F}}{\mathbf{H_F}}\right)^2}\right)-\ln\left(\frac{\mathbf{V_F}-\boldsymbol{\omega}\mathbf{L}}{\mathbf{H_F}}+\sqrt{1+\left(\frac{\mathbf{V_F}-\boldsymbol{\omega}\mathbf{L}}{\mathbf{H_F}}\right)^2}\right)\right]+\frac{\mathbf{H_F}\mathbf{L}}{\mathbf{EA}} \quad (36)$$

$$\mathbf{z}(\mathbf{H_F},\mathbf{V_F}) = \frac{\mathbf{H_F}}{\boldsymbol{\omega}}\left[\sqrt{1+\left(\frac{\mathbf{V_F}}{\mathbf{H_F}}\right)^2}-\sqrt{1+\left(\frac{\mathbf{V_F}-\boldsymbol{\omega}\mathbf{L}}{\mathbf{H_F}}\right)^2}\right]+\frac{1}{\mathbf{EA}}\left(\mathbf{V_F}\mathbf{L}-\frac{\boldsymbol{\omega}\mathbf{L}^2}{2}\right) \quad (37)$$

where $x(H_F, V_F)$ and $z(H_F, V_F)$ are, respectively, the horizontal and vertical spans of the line, H_F and V_F are the horizontal and vertical tensions at the fairlead, L is the length of the line, ω is the underwater linear weight of the line, E is the Young's modulus of the line and A is the line section. These equations are written for the case where the line does not lie on the sea bottom, but they can be rewritten to add that boundary condition, as shown in (Faltinsen, 1999). An iterative method is required to find the solution of the non-linear catenary equations. The hydrodynamic drag and added mass, together with cable inertia are neglected. The main benefit of this model is that it can achieve a high computational efficiency (Masciola, Jonkman, & Robertson,

Implementation of a multisegmented, Quasi-Static cable model, 2013a). The main drawback of this approach is that the dynamics of the line greatly affects its loading, and as a consequence this approach is inaccurate in predicting loads in the mooring system. It is also hard to implement quasi-static models for complex lines configurations which include line sections of different properties, clump weights, risers, or crowfoot lines (also known as delta lines or "Y" shaped lines).

Dynamic models

A dynamic model instead considers the dynamic characteristics of the line, and includes inertia, viscous drag and added mass, at the expenses of increased complexity of the model. A dynamic model accounts for the propagation of longitudinal and transverse vibrations, which is accomplished by solving the wave equation

$$\omega \frac{\partial \mathrm{r}(\mathrm{s},\mathrm{t})}{\partial \mathrm{t}^2} = \frac{\partial \mathrm{F}(\mathrm{s},\mathrm{t})}{\partial \mathrm{s}} + \mathrm{f}(\mathrm{s},\mathrm{t}) \left|\frac{\partial \mathrm{r}}{\partial \mathrm{s}}\right| \qquad (\textbf{\textit{38}})$$

where $s \in [0, L]$ is the arc-length parameter, t is time, $\mathrm{r} \in \mathbb{R}^3$ is the position of the line in space, $\mathrm{F} \in \mathbb{R}^3$ is the internal force in the line, which usually includes only axial tension and internal damping, but can also include bending and torsion effects which could be important for cables, see (Escalante, Sampaio, Rosales, & Ritto, 2011) and (Tahar & Kim, 2008). Finally, $\mathrm{f} \in \mathbb{R}^3$is the external force on the line per unit of length, and is composed by the sum of several forces such as gravity, buoyancy, hydrodynamic damping and added mass, or sea-floor contact forces. For the sea-floor forces, the dynamic models present a significant advantage since they allow to implement the dynamic friction effects for different sea-floor materials and bathymetries, see (Barrera C. , Guanche, Losada, Armesto, & Dolores, 2018) and (Jaiswal, Vishnubhotla, Cole, Gordon, & Sharma, 2016). Several boundary conditions can be easily imposed to this equation, including line-to fairlead, line-to-anchor or line-to-line joints, risers, and clump weights.

A common way to solve dynamic models is the lumped mass approximation, where the cable is discretized as in a FEM approach and the mass of each element is lumped at the two end nodes. Examples of this approach are reported in (Azcona, Munduate, Gonzalez, & Nygaard, 2017; Hall & Goupee, 2015). Several other FEM models without lumped elements can also be used, as presented in (Aamo & Fossen, 2000), and also higher order FEM models with high accuracy at shock loads prediction, see (Palm, Moura Paredes, Eskilsson, Taveira Pinto, & Bergdahl, 2013). Although it is computationally expensive, this is the approach most suited for the calculation of loads in the mooring systems.

4.3.2 Static truncation

The objective for the static truncation is to replicate the static force-deformation or static offset curves computed for the real line. In other words, the fairlead is imposed to a constant position and the tension at the fairlead is computed considering that the line is at rest, using a quasi-static model. This is done for the reference position of the mooring line, using the fairlead position with the platform at rest and also for some offset positions along the horizontal and vertical axis. The vertical and horizontal forces of the line are considered. The static offset for an objective and a truncated line is shown in *Figure **4-1***, where the horizontal axis shows horizontal or vertical offsets for the first and second columns, respectively, and the vertical axis shows horizontal and vertical force for the first and second rows, respectively.

Considering the four curves shown in the *Figure **4-2***, the mean of the four "mean square normalized errors", shown in Equation 39, is considered as the objective function to minimize for the static truncation. In this equation, the sub-index "o" stands for objective line and the subindex "t" stands for truncated line, also, $F_x(x,z)$ and $F_z(x,z)$ are horizontal and vertical force at the for a (x,z) offset and n_x and n_z are the number of points along the vertical and horizontal offsets.

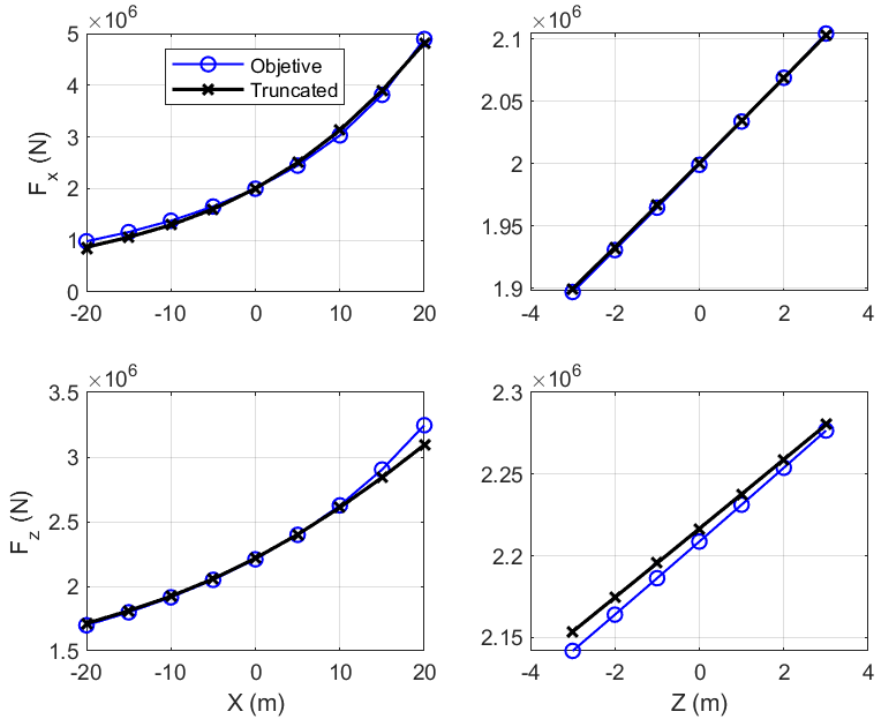

Figure 4-2. Errors of the horizontal (first row) and vertical forces (second row) in the line along the horizontal (first column) and vertical axis (second column).

$$f = \frac{1}{4}\cdot\left[\frac{1}{n_x}\sum_{i=1}^{n_x}\left(\frac{F_{x,t}(x_i,0)-F_{x,o}(x_i,0)}{F_{x,o}(0,0)}\right)^2+\frac{1}{n_x}\sum_{i=1}^{n_x}\left(\frac{F_{z,t}(0,x_i)-F_{z,o}(0,x_i)}{F_{z,o}(0,0)}\right)^2\right.$$
$$+\frac{1}{n_z}\sum_{i=1}^{n_z}\left(\frac{F_{x,t}(0,z_i)-F_{x,o}(0,z_i)}{F_{z,o}(0,0)}\right)^2 \qquad (39)$$
$$\left.+\frac{1}{n_z}\sum_{i=1}^{n_z}\left(\frac{F_{z,t}(0,z_i)-F_{z,o}(0,z_i)}{F_{z,o}(0,0)}\right)^2\right]$$

The truncated line variables that can be modified in order to solve the minimization problem are the following:

- Anchor position
- Line length
- Line properties
- Anchor spring stiffness and properties.
- Number of intermediate weights/floaters.
- Position of the intermediate bodies.

In order to simulate complex mooring lines with intermediate bodies and springs, the quasi-static methods are used for each line segment and the equilibrium positions of the segment's ends are found with iterative non-

linear systems solvers. Some of these variables are discrete, such as the number of intermediate bodies or the properties of the line (chosen out of a catalog). Also, the objective function can be noisy due to convergence problems with the quasi-static method. For these reasons, the optimization solver used in this case is a constrained genetic algorithm that can find several local minimums of the objective function. The genetic algorithm, implemented in MATLAB, is hybridized with a pattern search algorithm, to improve the solutions found (Goldberg, 1989) (Audet, 2003). Previous experience in line truncation is used to create an appropriate initial population.

To test this first step of the truncation, we design the static equivalent truncated mooring line to be fitted inside the Cantabria Coastal and Ocean Basin (CCOB). For this FIHAC facility with 30 m length, 44 m width and 3 m depth, an appropriate length scale is 1/40. Catenary mooring lines of the Activefloat platform have a length of 614 m (557.5 m footprint and 185 m depth). At the Site B (Gran Canaria), we have modelling limitations related to water depth of 200 m.

In order to replicate the real axial stiffness of the prototype, we place two calibrated springs at the anchor whose stiffnesses are added to the one from the mooring line. Besides, three clump weights are also included in the truncated mooring line. *Figure **4-3*** shows the resulting truncation design of the static load optimisation for a single mooring line. The restoring force of a single mooring line as a function of platform surge displacement is represented in *Figure **4-4***.

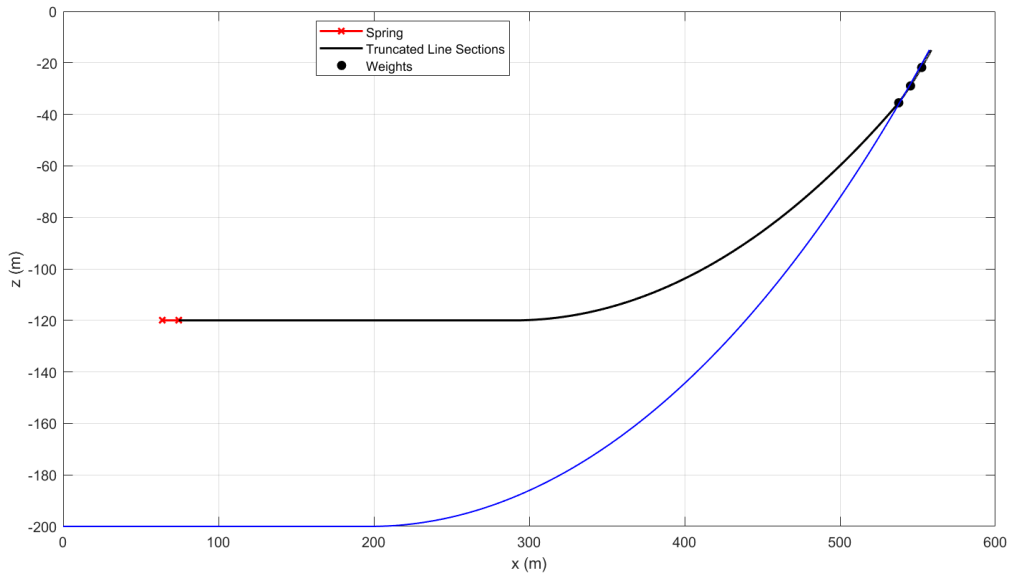

Figure 4-3. Truncation design of catenary mooring line.

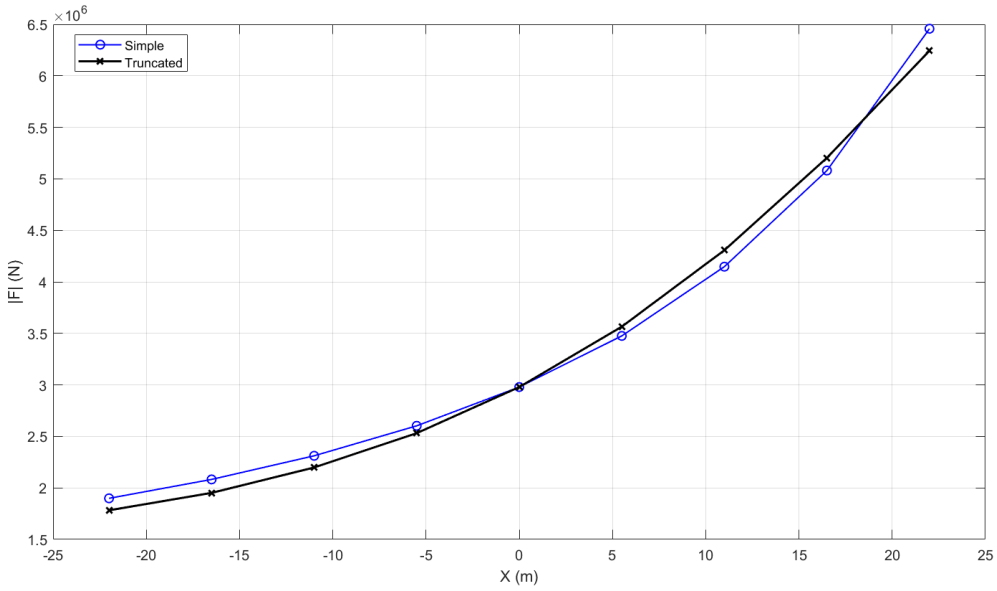

Figure 4-4. Force-displacement curve.

The discrepancies due to the truncation procedure imply uncertainties that will require to be assessed by means of an uncertainty analysis.

4.3.3 Dynamic and full system truncation

The static truncation technique presented can yield many more than only one candidate for the best truncated line. Usually, the best candidate is chosen, but it is observed that many of the candidates present small static discrepancies with the objective line. For this reason, for the dynamic truncation, all the candidates that present a satisfactory static offset, with different numbers of intermediate bodies or configurations, are considered for the dynamic truncation. The methodology is based in imposing regular and irregular forced oscillations on the fairlead and simulating the real line, and the truncated line candidates with the dynamic models, and comparing the observed mean peak tensions.

The candidates with least dynamic discrepancies are chosen. If there are still more than one good candidates, these are finally tested in the full mooring system simulation, where both the platform movements and the lines loads are compared in order to choose the best candidate. If at the end there is a doubt among different candidates, the simpler option is chosen, since it will be easier to set up in the lab and the uncertainties will be smaller.

5 REFERENCES

Aamo, O., & Fossen, T. (2000). Finite element modelling of mooring lines. *Mathematics and Computers in Simulation, 53*(4-6), 415-422.

Argyros, A., Langley, R. S., & Ahilan, R. V. (2011). Simplifying mooring analysis for deepwater systems using truncation. *Proceedings of the 21st International Offshore and Polar Engineering Conference.* Maui, IH, USA.

Audet, C. a. (2003). Analysis of Generalized Pattern Searches. *SIAM Journal on Optimization*, 889-903.

Azcona, J., Bouchotrouch, F., Gonzalez, M., Garciandia, J., Munduate, X., Kelberlau, F., & Nygaard, T. A. (2014a). Aerodynamic thrust modelling in wave tank tests of offshore floating wind turbines using a ducted fan. *Journal of Physics: Conference Series*(524).

Azcona, J., Bredmose, H., Campagnolo, F., Manjock, A., Pereira, R., & Sandner, F. (2014b). *D4.22: Methods for performing scale-tests for method and model validation of floating wind turbines.* INNWIND.EU.

Azcona, J., Munduate, X., Gonzalez, L., & Nygaard, T. A. (2017). Experimental validation of a dynamic mooring lines code with tension and motion measurements of a submerged chain. *Ocean Engineering, 129*, 415-427.

Baarholm, R., Fylling, I., Stansberg, C. T., & Oritsland, O. (2006). Model testing of ultra-deepwater floater systems: Truncation and software verification methodology., *1*, págs. 527–537. Hamburg (Germany). doi:10.1115/OMAE2006-92492

Barrera, C., Battistella, T., Guanche, R., & Losada, I. J. (2020a). Mooring system fatigue analysis of a floating offshore wind turbine. *Ocean Engineering, 195*, 1–17. doi:10.1016/j.oceaneng.2019.106670

Barrera, C., Guanche, R., & Losada, I. J. (2019a). Experimental modelling of mooring systems for floating marine energy concepts. *Marine structures*(63), 153-180.

Barrera, C., Guanche, R., Losada, I., Armesto, J., & Dolores, D. (2018). Numerical and experimental modelling of mooring systems: effects of wave groupiness on extreme loads. *Proceedings of the ASME 2018 37th International Conference on Ocean, Offshore and Arctic Engineering*.

Barrera, C., Guanche, R., Rodríguez, Á., Armesto, J. A., & Losada, I. J. (2020b). On the importance of mooring system parametrisation for accurate floating structure designs. *Marine Structures, 72*. doi:10.1016/j.marstruc.2020.102765

Barrera, C., Losada, I. J., Guanche, R., & Johanning, L. (2019b). The influence of wave parameter definition over floating wind platform mooring systems under severe sea states. *Ocean Engineering, 172*, 105–126. doi:10.1016/j.oceaneng.2018.11.018

Battistella, T., Meseguer, A., & Guanche, R. (2019). Real time hybrid model testing including complex aerodynamic loading for TRL+ project. *Poster of the Offshore Wind Europe 2019.* Copenhagen (Denmark).

Battistella, T., Paradinas, D. D., M, U. A., & G, G. R. (2018). High fidelity simulation of multi-MW rotor aerodynamics by using a multifan. *Proceedings of the ASME 2018 37th International Conference on Ocean, Offshore and Arctic Engineering.* Madrid, Spain.

Bayati, I., Facchinetti, A., Fontanella, A., Giberti, H., & Belloli, M. (2018). A wind tunnel/HIL setup for integrated tests of floating offshore wind turbines. *Journal of Physics: Conference Series*(1037).

Bayati, I., Facchinetti, A., Fontanella, A., Taruffi, F., & Belloli, M. (2020). Analysis of FOWT dynamics in 2-DOF hybrid HIL wind tunnel experiments. *Ocean Engineering*(195).

Belloli, M., Bayati, I., Facchinetti, A., Fontanella, A., Giberti, H., La Mura, F., . . . Zasso, A. (2020). A hybrid methodology for wind tunnel testing of floating offshore wind turbines. *Ocean Engineering, 210*. doi:10.1016/j.oceaneng.2020.107592

Bergdahl, L., Palm, J., Eskilsson, C., & Lindhal, J. (2016). Dynamically scaled model experiment of a mooring cable. *Marine Science and Engineering*.

Bredmose, H., Larsen, S. E., Matha, D., Rettenmeier, A., & Marino, E. S. (2012). *Collation of offshore wind-wave dynamics.* MARINET.

Bredmose, H., Rinker, J., Skrzypinski, W., Zahle, F., Meng, F., Dykes, K., . . . Shields, M. (2019). *COREWIND D1.1: Definition of the 15MW Reference Wind Turbine.* Tech. rep., DTU, NREL.

Chabaud, V., Steen, S., & Skjetne, R. (2013). Real-time hybrid testing for marine structures: challenges and strategies. *Proceedings of the ASME International Conference on Ocean, Offshore and Arctic Engineering.* Nantes.

Chakrabarti, S. (1998). Physical model testing of floating offshore structures. *Proceedings of the Dynamic Positioning Conference.* Houston (TX, USA).

Desmond, C. J., Hinrichs, J. C., & Murphy, J. (2019). Uncertainty in the physical testing of floating wind energy platforms' accuracy versus precision. *Energies, 12*. doi:10.3390/en12030435

DNVGL-RP-0286. (2018). *Coupled analysis of floating wind turbines.*

Escalante, M., Sampaio, R., Rosales, M., & Ritto, T. (2011). A reduced order model of a 3D cable using proper orthogonal decomposition. *Asociación Argentina de Mecánica Computacional, XXX*, 1143-1158.

Faltinsen, O. (1999). *Sea loads on ships and o.* Cambridge ocean technology series.

Fan, T., Qiao, D., & Ou, J. (2012). Optimized design of equivalent truncated mooring system based on similarity of static and damping characteristics., (págs. 959–966).

Fan, T., Qiao, D., & Ou, J. (2014). Innovative approach to design truncated mooring system based on static and damping equivalent. *Ships and Offshore Structures, 9*, 557–568. doi:10.1080/17445302.2013.867631

Fan, T., Qiao, D., Yan, J., Chen, C., & Ou, J. (2017). An improved quasi-static model for mooring-induced damping estimation using in the truncation design of mooring system. *Ocean Engineering, 136*, 322–329. doi:10.1016/j.oceaneng.2016.05.042

Ferreira, F. M., Lages, E. N., Afonso, S. M., & Lyra, P. R. (2016). Dynamic design optimization of an equivalent truncated mooring system. *Ocean Engineering, 122*, 186–201. doi:10.1016/j.oceaneng.2016.06.021

Fowler, M. J., Goupee, A. J., Allen, C., Viselli, A., & Dagher, H. (2017). 1:52 scale testing of the first commercial scale floating wind turbine, VolturnUS: testing overview and the evolution of scale model testing

methods. *Proceedings of the ASME International Conference on Ocean, Offshore and Arctic Engineering.* Trondheim.

Goldberg, D. E. (1989). *Genetic Algorithms in Search, Optimization & Machine Learning.* Addison-Wesley.

Guanche, R., Vidal, C., Piedra, A., & Losada, I. J. (2011). IDERMAR METEO: Offshore wind assessment at high and very high water depths. *Proceedings of the OCEANS 2011 IEEE - Spain.* Santander (Spain). doi:10.1109/Oceans-Spain.2011.6003525

Guyedon, S., Lindeboom, R., van Kampen, W., & de Ridder, E. J. (2018). Comparison of two wind turbine loading emulation techniques based on tests of a TLP-FOWT in combined wind waves and current. *Conference proceedings of the ASME International Offshore Wind Technical Conference IOWTC2018.* San Francisco.

Hall, M., & Goupee, A. (2015). Validation of a lumped-mass mooring line model with DeepCwind semisubmersible model test data. *Ocean Engineering, 104*, 590-603.

Hall, M., Goupee, A., & Jonkman, J. (2018). Development of performance specifications for hybrid modeling of floating wind turbines in wave basin tests. *Journal of Ocean Engineering and Marine Energy, 4*. doi:10.1007/s40722-017-0089-3

Hughes, S. A. (1993). *Physical models and laboratory techniques in coastal engineering.* doi:10.1142/2154

IEC 61400-3. (2009). *Wind turbines — Part 3: design requirements for offshore wind turbines.* Geneve (Switzerland). doi:10.1021/es0620181

Jaiswal, V., Vishnubhotla, S., Cole, S., Gordon, R., & Sharma, P. (2016). Impact of Bathymetry on the Mooring Design of an Offshore Floating Unit. *Proceedings of the ASME 2016 35th International Conference on Ocean, Offshore and Arctic Engineering., 1*.

Ji, C., & Xu, S. (2014). Verification of a hybrid model test method for a deep water floating system with large truncation factor. *Ocean Engineering, 92*, 245–254. doi:10.1016/j.oceaneng.2014.09.047

Jonkman, J. M., & Buhl Jr, M. L. (2005). *FAST user's guide.* Tech. rep., National Renewable Energy Laboratory, Golden (CO, USA).

Jung, H. W., Kim, Y. H., Cho, S. K., Hwang, S. C., & Sung, H. G. (2015). Design of truncated mooring line model in KRISO's deepwater ocean engineering basin. *Journal of Advanced Research in Ocean Engineering, 1*, 227–238. doi:10.5574/JAROE.2015.1.4.227

Kang, Z., Zhang, C., & Sun, L. (2017). Research on truncation method of FPSO and offloading system in model test. *Applied Ocean Research, 67*, 94–108. doi:10.1016/j.apor.2017.06.007

Kim, Y., & Hermansky, G. (2014). Uncertainties in seakeeping analysis and related loads and response procedures. *Ocean Engineering, 86*, 68–81. doi:10.1016/j.oceaneng.2014.01.006

Lie, H., Braaten, H., Kristiansen, T., & Nielsen, F. G. (2007). Free-span VIV testing of full-scale umbilical., (págs. 2764–2771).

Luo, Y., & Baudic, S. (2003). Predicting FPSO responses using model tests and numerical analysis., (págs. 167–174).

Lyons, G. J., Brown, D. T., Cook, H. H., Walls, B., & Barnay, G. (1998). The Foinaven umbilical performance monitoring system - a new approach. Houston (TX, USA).

Ma, G., Wang, H., Sun, L., & Jiang, Y. (2018). Dynamic truncation method for mooring lines with tension estimation combined in the time and frequency domains. *Ships and Offshore Structures, 13*, 310–319. doi:10.1080/17445302.2017.1377049

Ma, G., Zhong, L., Wang, H., Kang, Z., & Sun, L. (2019). Truncation analysis of mooring line based on dynamic similarity with consistent nonlinearity. *Ocean Engineering, 176*, 46–56. doi:10.1016/j.oceaneng.2019.02.027

Mahfouz, M. Y., Salari, M., Hernández, S., Vigara, F., Molins, C., Trubat, P., . . . Pegalajar-Jurado, A. (2020). *COREWIND D1.3: Public design and FAST models of the two 15MW floater-turbine concepts.* Tech. rep., USTUTT, ESTEYCO, UPC, DTU.

Marinet2. (2020). *Offshore wind facilities*. Obtenido de http://www.marinet2.eu/facilities/offshore-wind/

Marta, M., Mueller-Schuetze, S., Ottersberg, H., Isus-Feu, D., Johanning, L., & Thies, P. R. (2015). Development of dynamic submarine MV power cable design solutions for floating offshore renewable energy applications. Paris (France).

Martin, H. R., Kimball, R. W., Viselli, A. M., & Goupee, A. J. (2014). Methodology for wind/wave basin testing of floating offshore wind turbines. *Journal of Offshore Mechanics and Arctic Engineering, 136*. doi:10.1115/1.4025030

Martinelli, L., Lamberti, A., Ruol, P., Ricci, P., Kirrane, P., Fenton, C., & Johanning, L. (2010). Power umbilical for ocean renewable energy systems - feasibility and dynamic response analysis. Bilbao (Spain).

Masciola, M., Jonkman, J., & Robertson, A. (2013a). Implementation of a multisegmented, Quasi-Static cable model. *Proceedings of the 23rd International Offshore and Polar Engineering Conference.* Anchorage, Alaska, USA.

Masciola, M., Robertson, A., Jonkman, J., Coulling, A., & Goupee, A. (2013b). Assessment of the importance of mooring dynamics on the globla response of the DeepCWind floating semisubmersible offshore wind turbine. *Proceedings of the 23rd International Offshore and Polar Engineering Conference.* Anchorage, Alaska, USA.

Matha, D., Bischoff, O., Fetcher, U., & Kuhn, M. (2011). Non-linear Multi-Body mooring system model for floating offshore wind turbines. *EWEA Offshore 2011.* Amsterdam, The Netherlands.

Meseguer, A., & Guanche, R. (2019). Wind turbine aerodynamics scale-modeling for floating offshore wind platform testing. *Journal of Wind Engineering and Industrial Aerodynamics, 186*, 49–57. doi:10.1016/j.jweia.2018.12.021

Molins, C., Trubat, P., Gironella, X., & Campos, A. (2015). Design optimization for a truncated catenary mooring system for scale model test. *Journal of Marine Science and Engineering, 3*, 1362–1381. doi:10.3390/jmse3041362

Müller, K., Lemmer, F., & Yu, W. (2013). *Deliverable D4.2 Public Defininition of Two LIFES50+ 10MW Floater Concepts .*

Muller, K., Sandner, F., Bredmose, H., Azcona, J., Manjock, A., & Pereira, R. (2014). Improved tank test procedures for scaled floating offshore wind turbines. *International Wind Engineering Conference.*

Ormberg, H., Stansberg, C. T., Yttervik, R., & Kleiven, G. (1999). Integrated vessel motion and mooring analysis applied in hybrid model testing. *Proceedings of the 1999 Ninth International Offshore and Polar Engineering Conference*, *1*, págs. 339–346. Brest (France).

Palm, J., Moura Paredes, G., Eskilsson, C., Taveira Pinto, F., & Bergdahl, L. (2013). Simulation of mooring cable dynamics using a discontinuous Galerkin method. *In 5th International Conference on Computational Methods in Marine Engineering, MARINE 2013;*.

Park, D.-M., Kim, Y., & Song, K.-H. (2013). Sensitivity in numerical analysis of parametric roll. *Ocean Engineering, 67*, 1–12. doi:10.1016/j.oceaneng.2013.04.008

Robertson, A. (2017). Uncertainty analysis of OC5-DeepCwind floating semisubmersible offshore wind test campaign. *Proceedings of the International Society of Offshore and Polar Engineers' International Ocean and Polar Engineering Conference.* San Francisco (CA, USA).

Robertson, A. N., Bachynski, E. E., Gueydon, S., Wendt, F., Schünemann, P., & Jonkman, J. (2018). Assessment of experimental uncertainty for a floating wind semisubmersible under hydrodynamic loading. *Proceedings of the ASME 2018 37th International Conference on Ocean, Offshore and Arctic Engineering.* Madrid (Spain).

Robertson, A. N., M, J. J., D, M. M., & P, M. (2013). Summary of conclusions drawn from the DeepCWind scaled floating offshore wind system test campaign. *ASME International Conference on Ocean, Offshore and Arctic Engineering*. Nantes.

Sandner, F., Bredmose, H., Jose, A., & Muller, K. (2014). *InnWind.EU design basis (4.22: Methods for performing scale-tests for method and model validation).* FP7 - InnWind.EU.

Sarmiento, J., Iturrioz, A., Ayllón, V., Guanche, R., & Losada, I. J. (2019). Experimental modelling of a multi-use floating platform for wave and wind energy harvesting. *Ocean Engineering, 173*, 761–773. doi:10.1016/j.oceaneng.2018.12.046

Sauder, T., Chabaud, V., Thys, M., Bachynski, E., & Saether, L. O. (2016). Real time hybrid model testing of a braceless semi-submersible wind turbine. Part I: the hybrid approach. *ASME International Conference on Ocean, Offshore and Arctic Engineering.* Busan.

Stansberg, C. T., Karlsen, S. I., Ward, E. G., Wichers, J. E., & Irani, M. B. (2004). Model testing for ultradeep waters., *2*, págs. 1153–1161.

Stansberg, C. T., Oritsland, O., & Ormberg, H. (2001). Challenges in deep water experiments: hybrid approach. *Proceedings of the 20th International Conference on Offshore Mechanics and Arctic Engineering.* Rio de Janeiro, Brazil.

Stansberg, C. T., Ormberg, H., & Oritsland, O. (2002). Challenges in deep water experiments: Hybrid approach. *Journal of Offshore Mechanics and Arctic Engineering, 124*, 90–96. doi:10.1115/1.1464129

Tahar, A., & Kim, M. (2008). coupled-dynamic analysis of floating structures with polyester mooring lines. *Ocean Engineering*(35), 1676-1685.

Taninoki, R., Abe, K., Sukegawa, T., Azuma, D., & Nishikawa, M. (2017). Dynamic cable system for floating offshore wind power generation. *SEI Technical Review, 84*, 53–-58.

Thys, M., Fontanella, A., Taruffi, F., Manjock, A., & Belloli, M. (2019). *LIFES50+ D7.9: Guidance and recommended methods for hybrid/HIL-based FOWT experimental testing.* Tech. rep., SINTEF Ocean, POLIMI, DNV-GL.

Vigara, F., Cerdán, L., Durán, R., Muñoz, S., Lynch, M., Doole, S., . . . Guanche, R. (2019). *COREWIND D1.2: Design load basis.* Tech. rep., ESTEYCO, COBRA, INNOSEA, JDR, UPC, FIHAC, UL INT GMBH.

Waals, O., & VanDijk, R. R. (2004). Truncation methods for deep water mooring systems for a catenary moored FPSO and a Semi taut moored semi submersible. *Proceedings of the Deep Offshore Technology International Conference.* Houston (TX, USA).

Wang, H.-W., Luo, Y., Hu, K.-Y., & Li, T.-T. (2010). Mooring truncation design of a deepwater SPAR. *Journal of Marine Science and Application, 9*, 168–174. doi:10.1007/s11804-010-9069-x

Wei, H., Xiao, L., Tian, X., & Feng, W. (2018). Hybrid model testing using pre-offset and asymmetric truncation design for deepwater semi-submersible with highly compliant mooring system. *Journal of Marine Science and Technology (Japan), 23*, 536–556. doi:10.1007/s00773-017-0491-5

Wei, H., Xiao, L., Tian, X., & Kou, Y. (2017). Four-level screening method for multi-variable truncation design of deepwater mooring system. *Marine Structures, 51*, 40–64. doi:10.1016/j.marstruc.2016.10.003

Xu, S., & Ji, C.-Y. (2014). Dynamics of large-truncated mooring systems coupled with a catenary moored semi-submersible. *China Ocean Engineering, 28*, 149–162. doi:10.1007/s13344-014-0012-9

Zhang, H. M., Huang, S. H., & Guan, W. B. (2014). Optimal design of equivalent water depth truncated mooring system based on baton pattern simulated annealing algorithm. *China Ocean Engineering, 28*, 67–80. doi:10.1007/s13344-014-0005-8

Zhang, H. M., Sun, Z. L., Yang, J. M., & Gao, M. Z. (2009). Investigation on optimization design of equivalent water depth truncated mooring system. *Science in China, Series G: Physics, Mechanics and Astronomy, 52*, 277–292. doi:10.1007/s11433-009-0044-y

Zhang, H., Gao, W., Wang, Q., Jiang, J., & Zhao, Z. (2012). Investigation on optimization design of an equivalent water depth truncated mooring system based on INSGA-II. *Journal of Marine Science and Application, 11*, 208–215. doi:10.1007/s11804-012-1124-3